A NOVEL HYDROPHOBIC ZrO₂-SiO₂ BASED HETEROGENEOUS ACID CATALYST FOR THE ESTERIFICATION OF GLYCEROL WITH OLEIC ACID

KONG PEI SAN

**FACULTY OF ENGINEERING
UNIVERSITY OF MALAYA
KUALA LUMPUR**

2018

A NOVEL HYDROPHOBIC ZrO$_2$-SiO$_2$ BASED HETEROGENEOUS ACID CATALYST FOR THE ESTERIFICATION OF GLYCEROL WITH OLEIC ACID

KONG PEI SAN

THESIS SUBMITTED IN FULFILMENT OF THE REQUIREMENTS FOR THE DEGREE OF DOCTOR OF PHILOSOPHY

FACULTY OF ENGINEERING
UNIVERSITY OF MALAYA
KUALA LUMPUR

2018

UNIVERSITY OF MALAYA
ORIGINAL LITERARY WORK DECLARATION

Name of Candidate: KONG PEI SAN

Matric No: KHA140003

Name of Degree: DOCTOR OF PHILOSOPHY

Title of Project Paper/Research Report/Dissertation/Thesis ("this Work"):

A NOVEL HYDROPHOBIC ZrO_2-SiO_2 BASED HETEROGENEOUS ACID CATALYST FOR THE ESTERIFICATION OF GLYCEROL WITH OLEIC ACID

Field of Study: REACTION ENGINEERING

I do solemnly and sincerely declare that:

(1)   I am the sole author/writer of this Work;
(2)   This Work is original;
(3)   Any use of any work in which copyright exists was done by way of fair dealing and for permitted purposes and any excerpt or extract from, or reference to or reproduction of any copyright work has been disclosed expressly and sufficiently and the title of the Work and its authorship have been acknowledged in this Work;
(4)   I do not have any actual knowledge nor do I ought reasonably to know that the making of this work constitutes an infringement of any copyright work;
(5)   I hereby assign all and every rights in the copyright to this Work to the University of Malaya ("UM"), who henceforth shall be owner of the copyright in this Work and that any reproduction or use in any form or by any means whatsoever is prohibited without the written consent of UM having been first had and obtained;
(6)   I am fully aware that if in the course of making this Work I have infringed any copyright whether intentionally or otherwise, I may be subject to legal action or any other action as may be determined by UM.

Candidate's Signature   Date:

Subscribed and solemnly declared before,

Witness's Signature   Date:

Name:

Designation:

A NOVEL HYDROPHOBIC ZrO_2-SiO_2 BASED HETEROGENEOUS ACID CATALYST FOR THE ESTERIFICATION OF GLYCEROL WITH OLEIC ACID

ABSTRACT

The inevitably low value of glycerol has led to extensive investigations on glycerol conversion to value-added derivatives. This work focuses on industrially important catalytic esterification of glycerol with oleic acid due to its high commercial value. In this work, a novel heterogeneous acid catalyst featuring hydrophobic surface was developed on ZrO_2-SiO_2 support as water tolerant solid acid catalyst is vital for two phase esterification reactions producing water. The synthesized catalyst (ZrO_2-SiO_2-Me&Et-$PhSO_3H$) was prepared through silication and surface modification using trimethoxymethylsilane (TMMS) and 2-(4-chlorosulfonylphenyl)ethyltrimethoxysilane. The surface morphology, physiochemical and textural properties, acidity and hydrophobicity were characterized. The mechanism of the catalyst surface modification is thereof proposed according to comprehensive characterization results. A novel technique to control acidity and hydrophobicity level of the designed catalyst is disclosed in this work. The acidity and hydrophobicity of the catalyst were tuned by controlling the amount of surface modification agents. It was found that the hydrophobicity of the catalyst is decreased as its acidity increased. ZrO_2-SiO_2-Me&Et-$PhSO_3H$_70 catalyst with 70 mol% of TMMS and 0.62 mmol/g acidity is the optimal catalyst for glycerol esterification with oleic acid. Furthermore, the role of hydrophobicity in catalytic reaction was investigated herein. It was found that at constant catalyst acidity, the more hydrophobic catalyst showed better yield. The conversion obtained with the designed catalyst (ZrO_2-SiO_2-Me&EtPhSO_3H$_70) is 88.2% with 53.5% glycerol monooleate selectivity and 40.0% glycerol dioleate

selectivity (combined 94% selectivity of glycerol monooleate and dioleate) at equimolar oleic acid-to-glycerol ratio, 160 $^{\circ}$C, reaction temperature, 5 wt% catalyst concentration with respect to weight of oleic acid, solvent-less reaction conditions and 8 h reaction time. This work reveals hydrophobicity and pore volume of the designed catalyst affect the selectivity of product significantly. In addition, the performance of the hydrophobic designed ZrO_2-SiO_2-Me&Et-$PhSO_3H$_70 catalyst was used to benchmark with catalytic activity of sulfated zirconia (SO_4^{2-}/ZrO_2) and commercial catalysts (Amberlyst 15 and Aquivion). The correlation results showed that pore volume (pore size) influenced the product selectivity when ZrO_2-SiO_2-Me&Et-$PhSO_3H$_70 catalyst was compared to three SO_4^{2-}/ZrO_2 catalysts that were developed from different zirconium precursors. Whereby, the higher pore volume catalyst is favourable to glycerol dioleate production at identical reaction conditions. It can be concluded pore volume and size can be used to control the selectivity of the products. In addition, this study also revealed hydrophobicity characteristic facilitated initial reaction rate effectively.

Keywords: Silica-based catalyst, hydrophobic, esterification, glycerol, oleic acid

A NOVEL HYDROPHOBIC ZrO$_2$-SiO$_2$ BASED HETEROGENEOUS ACID CATALYST FOR THE ESTERIFICATION OF GLYCEROL WITH OLEIC ACID

ABSTRAK

Kejatuhan harga gliserol yang terlampau rendah menyebabkan penyelidik saintifik memulakan pemprosesan gliserol kepada produk tambah nilai. Kerja ini mengaji pengesteran gliserol dengan asid oleik meggunakan pemangkin asid heterogen kerana nilai komersial produk yang tinggi. Novel pemangkin asid heterogen yang mempunyai sifat hidrofobik akan direkakan dengan menggunakan pepejal ZrO$_2$-SiO$_2$. Pemangkin asid heterogen yang bersifat hidrofobik adalah sangat penting terutamanya bagi tindak balas dwifasa bahan dan proses pengesteran yang menghasilkan air. Pemangkin asid heterogen, ZrO$_2$-SiO$_2$-Me&Et-PhSO$_3$H direkakan dengan menggunakan proses lapisan silika atas pepejal zirconia dan pertukaran sifat permukaan pemangkin melalui ejen hidrofobik. Penyiasatan sifat-sifat pemangkin seperti morfologi permukaan, keasidan, tekstur, hidrofobik dan fizikokimia telah dikaji untuk menentukan ciri-ciri keistimewaan pemangkin asid heterogen ini. Selain daripada itu, kerja ini membentangkan teknik mengawal keasidan dan kehidrofobikan pemangkin asid heterogen. Mekanisme permukaan pemangkin yang direkakan ini dicadangkan berasaskan keputusan pencirian ujikaji pemangkin yang lengkap. Teknik novel untuk mengawal keasidan dan kehidrofobikan bagi pemangkin ini telah didedahkan dalam tesis ini. Kerja ini telah membuktikan keasidan dan kehidrofobikan pemangkin ZrO$_2$-SiO$_2$-Me&Et-PhSO$_3$H boleh dikawal dengan penggunaan kuantiti ejen modifikasi permukaan yang sesuai. Apabila sifat kehidrofobikan pemangkin semakin berkurang, keasidan pemangkin akan bertambah telah ditemui dalam kerja ini. Pemangkin ZrO$_2$-SiO$_2$-Me&Et-PhSO$_3$H_70 dengan 70 mol% hidrofobik dan keasidan 0.62 mmol/g adalah pemangkin optimum bagi reaksi pengesteran gliserol dengan asid oleik. Kajian peranan sifat hidrofobik dalam pemangkin asid heterogen atas reaksi pengesteran telah dijalankan dan mendapati

pemangkin yang lebih hidrofobik memperoleh hasil yang lebih tinggi apabila keasidan pemangkin yang sama digunakan. Pemangkin ZrO_2-SiO_2-Me&EtPhSO$_3$H_70 mencapai pertukaran 88.2%, 53.5% kememilihan gliserol monooleate dan 40.0% kememilihan gliserol dioleate dalam keadaan tindak balas 160 $^{\circ}$C, 5 wt% kepekatan mangkin dan sama molar gliserol-asid oleik. Kerja ini membuktikan kehidrofobikan dan isipadu liang pemangkin mempengaruhi kememilihan hasil keluaran Selain itu, prestasi pemangkin hidrofob yang direka, ZrO_2-SiO_2-Me&Et-PhSO$_3$H_70 telah dibandingkan dengan aktiviti pemangkin zirkonia sulfat (SO_4^{2-}/ZrO_2) dan pemangkin komersil (Amberlyst 15 dan Aquivion). Keputusan korelasi menunjukkan bahawa isipadu liang (saiz liang) mempengaruhi kememilihan produk apabila pemangkin ZrO_2-SiO_2-Me&Et-PhSO$_3$H_70 dibandingkan dengan tiga pemangkin SO_4^{2-}/ZrO_2 yang dihasilkan dari prekursor zirkonium yang berbeza. Di mana, isipadu liang pemangkin yang lebih tinggi adalah lebih baik bagi pengeluaran gliserol dioleik dalam keadaan tindak balas yang sama. Kerja ini boleh menyimpulkan isipadu liang dan saiz liang boleh mengawal kememilihan produk. Di samping itu, kajian ini juga mendedahkan ciri hidrofobisiti pemangkin mempercepatkan kadar reaksi awal.

Kata kunci: Pemangkin jenis silica, hidrofobik, pengesteran, gliserol, asid oleik

ACKNOWLEDGEMENTS

TABLE OF CONTENTS

LIST OF FIGURES

LIST OF TABLES

LIST OF SYMBOLS AND ABBREVIATIONS

List of Abbreviations

ACN	:	Acetonitrile
Al	:	Aluminum
BaO	:	Barium oxide
BET	:	Brunauer, Emmett and Teller
CAGR	:	Compound annual growth rate
CaO	:	Calcium oxide
CG	:	Crude glycerol
CSPETS	:	2-(4-chlorosulfonylphenyl)ethyltrimethoxysilane
DMC	:	Double metal cyanide
FAEs	:	Fatty acid esters
FAMEs	:	Fatty acid methyl esters
FeO	:	Ferrous oxide
FESEM	:	Field Emission Scanning Electron Microscope
FFAs	:	Free fatty acids
FTIR	:	Fourier-transform infrared
GMO	:	Glycerol monooleate
GDO	:	Glycerol dioleate
GTO	:	Glycerol trioleate
HCl	:	Hydrochloric acid
H_2O	:	Water
H_2SO_4	:	Sulfuric acid
HNO_3	:	Nitric acid
HPAs	:	Heteropolyacids

HPLC	:	High performance liquid chromatography
HPMo	:	Phosphomolybdic acid
HPW	:	Phosphotungstic acid
HSiW	:	Silicotungstic acid
LDH	:	Layered double hydroxide
MCM-41	:	Mobil Composition of Matter No. 41
MeOH	:	Methanol
MgO	:	Magnesium oxide
MONG	:	Matter organic non glycerol mattress
MR	:	Molar ratio
OA	:	Oleic acid
PG	:	Pure glycerol
PSD	:	Particle size distribution
*p*TSA	:	p-toluene sulfonic acid
RI	:	Refractive index
SBA	:	Santa Barbara Amorphous
SnO	:	Stannous oxide
SrO	:	Strontium oxide
TEOS	:	Tetraethyl orthosilicate
TFA	:	Trifluoroacetic acid
TGA	:	Thermogravimetric analysis
THF	:	Tetrahydrofuran
Ti	:	Titanium
TMMS	:	Trimethoxymethylsilane
USP	:	United States Pharmacopeia
XPS	:	X-ray photoelectron spectra

| XRD | : | Powder X-ray diffraction |
| ZnO | : | Zinc oxide |

List of Symbols

C	:	Conversion (%)
hL	:	Hectoliter (equivalent to 100 litres)
PD	:	Pore diameter (nm)
pK	:	Dissociation constant
P/P_0	:	Relative pressure
PV	:	Pore volume (cm^3/g)
PSD	:	Particle size distribution (μm) or (nm)
S	:	Selectivity (%)
S_{GMO}	:	Selectivity of GMO (%)
S_{GDO}	:	Selectivity of GDO (%)
S_{GTO}	:	Selectivity of GTO (%)
SSA	:	Specific surface area (m^2/g)
Y	:	Yield (%)

LIST OF APPENDICES

CHAPTER 1: INTRODUCTION

1.1   Glycerol Characteristics and Production

Glycerol is a colorless, odorless, viscous, and hygroscopic liquid substance with a slightly sweet taste. It is the simplest trihydric alcohol that can be reacted as an alcohol but can remain stable under most conditions. Glycerol was first discovered by C. W. Scheele in 1779 through the saponification of olive oil with lead oxide. The name "glycerol" was first used by M. E. Chevreul in 1813; until the 1930s, glycerol was mainly produced via a fat-splitting process. Pasteur (1857) showed that glycerol, together with succinic acid, can be produced from sugars via a biochemical pathway called alcoholic fermentation. In World War I and II, glycerol was also produced through fermentation or carbohydrate hydrogenolysis (Anneken et al., 2000; Pagliaro & Rossi, 2010; The Soap and Detergent Association, 1990; USDA AMS Agricultural Analytics Division, 2013).

Glycerol has also been synthetically produced from petrochemical feedstock since 1943 (I. G. Farben); synthetically produced glycerol accounted for approximately 60% of the total market in 1965 (Pagliaro & Rossi, 2010). However, the use of synthetic glycerol has lost popularity over renewable-derived glycerol because of cost-ineffective production (Quispe, Coronado, & Carvalho Jr, 2013). Three common pathways have concurrently generated excess agriculture-based glycerol: hydrolysis, saponification, and biodiesel production (Brockmann et al., 1987; Kirk-Othmer, 2013).

The quantity and quality of glycerol generated from three major commercial productions are elucidated comprehensively herein. It has been revealed that excess crude glycerol (CG) is attributed not only to biodiesel production but also to alternate

chemical routes employed in the oleochemical industry. Glycerol that has not undergone chemical treatment, purification, or separation is known as CG. The quality of CG strongly depends on processes and materials. Different impurities, such as monoglycerides, diglycerides, alkali metals, fatty acid esters (FAEs), soaps, salts, or diols are formed with their corresponding processing technologies. The common processes of glycerol production, operating conditions and the quality of CG produced through different routes are summarized in Table 1.1. Among the three processes, hydrolysis produces the least amount of impurities: 2.2%, 14.1%, and 16% of the total impurities consisting of ash, matter organic non glycerol (MONG), and polyol are obtained through hydrolysis, soap production, and biodiesel production, respectively. Despite the highest content of impurities obtained through biodiesel production, biodiesel-based CG is the major source of glycerol.

Table 1.1: Summary of commercially available glycerol production routes and their impurities

	High pressure splitting (hydrolysis)	Soap making process (saponification)	Biodiesel production (transesterification)
Mechanism	Triglycerides + 3water ⟷ fatty acids + glycerol	Triglycerides + 3NaOH ⟶ soaps + glycerol	Triglycerides + 3.methanol ⟷ Methyl esters + glycerol
Theoretical yield	Theoretically 1 ton oil produces 100 kg glycerol, approximately 10 wt% concentration of glycerol obtainable for hydrolysis, saponification and transesterification		
Operating conditions	• T= 250-260 ^{o}C • P= 70-80 bar • t= 2-3 h • Catalyst= absence	• T= 125 ^{o}C • P= atmosphere • Extra chemical dosing= brine, electrolytes and lye solution	• T= 60-80 ^{o}C • P= atmosphere • t= 1 h • Molar ratio of methanol to oil= 6:1 • Base homogeneous catalyst= sodium methoxide, potassium hydroxide, sodium hydroxide, potassium methoxide • Base heterogeneous catalyst= alkaline metal oxide (MgO, CaO, SrO, BaO), supported metal oxide, binary metal oxide, hydrotalcite and others.
Diluted glycerol	Sweet water consists of 10 to 16% concentration of glycerol	Spent soap lye contains 8-12% of glycerol	± 50 wt% glycerol (vary according to biodiesel processes)
Common impurities	Large amount of water, inorganic salts, fats, low molecular weight organic compounds, glycerol oligomers and polymers	Glycerol mixture with spent lye or neutral lye; around 6 to 8 % high salt content	CG with abundance of impurities such as triglyceride, mono-,diglyceride, inorganic salts, polyols, soap, ash, methanol, moisture, MONG, FAEs, FFAs and FAMEs

Table 1.1 continued

Demethylated glycerol			
Components			
Glycerol	88-90%	83-84%	65-80%
Ash	0.7-1%	8.5-9.5%	4-6%
Water	8-9%	6-7%	10%
MONG	0.7-1%	3-4%	5%
Polyols	0.2%	0.1%	1%
Processing for technical/USP/Kosher grade glycerol	Yes	Rarely	Yes

Note: pH measurement for demethylated biodiesel-derived glycerol is possible only while using heterogeneous catalyst, or appears only after previous neutralization of homogeneous catalyst.

The Table was summarized from (Ayoub & Abdullah, 2012; CIMBRIA SKET, 2008; International Process Plants, 2009; Kirk-Othmer, 2013; Ma & Hanna, 1999; Quispe et al., 2013; Thompson & He, 2006))

1.1.1 Production capacity and current market trend for glycerol

Market statistics has revealed that the highest glycerol production capacity is attributed to biodiesel manufacturing, followed by fatty acid splitting, and fatty alcohol separation (Oleoline, 2012). Glycerol comprises 10 wt% of the total biodiesel production. The global biodiesel market was expected to reach 37 billion gallons by 2016, with an average growth of 42% per year, and is predicted to produce approximately 4 billion gallons of CG by 2016 (Quispe et al., 2013; Yang, Hanna, & Sun, 2012). The recent biodiesel market analysis report published on mid of 2017 indicates that the world biodiesel production was approximately 82 million tonnes in 2016 (BP, June 2017).

Nevertheless, the sudden decline in petroleum oil prices has significantly reduced the prices of biodiesel during the second half of 2014. Figure 1.1 shows the biodiesel prices declined strongly from 112 USD/hL (2013) to less than 80 USD/hL (2014); the ten-year forecast for biodiesel prices are expected to recover in nominal terms close to those in 2014 level (prices vary from 85-90 USD/hL). Figure 1.2 indicates that the global biodiesel production is expected to reach almost 39 billion liters by 2024. The projected production volume of biodiesel is stable and is mostly policy driven (Food and Agriculture Organization of the United Nations (OECD), 2015). The conventional glycerol commodity market is very narrow, and any increase in biodiesel production causes a sharp decrease by more than 50% of its current value (Babajide, 2013). As such, glycerol derivatives can potentially occupy a large segment in the current market. To date, the reported CG and refined glycerol price are \$0.24/kg and \$0.8/kg, respectively in the mid of 2017 (Oleoline, 2017).
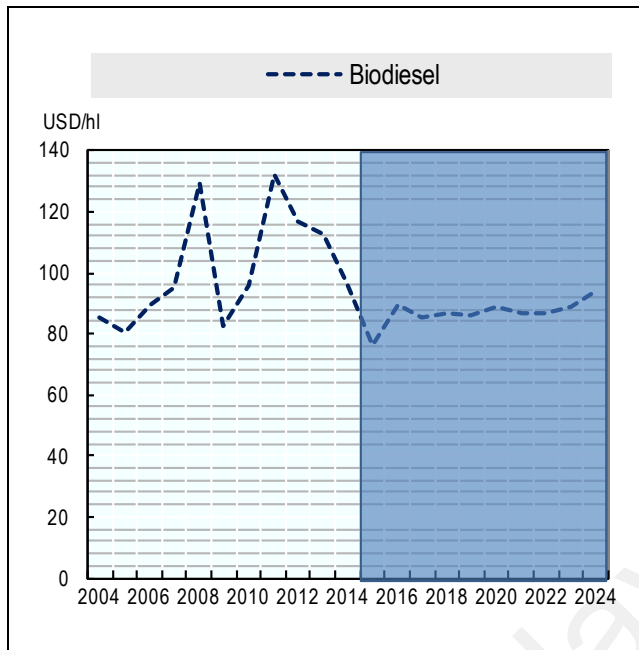
Figure 1.1: Evolution of biodiesel world price

(OECD 2015 market report)
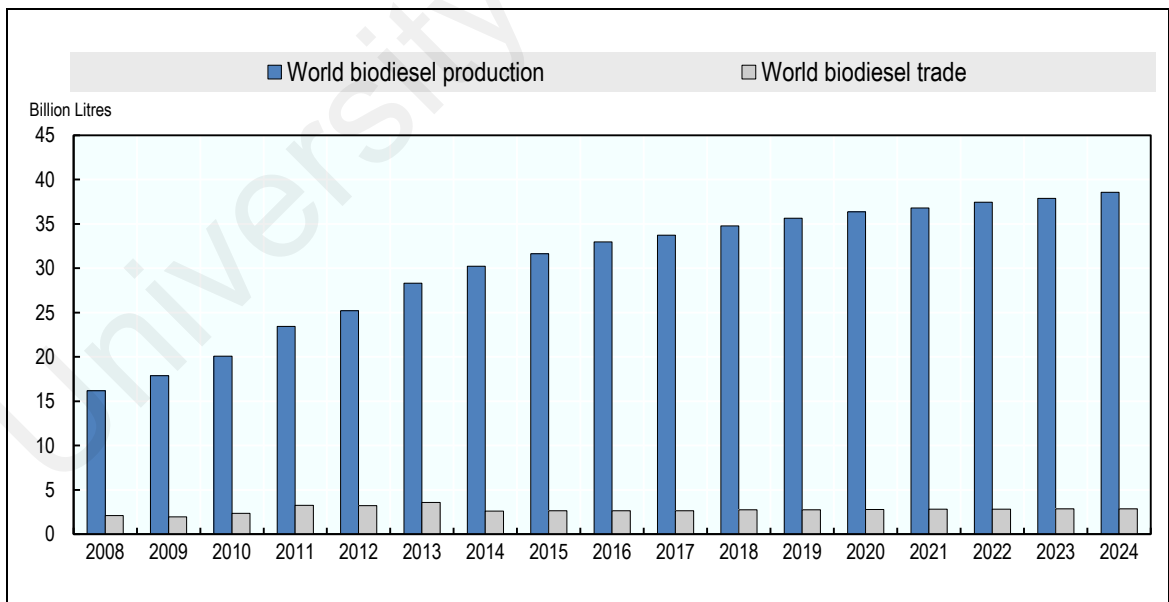
Figure 1.2: Development of the world biodiesel market

(OECD 2015 market report)

1.1.2 Transformation of glycerol to value-added derivatives

A fundamental understanding of different industrial processes, such as hydrogenation, hydrolysis, oxidation, chlorination, etherification, esterification, transesterification, and reforming, is necessary to investigate the transformation of glycerol into different derivatives (Soares, Lachter, Rodrigues Jr, Batista, & Nascimento, 2011). Figure 1.3 shows examples of possible glycerol derivatives via different pathways. Potential glycerol derivatives, such as propylene glycol, acrolein, dihydroxyacetone, glyceric acid, tartronic acid, epichlorohydrin, glycerol tertiary butyl ether, polyglycerols, glycerol esters, hydrogen gas, fuel additives, lubricant additives and glycerol carbonate, have been widely considered in global market for the transformation of glycerol into value-added chemicals (Gu, Azzouzi, Pouilloux, Jérôme, & Barrault, 2008; Kong, Aroua, & Daud, 2016; Leoneti, Aragão-Leoneti, & de Oliveira, 2012).

The rise in demand toward renewable sources, combined with the surplus of biodiesel production, has provided an attractive platform to all the industry players and researchers to work on glycerol transformation. The excess of glycerol produced from biodiesel production, together with society's concerns on biodegradable resources, has renewed the interest of researchers in catalytic esterification of glycerol. Consequently, direct-catalytic esterification of glycerol with oleic acid (OA) to produce glycerol monooleate (GMO), glycerol dioleate (GDO) and glycerol trioleate (GTO) will be described in Chapter 2 (Literature review).
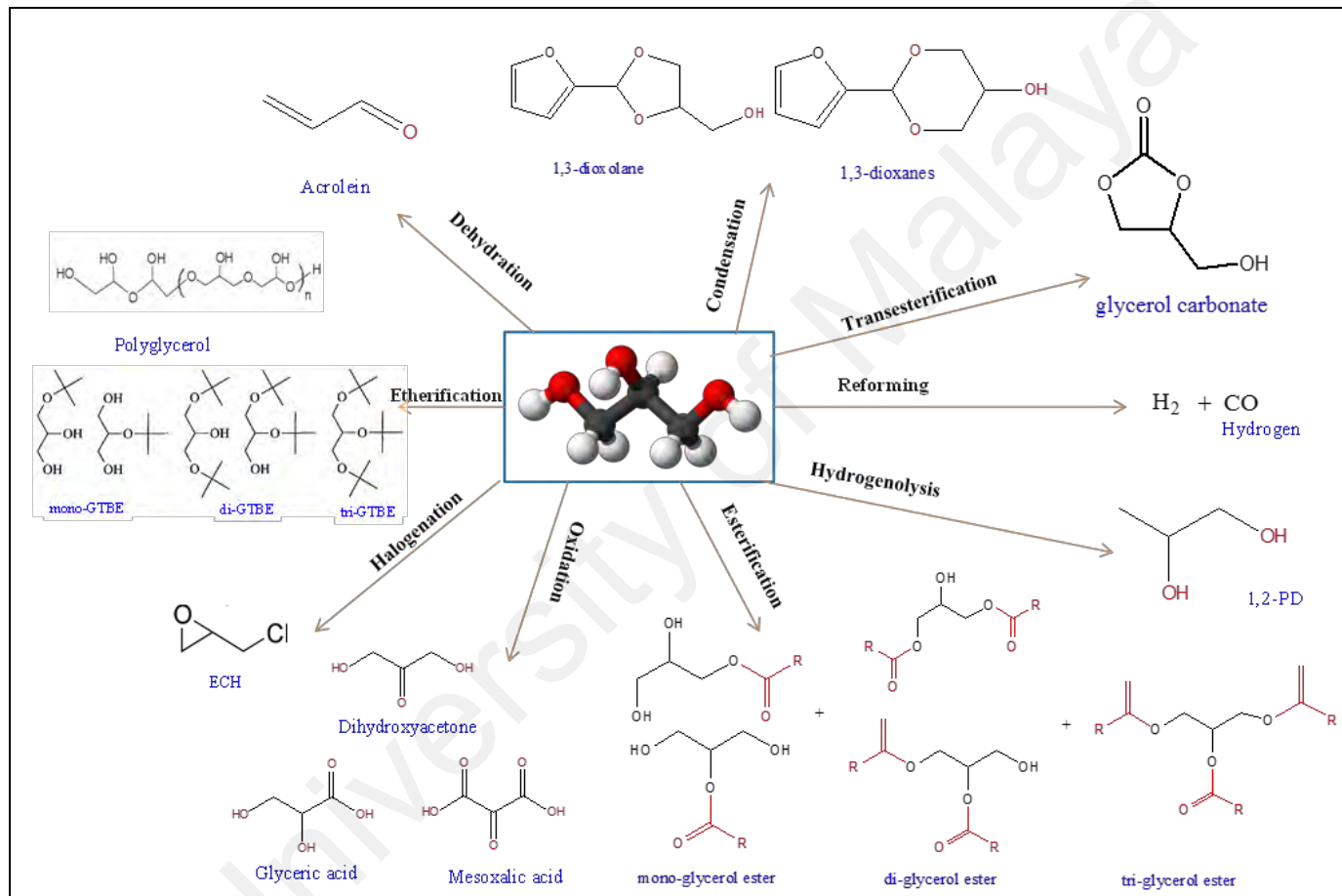
Figure 1.3: Possible glycerol derivatives via different pathways

(Kong, Aroua, & Daud, 2016)

1.2 Problem statement

The inevitably low value of glycerol has led to extensive investigations on glycerol conversion to value-added chemicals. This work focuses on the development of water tolerant solid acid catalyst for industrially important catalytic esterification of glycerol with OA. The use of glycerol as a starting material to produce glycerol-derivatives is challenging. The high viscosity of glycerol could encounter diffusion problem in reaction media. Moreover, it has been reported that the reaction, involving reactants in two different phases, is complicated as poor interaction of OA and glycerol leads to low reactivity (Jérôme, Pouilloux, & Barrault, 2008). Secondly, the presence of water by-product in typical esterification reaction can easily deactivate the acid sites of solid acid catalyst and negatively affect the equilibrium of reaction.

To date, heterogeneous acid catalysts such as ion exchange resins (Åkerman, Gaber, Ghani, Lämsä, & Hatti-Kaul, 2011), zeolites (Singh, Patidar, Ganesh, & Mahajani, 2013), double-metal cyanide complexes (Kotwal, Deshpande, & Srinivas, 2011), heteropolyacids-supported catalysts (L. H. Wee et al., 2013), hydrotalcite (Hamerski & Corazza, 2014; Hamerski, Prado, da Silva, Voll, & Corazza, 2016) and sulfated metal oxides catalysts (Kong, Aroua, & Daud, 2015) have been studied for catalytic glycerol esterification with OA. It was reported that Sn-beta zeolite-catalyzed esterification was inefficient with only 4 % of OA conversion after 20 h reaction at equimolar ratio, 150 ^{o}C and solvent-added condition, even below the conversion without adding any catalyst (20 %) at identical reaction parameters. Thus, design of a reliable heterogeneous acid catalyst featuring with hydrophobic surface for water sensitive esterification of glycerol with fatty acid is essential in current research stage.

It was reported that hydrophobicity surface of a heterogeneous acid catalyst enhances miscibility phase between glycerol and OA. Some of the researchers elucidate that

hydrophobicity-enhanced acid catalysts can improve reactivity as well as selectivity, especially when one of the reactants is highly hydrophilic (Estevez et al., 2016; Gaudin, Jacquot, Marion, Pouilloux, & Jérôme, 2011; Konwar et al., 2016). In this work, a novel and environment benign heterogeneous acid catalyst that developed from SiO_2-ZrO_2 support featuring with hydrophobic surface characteristic is designed. The catalyst synthesis, characterization and catalytic activity of the process will be studied insight. Process optimization to maximize GMO and GDO yield is evaluated using suitable molar ratio of reactants. Further, the comparative study of designed catalyst with commercial and sulfated zirconia is evaluated in this work.

1.3 Objectives of the study

The aim of this work is to study the catalytic esterification of glycerol with OA for the formation of GMO and GDO. The main objectives of this study are as follows:

i. To synthesize and characterize a novel hydrophobic ZrO_2-SiO_2 based acid catalyst for the catalytic esterification of glycerol with OA.

ii. To evaluate the catalyst performance under various operating conditions such as reactants molar ratio, catalyst concentration, reaction temperature and reaction time.

iii. To benchmark the performance of the novel catalyst to that of conventional sulfated zirconia (SO_4^{2-}/ZrO_2) and commercial catalysts (Amberlyst 15; Aquivion).

1.4   Scope of the study

This work focuses on design and synthesis of hydrophobic-enhanced heterogeneous acid catalyst for glycerol oleate synthesis. The catalyst is synthesized by coating SiO_2 on zirconia support, followed by adding hydrophobic agent trimethoxymethylsilane (TMMS) and atom transfer radical polymerization initiator, 2-(4-chlorosulfonylphenyl)ethyltrimethoxysilane (CSPETS) and sulfonation process. The important catalyst properties such as morphology, physiochemical, textural, surface composition, and hydrophobicity level are examined for synthesized catalyst. The effect of TMMS and CSPETS loading amount used in catalyst synthesis towards hydrophobicity and acidity is insight studied. In addition, the mechanism for surface functionalization on SiO_2-ZrO_2 support is proposed based on the analytical and characterization results.

Process optimization under various operating conditions such as reactants molar ratio, catalyst concentration, reaction temperature and reaction time are included. In addition, the performance of the novel designed catalyst is compared with three conventional sulfated zirconia catalysts (SO_4^{2-}/ZrO_2) that developed from different zirconium precursors and commercial catalysts (Amberlyst 15; Aquivion).

1.5 Thesis outlines

This thesis consists of five chapters dealing with different aspects relevant to the topic of the study as follows:

i.   Chapter 1: Introduction

This chapter gives a general introduction of current glycerol production capacity, market value and commercially available process routes for glycerol; as well as potential value-added derivatives transformed from glycerol. The problem statement, main objectives and scope of this study are described in this chapter.

ii.   Chapter 2: Literature Review

Chapter 2 describes the common production routes of GMO and GDO and the reasons why heterogeneous acid catalyst is favorable in the production of GMO and GDO. The different type of heterogeneous acid catalysts and their important characteristics (such as textural properties, acidity, surface wettability, and catalyst sites) toward catalytic esterification of glycerol with OA are critically reviewed in this chapter. In addition, this chapter also reviews the impacts of operating parameters (molar ratio of glycerol to OA, reaction temperature, reaction time and catalyst concentration) on conversion and products selectivity.

iii. Chapter 3: Methodology

The chemical and materials, different catalyst preparation methods, different catalyst characterizations analysis instruments, product analysis techniques and catalytic activity testing method are elucidated in Chapter three.

iv.   Chapter 4: Results and Discussion

This chapter is divided into three parts: the first part is to investigate the preparation method of highly hydrophobic ZrO_2-SiO_2 based acid catalyst and the novel technique to control hydrophobicity and acidity of designed catalyst. The second part deals with the optimization of process parameters over the designed hydrophobic ZrO_2-SiO_2 based catalyst. The third part investigates the preparation methods and properties of SO_4^{2-}/ZrO_2 catalysts that were developed from three different precursors (zirconium (IV) propoxide, zirconium oxychloride and zirconium(IV) hydroxide). Subsequently, the catalytic activities of commercial available Amberlyst 15, Aquivion, SO_4^{2-}/ZrO_2 catalysts are benchmarked with the designed hydrophobicity-enhanced acid catalyst. All catalysts are subjected to an extensive characterization. Moreover, the relationships between conversion/selectivity and catalyst properties are insight studied in this work.

v.   Chapter 5: Conclusion and Recommendation

This chapter summarizes and concludes the findings of this research. The recommendation for future studies is suggested in this chapter.

CHAPTER 2: LITERATURE REVIEW

2.1   Catalytic-esterification of glycerol with oleic acid

The application of heterogeneous acid catalysts in conversion of glycerol into valuable derivatives includes dehydration to acrolein, acetylation to triacetin, esterification to glycerol esters, etherification to polyglycerols or glycerol ether as well as condensation to 1,3-dioxolanes and 1,3-dioxanes (Kong, Aroua, Daud, Lee, et al., 2016; Suprun, Lutecki, Haber, & Papp, 2009; Vol'eva et al., 2012). One promising option is the catalytic esterification of glycerol with fatty acids to obtain mono-, and di-esters. Typically, esterification reaction of glycerol with oleic acid (a common unsaturated fatty acid with C18:1 carbon chain, OA) is a feasible and economic method to change the fatty acid profile of a triglyceride. Mixture of glycerol monooleate (GMO), glycerol dioleate (GDO) and glycerol trioleate (GTO) can be produced over heterogeneously acid-catalyzed esterification reaction with acid, multi-valent metal salt type heterogeneous catalyst as well as biocatalysts (Bagheri, Julkapli, & Yehye, 2015). Figure 2.1 shows the possible derivatives produced from glycerol esterification with OA produces mixtures of GMO, GDO and GTO.
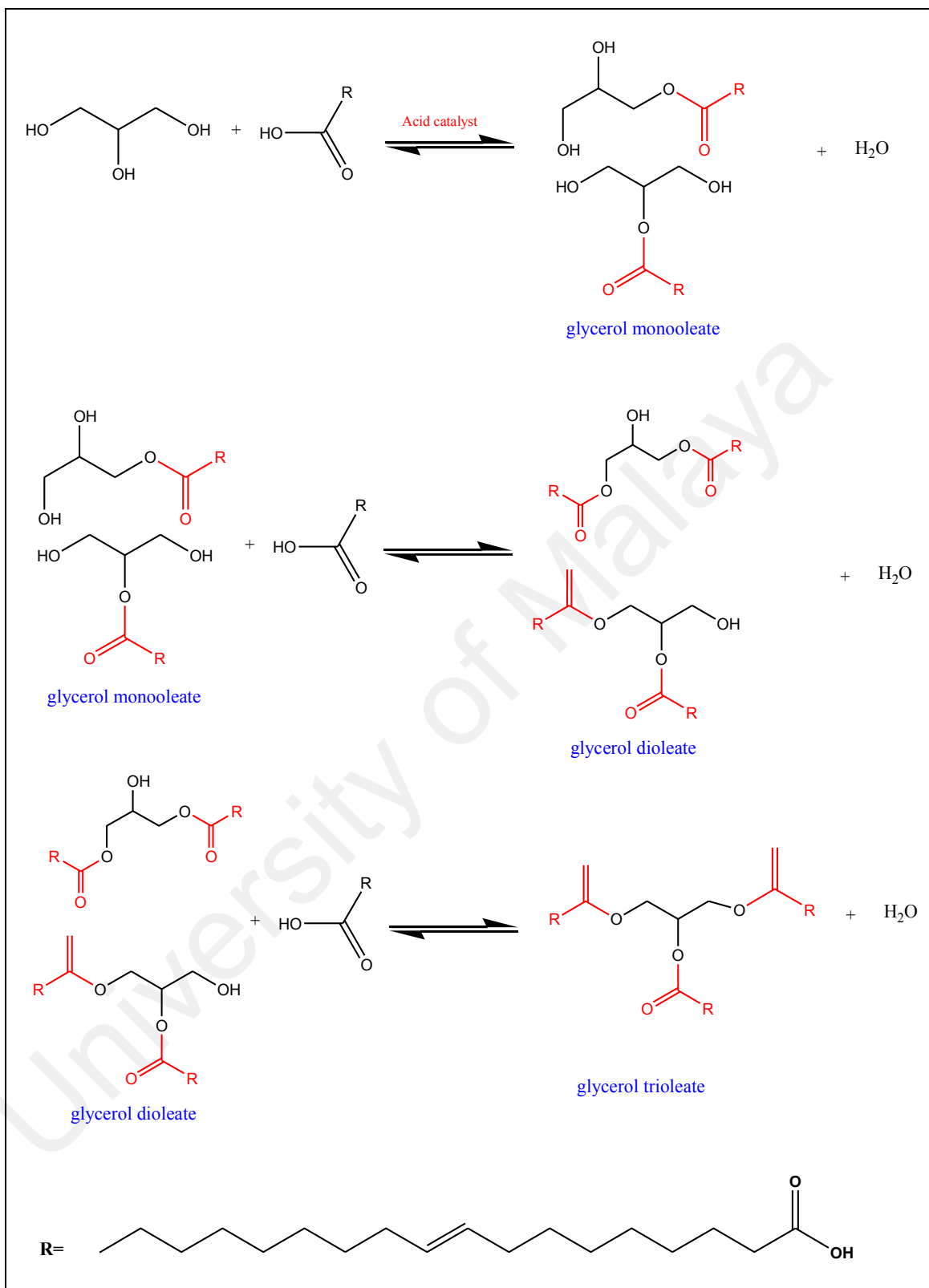
Figure 2.1: Reaction scheme for esterification of glycerol with OA in GMO, GDO and GTO production

It has been known that the fatty acid profile of a naturally occurring triglyceride contains various ratio of fatty acids. Triglycerides are generally composed of different alkyl chain lengths and saturation degrees from short, medium, long, saturated to eventually polyunsaturated alkyl groups (Refaat, 2009). For instance, the composition of palm oil comprises approximately 50% saturated fatty acids, with 44% palmitic acid (C16:0), 5% stearic acid (C18:0), and trace amounts of myristic acid (C14:0). The unsaturated fatty acids are approximately 40% OA (C18:1) and 10% polyunsaturated linoleic acid (C18:2) and linolenic acid (C18:3) (Montoya et al., 2014). From industry point of view, esterification of glycerol with fatty acid C18:1 is an alternative feasible way to transform fatty acid profile of a triglyceride. Glycerol esterification with longer molecular chain C18:1 requires longer reaction time than those medium or short chain fatty acids.

The common pathways to produce GMO, GDO are: (i) alkali MgO catalyst glycerolysis of GTO with glycerol at elevated temperature of 250 ^{o}C (A. Corma, Iborra, Miquel, & Primo, 1998); (ii) alkali glycerolysis of methyl oleate (Avelino Corma, Hamid, Iborra, & Velty, 2005; C. A. Ferretti et al., 2012; Cristián A. Ferretti, Soldano, Apesteguía, & Di Cosimo, 2010); (iii) biocatalyst glycerolysis of oil (Novozym 435) in a low-temperature reaction(40-70 ^{o}C) (Krüger et al., 2010; Voll et al., 2011); (iv) direct catalytic-esterification (Díaz, Mohino, Blasco, Sastre, & Pérez-Pariente, 2005; Hermida, Abdullah, & Mohamed, 2011; L. Wee et al., 2013). Table 2.1 summarizes the production efficiency of GMO and GDO in different production routes.

The advantages of catalytic-esterification of glycerol are that it is operated under milder reaction conditions (less than 180 ^{o}C) and processes directly without prerequisite of transesterification/esterification reactions at elevated temperature of 250 ^{o}C. In this

review, esterification route is being studied in-depth as this route is expected to be more selective and cost-effective compared to the other options (Singh et al., 2013).

Table 2.1: Comparative performance of GMO and GDO produced via different routes

Starting materials	Production Routes	Catalysts	Operating conditions	Performance	References
GTO; glycerol	Esterification and glycerolysis	MgO	T= 240 ^{o}C Gly/GTO= 12 t= 5 h Cat.= 4 wt%	C= 97% S_{GMO}= 75% S_{GDO}= 24%	(A. Corma et al., 1998)
Methyl oleate; glycerol	Trans-esterification and glycerolysis	MgO	T= 220-250 ^{o}C Gly/methyloleate= 2-6 t= 2 h Cat.=4 wt%	C= 70% S_{GMO}= 77% S_{GDO}= 24%	(Cristián A. Ferretti et al., 2010)
Olive oil	Glycerolysis	Novozym 435	T= 55 ^{o}C Oil/gly.= 6 t= 12 h Cat.=10 wt% Tert-butanol as solvent	S_{GMO}= >60 % S_{GDO}= >50 %	(Voll et al., 2011)
OA; glycerol	Esterification	STA-IL ionic liquid grafted acid catalyst	T= 100 ^{o}C t= 9 h Cat= 7 wt% OA/gly= 6	C= 96% S_{GMO}= 90%	(Wan N. R. W. Isahak, Ramli, Ismail, & Yarmo, 2014)

Heterogeneous acid catalytic system is environmental sustainable compared to homogeneous catalyst due to lesser waste production, easier operation and possible recycling. However, catalytic activity of heterogeneous catalyst is generally lower than that of homogeneous catalyst due to the poor accessibility of the embedded catalytic sites. The highly desirable selectivity of product can be obtained using heterogeneous catalyst system as the textural property of catalyst such as porosity might influence product selectivity. In fact, the use of glycerol as a starting material to produce glycerol-

derivatives is challenging. The high viscosity of glycerol could lead to diffusion problem in reaction media. Moreover, it has been reported that the reaction involving two immiscible phase reactants is complicated as poor interaction of OA and glycerol has led to low reactivity (Jérôme et al., 2008).

Some of the researchers elucidate that hydrophobicity-enhanced acid catalysts can improve reactivity as well as selectivity; especially when one of the reactants is highly hydrophilic such as glycerol (Estevez et al., 2016; Gaudin et al., 2011; Konwar et al., 2016). Moreover, the presence of water by-product in typical esterification reaction can easily deactivate the acid sites of solid acid catalyst and negatively affect the equilibrium of reaction (Kong, Aroua, Daud, Cognet, & Pérès, 2016). Consequently, water tolerable solid acid catalyst featuring hydrophobic surface characteristic is vital for esterification of glycerol with fatty acid (Chen, Chen, Zhang, Gao, & Yang, 2016). The recent published literatures for catalytic-esterification of glycerol with OA and their affecting parameters are discussed in this chapter. In addition, the limitation and unfavourable features of homogenous acid catalysts are addressed.

2.2   Applications, market and demand for glycerol oleate

GMO and GDO are lipids with amphiphilic, non-ionic and excellent emulsifying properties. They are widely applied in food, cosmetic and pharmaceutical industries, and aqueous fiber finishing (Macierzanka & Szeląg, 2004; Thengumpillil, Penumarthy, & Ayyagari, 2002). GMO featuring a polar head group and a non-polar hydrocarbon chain (significant amphiphilic properties). This allows GMO self-assemble into different liquid crystalline structures under varying conditions of temperature and solvent composition (Kulkarni, Wachter, Iglesias-Salto, Engelskirchen, & Ahualli, 2011). It is also introduced in specific fields such as in oil well drilling operations, lipophilic emulsifier for water-in-oil applications and anti-friction agent of lubricant and

fine mechanical oils (Wan N. R. W. Isahak et al., 2014; Organic Materials Review Institute, 2001).

In terms of market demand, the gradual slowdown in the food and plastics sectors have inhibited the growing rate of GMO, conversely, actively growing industries such as personal care, pharmaceuticals and lubricants have provided alternate outlets for GMO (Frost & Sullivan Research Service, 2014). Henceforward, the demand of GMO is correlated to personal care or lubricant market due to the saturated demand in food and plastic industries.

Whereby, GTO is one of the common biolubricants with symmetrical structure with that of triglyceride. Monounsaturated OA was selected in biolubricant synthesis because the conjugated bond of OA exhibits lower pour point, cloud point and low-temperature stability lubricant (Gryglewicz, Piechocki, & Gryglewicz, 2003). GTO is widely applied in two-stroke engines, rolling metal, casting aluminium, tire tread and as a stabilizing oil component (Labauze & Vasseur, 2007; Yoneda, 2009). In addition, the fields that use machinery for food processing, medicine and textile have almost declined the use of white mineral oils due to their toxicity. Subsequently, the combination of lubricity, biodegradability, renewability and non-toxicity of GTO lubricants has the potential to lead towards the growth in this market. Table 2.2 demonstrates the general industrial applications for GMO, GDO and GTO.

Table 2.2: The industrial applications for GMO, GDO and GTO

Products	Industrial applications	References
GMO	Defoamer in food processing, lipophilic emulsifier for water-in-oil applications or personal care, as antifriction agent in engine, lubrication additive; monoolein-based nano-particulate liquid dispersions for drug delivery; surfactant	(Wan N. R. W. Isahak et al., 2014; Organic Materials Review Institute, 2001)
GDO	Used in drug delivery applications; as safe plasticizers for the polymer industry	(Barauskas, Misiunas, Gunnarsson, Tiberg, & Johnsson, 2006; Zhang et al., 2017)
GTO	Metal working and textile lubricant in two-cycle engines, rolling metal, casting aluminum, tire tread; as a stabilizing oil component	(Labauze & Vasseur, 2007; Yoneda, 2009)

The industrial price of GMO, GDO and GTO was traded approximately at, 3.46 $/kg 4.46-6 $/kg and 2.80 $/kg, respectively in 2017 (Zauba, 2016). While the global lubricant market experiences dramatic changes for the past 10 years. It can be observed worldwide that there is a relatively stable and constant lubricant demand since 1991 (about 35 million tons per year) (Mobaraki, Movassagh, & Karimi, 2014; Nagendramma & Kaul, 2012). To date, the world's lubricant demand is estimated to increase to 2.4 % per annum, with approximately 43.6 million metric tons in demand by 2017. It is reported that lubricants market worth over $74 billion by 2022 (GlobeNewswire, 2017). Figure 2.2 demonstrates the forecasted lubricant demand growth by region from 2005 to 2015. The diagram suggests Asia Pacific as having the highest prospect by examining their 3.5 % growing rate.
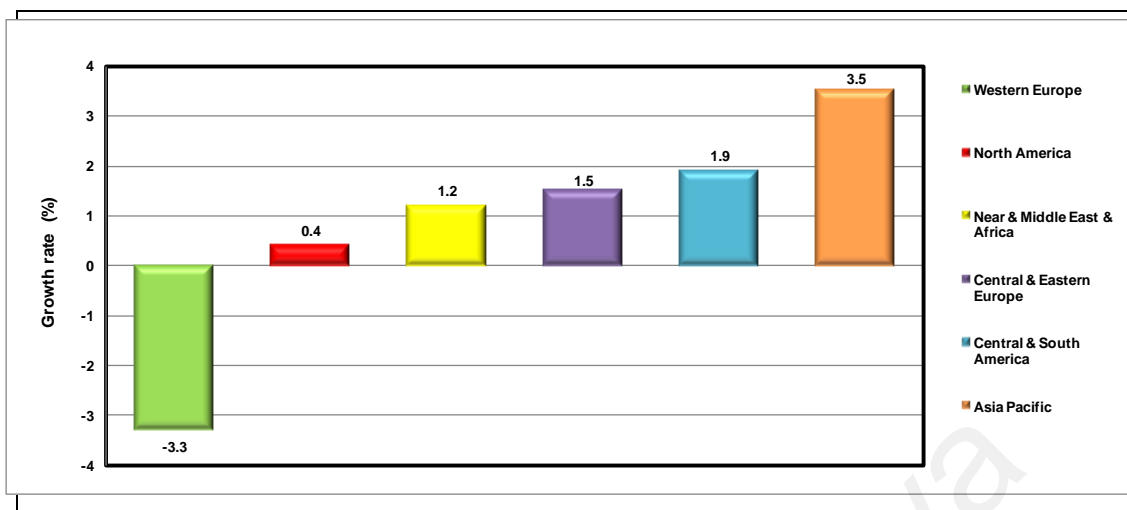
Figure 2.2: Forecast lubricants demand growth by region, 2005-2015

2.3   Mechanism of Brønsted and Lewis acid-catalysed esterification

2.3.1   General mechanism for glycerol esterification

Glycerol esterification using OA to produce GMO, GDO, and GTO can be extensively explained by the presence of three hydroxyl groups (−OH) that are attached to the glycerol backbone. OA is a long chain fatty acid and categorized as nonpolar lipid. In catalytic esterification of glycerol with OA, OA will selectively attach to any −OH of glycerol or any −OH from partially reacted glycerides; this phenomenon is related to the steric hindrance effect. Thus, the produced GMO and GDO normally present isomer forms depending on the position of esterification in the glycerol molecule. It has been reported the selectivity of GMO, GDO and GTO depends mostly on the catalyst features (surface acidity, pore structure, and catalyst stability) (Zięba, Drelinkiewicz, Chmielarz, Matachowski, & Stejskal, 2010) and reaction parameters (glycerol to OA molar ratio, temperature, catalyst amount, and reaction time) (L. Zhou, Al-Zaini, & Adesina, 2013). Generally, the acid-catalyzed glycerol esterification

involves two plausible reaction mechanisms based on the types of acid catalyst used: (i) Brønsted acid-catalyzed esterification and (ii) Lewis acid-catalyzed esterification.

2.3.2 Brønsted acid-catalysed esterification

The Brønsted acid-catalysed esterification is also named as Fischer esterification. Figure 2.3 illustrates a conventional reaction mechanism of the esterification reaction. Whereby, side chain R represents OA. This reaction mechanism involves addition of nucleophile (the glycerol) into OA followed by an elimination step, as follows (Troncea, Wuttke, Kemnitz, Coman, & Parvulescu, 2011):

i. The OA is initially protonated by the Brønsted-type acid catalyst.

ii. In the second step, the oxygen atom (two lone pairs) from the –OH of glycerol acts as a nucleophile and attaches to the sp2 carbon, leading to the loss of proton from the –OH.

iii. A series of fast equilibrium proton exchanges occurs in either of the –OH of acetic acid. In this step, a new ester bond forms between the carboxyl group carbon and the oxygen in glycerol.

iv. Water is then eliminated in either site.

v. In the final step, the excess proton leaves, regenerating a Brønsted acid catalyst.

vi. This process continues until all three strands of the glycerol backbone are converted into esters.
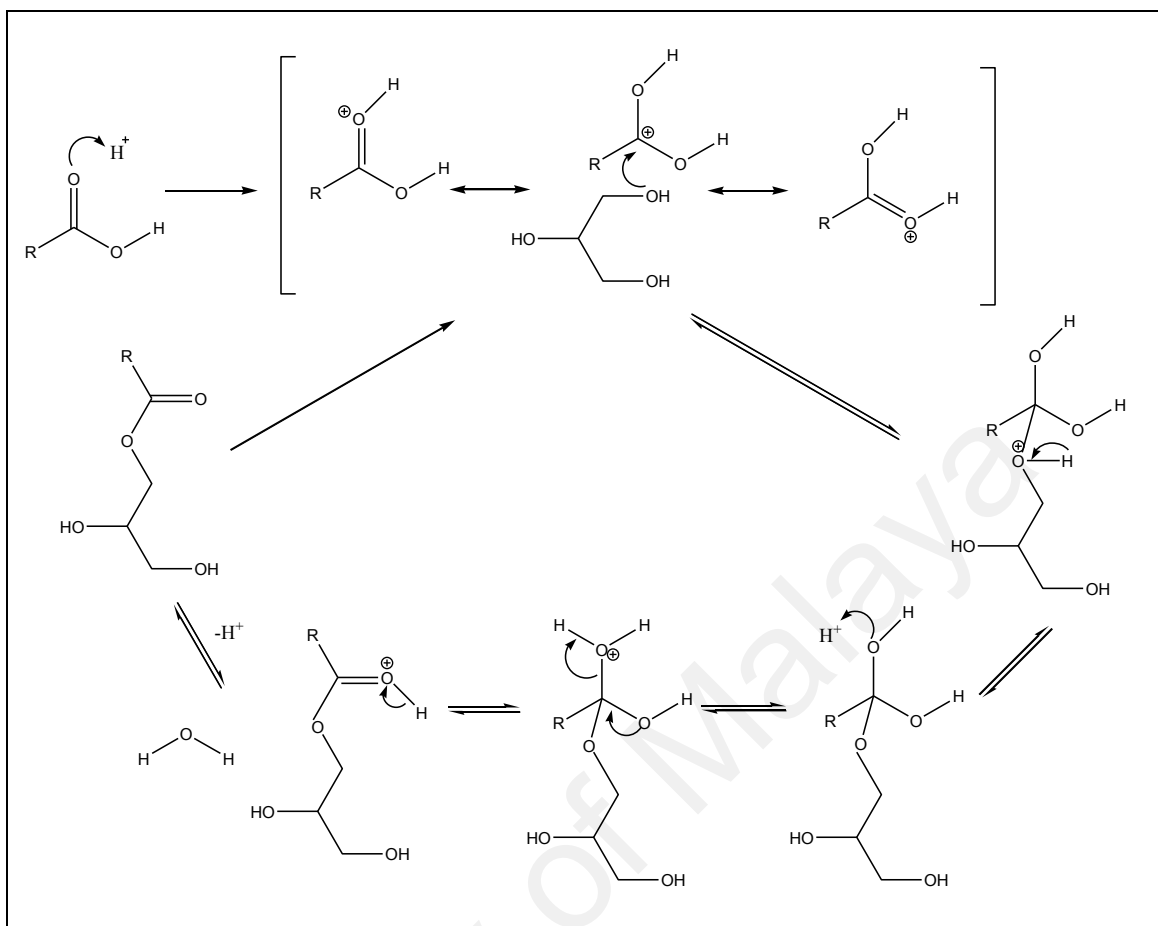
Figure 2.3: Brønsted-acid catalysed esterification mechanism

2.3.3 Lewis acid-catalysed esterification

Theoretically, Lewis acid-based esterification involves a reaction mechanism similar to that in Brønsted acid-based reaction. Nevertheless, Lewis acid-based esterification involves the attack of glycerol in a nucleophilic addition reaction. A slight difference between these two processes is that the Brønsted-catalysed reaction uses a proton generated from the acid catalyst. By contrast, the Lewis-based reaction involves a metal cation (Mn^+) as an electrophile to facilitate the interaction between the carbonyl oxygen from OA and the Lewis acidic site (L^+) of the catalyst to form carbocation. The nucleophile from glycerol attacks the carbon cation and produces tetrahedral

intermediates (Figure 2.4). During esterification, the tetrahedral intermediate eliminates water molecule to form an ester product (Yan, Salley, & Ng, 2009).
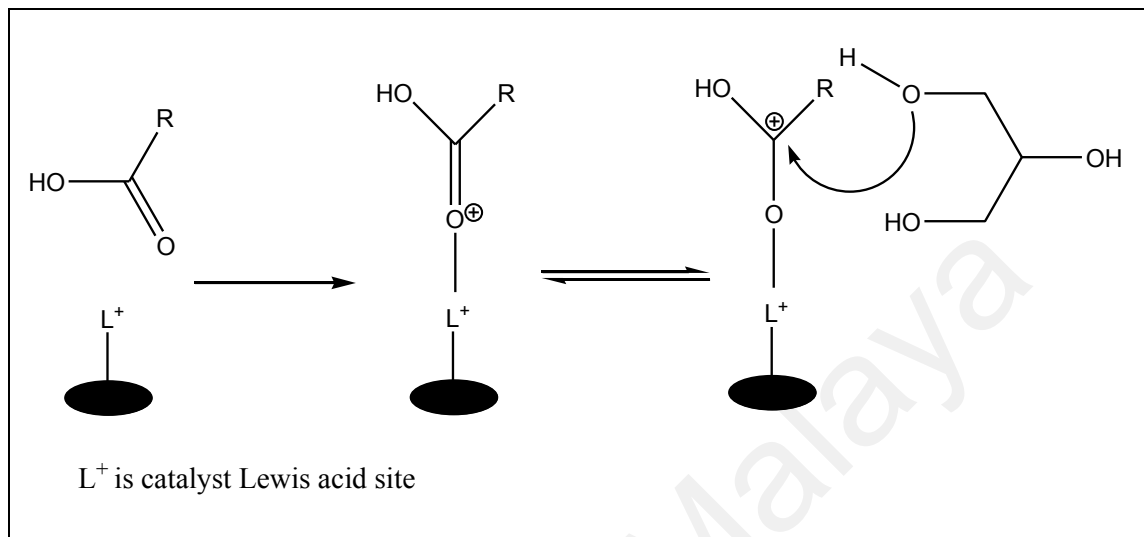
Figure 2.4: Lewis acid catalysed esterification mechanism

2.4   Homogeneous acid catalysts: limitation and drawbacks

The common homogeneous catalysts used in esterification production are sulfuric acid (H_2SO_4), hydrochloric acid (HCl), p-toluene sulfonic acid (pTSA) and methane sulfonic acid (MSA). Although H_2SO_4 is relatively cheap and recognised as an extremely acidic homogeneous catalyst, nonetheless, the corrosiveness of H_2SO_4 causes difficulty in storage, handling and operation. The double bond of unsaturated carboxylic acid can also react with H_2SO_4 to produce the undesirable ether side-product. On top of that, the dark colour appearance induced by H_2SO_4 cannot be eradicated by simple bleaching techniques.

Similar to H_2SO_4, HCl is also a chemical that is corrosive and difficult to handle. Meanwhile, for pTSA and MSA, both have similar acidity but differ in their physical appearance at ambient temperature (MSA is in liquid state at ambient temperature, while the closely related pTSA is in solid state). pTSA and MSA have lower reaction activity, subsequently making it easier for handling. Unlike H_2SO_4, their mild acidity does not attack the double bond of unsaturated carboxylic acid (Bondioli, 2004).

MSA or pTSA are considered the most suitable homogeneous acid catalysts for short chain ester production that requires lower operation temperature. However, they are undesirable to be applied in complex ester synthesis as complex esters usually require elevated reaction temperatures, which range from 180 to 250 ^{o}C. Although pTSA and MSA are low in acidity, they have slight effect on product colour. The complexity to obtain low colour product in pTSA-catalysed process was highlighted by (Sivaiah, Robles-Manuel, Valange, & Barrault, 2012). Table 2.3 shows examples of homogeneous acid-catalysed esterification reactions.

Table 2.3: Homogenous acid catalysed reaction studies

Homogeneous Catalysts	Raw materials	Reaction conditions	Conversion	References
H_2SO_4	MCPA acid; 2-ethyl hexanol	T= 120 ^{o}C t=2-3 h Catalyst= 0.1 M MR ethylhexanol:acid= 1.5	C= 98%	(Kong PS, Aroua MK, & Raman AA, 2011)
HCl	Fatty acid; methanol	T= 70 ^{o}C t=5 h Catalyst= 1 M MR methanol:fatty acid= 20:1	C= 98.44%	(Su, 2013)
MSA	Fatty acids; methanol	T= 130 ^{o}C t= 1 h Catalyst= 0.1 % w/w MR methanol/fatty acid= 3	C= >90%	(Aranda, Santos, Tapanes, Ramos, & Antunes, 2008)
pTSA	Myristic acid; isopropanol and *n*-propanol	T= 130 ^{o}C t= 3 h Catalyst= 0.03 M MR myristic acid/alcohol= 0.5	C= 80-90%	(de Jong, Feijt, Zondervan, Nijhuis, & de Haan, 2009)
Titanate	*Diisononyl phthalate;*pthalic anlydride	T= 200 ^{o}C t= 2 h Catalyst= 1.0 M	C= 99.9 %	(Johnson Matthey Catalysts VERTEC™, 2003)

Based on the above premises, homogeneous organic titanate catalyst was developed. The operation temperatures for titanate range from 180 to 220 °C. The recommended operating temperature shall not be lower than 160 °C to avoid premature hydrolysis of titanate (Johnson Matthey Catalysts VERTEC™, 2003). One of the major drawbacks of

the implementation of titanate is that the product is overloaded with titanium (Ti) content. Extra refining procedures such as steam stripping or hot water neutralisation are required to decrease Ti, but these procedures concurrently reduce the overall production yield. Moreover, the low Ti content requirement in product specifications resulted in business runners to turn to heterogeneous acid catalyst. Therefore, the development of applicable heterogeneous catalysts is vital to overcome the problems associated with homogeneous catalysts.

2.5 Heterogeneous acid catalysts for glycerol esterification

Heterogeneous acid catalysts play a crucial role in esterification reaction during esters production. In particular, solid acids have largely replaced the traditional homogeneous acid catalyst because of environmental, technological, and economic reasons. Generally, solid catalysts need to be stayed in a packed bed reactor for consecutive operations, exhibit longer catalyst lifetime than single-use homogeneous catalyst. A well-designed catalytic process system can overcome the drawbacks of homogeneous catalyst reaction by minimizing sludge and waste generation (Kiss, Dimian, & Rothenberg, 2008; Sivaiah et al., 2012).

A variety of solid acid catalysts have been studied for glycerol esterification. Their catalytic efficiency are also categorized into different groups (Table 2.4) (Gürbüz, Bond, Dumesic, & Román-Leshkov, 2013). It was reported that the key role of heterogeneous acid catalyst to attain high glycerol conversion rate and favorable selective glycerol oleate formation include: (i) acidity of catalyst (especially the Brønsted acid sites), (ii) texture properties, and (iii) surface morphology.

Table 2.4: Different groups of solid acid catalysts for glycerol esterification

Solid Acid Catalysts	Properties
Ion exchange resin	• Ion exchange resins are synthesized from polymers that are capable of exchanging particular ions. The drawback of the ion exchange resin catalyst is its low temperature stability.
Zeolites	• Crystalline solids composed of silicon and aluminum oxides arranged in a three-dimensional network of uniformly shaped micropores (< 2 nm) of tuneable topology and composition. • Brønsted acid sites in zeolites are commonly generated when protons balance the negatively charged framework induced by the presence of tetrahedrally coordinated aluminum (Al) atoms.
Heteropolyacids	• A class of metal salts wherein the oxo-anions are balanced by a wide range of cations with varying acid strength.
Metal oxides	• The Brønsted acid sites in metal oxides originate from highly polarized hydroxyl groups, acting as proton donors • The Lewis acid sites generated from coordinatively unsaturated cationic sites, which leave M^+ exposed to interact with guest molecules as an acceptor of pairs of electrons.
Mesoporous silica	• Mesoporous silica is a mesoporous form of silicate that consists of unique features: high surface area, chemical, thermal, and mechanical stability, highly uniform pore distribution and tunable pore size, high adsorption capacity, and an ordered porous network. • This material is potentially used as solid supported catalyst due to its recyclability, enhanced catalytic reactivity, and selectivity.
Carbon	• Porous carbon is an attractive catalytic material as it can be prepared from various low-cost waste carbon materials. • Carbon consists of suitable characteristics that can be used as a catalyst support, such as heat resistance, stability in both acidic and basic media, the possibility of easy recovery of precious metals supported on it and the possibility of tailoring both its textural and surface chemical properties.

Although many studies have demonstrated the high reactivity of glycerol esterification, most catalysts exhibit low thermal stability and unsatisfactory selectivity (Zięba et al., 2010). Furthermore, the hydrophilic character of catalyst surface is a challenge in active site deactivation resulting from the inevitable water formation during esterification, leading to leaching of active components into the reaction medium. The water-tolerant property of solid acid catalyst exhibiting a hydrophobic-enhanced surface is thus necessary to excellently perform glycerol esterification. Another reason of catalyst deactivation is the partial blockage of the catalyst's active sites by the reaction medium, such as glycerol and/or partial glycerides blocked within the pore structure of catalysts, thereby reducing the number of acid sites for continuous esterification until the desirable end-products are achieved (Khayoon, Triwahyono, Hameed, & Jalil, 2014).

2.5.1 Ion exchange resins

Ion exchange resins are effective catalysts for esterification, owing to their swelling capacity. Synthesis of monoglyceride through the esterification of glycerol with OA over ion exchange resins (Amberlyst 31 and Amberlyst 16) were studied by (Pouilloux, Abro, Vanhove, & Barrault, 1999). The conversion performance of Amberlyst 31 (68 %) is higher than Amberlyst 16 (37 %) under identical reaction condition due to the structure of resin; such that Amberlyst 16 is a macroporous resin while Amberlyst 31 is a gel-type resin. The gel type material of Amberlyst 31 demonstrates a 4 % low cross-linked structure. The Amberlyst 31 showed relatively low initial reaction rate but its reaction activity increased rapidly after 9 h of reaction due to the matrix swelling by OA. This study has shown the potential of sol-gel catalyst in glycerol GMO synthesis.

The effect of different operating temperatures towards reaction activity of using Amberlyst 31 catalyst was studied. A 68 % conversion at reaction temperature of 90 $^{\circ}$C

was recorded but experienced a decrease to 14 % conversion when the reaction temperature was increased to 140 $^{\circ}$C. This showed the loss of functional groups by the exposure to temperatures above the polymer thermal stability limit, whereby leading to the deactivation of cation exchange catalyst. Nevertheless, low surface areas and weak thermal stability are the major drawbacks of ion exchange resins (Frusteri et al., 2009).

2.5.2 Metal oxides

The use of metal oxide-based catalysts for esterification reaction has attracted attention of researchers owing to their strong surface acidity and high activity at low operating temperatures. The presence of Lewis acid (cations) and Brønsted acid (OH^- group)/Brønsted base (O^{2-} group) (anions) of metal oxides provided the required catalytic sites for esterification. Figure 2.5 illustrates the existence of Lewis and Brønsted sites in the metal oxide catalyst (Gürbüz et al., 2013). Moreover, functionalization of metal oxide via sulfonation (sulfated metal oxides such as sulfated-zirconia or tin oxide (SnO_2)) is a convenient means of enhancing the surface area and acidity of a catalyst.

$$ \text{Lewis acid} $$
$$ M^{n+} \text{——} O^{2-} \text{——} M^{n+} \text{——} O^{2-} \text{——} M^{n+} $$
$$ \text{Brønsted base} $$
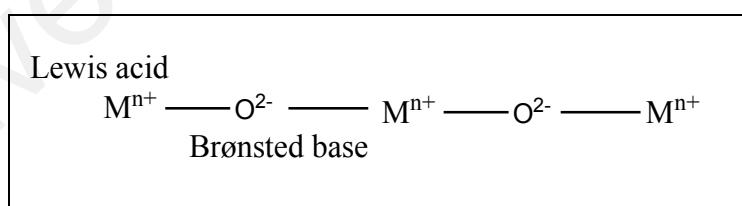
Figure 2.5: Lewis and Brønsted sites of metal oxide catalyst

The effectiveness of three metal oxides (zinc oxide (ZnO), ferrous oxide (FeO) and stannous oxide (SnO)) was compared by Bombos et al. in esterification of glycerol with OA (Dorin Bombos, Mihaela Bombos, Ion Bolocan, Gabriel Vasilievici, & Zaharia, 2010). It is revealed that ZnO was the outperforming catalyst when compared to FeO

and SnO due to the presence of large distribution acid center. Approximately 83.8 % conversion was obtained at equal molar ratio of OA to glycerol, 0.8 wt. % catalyst, 170 $^{\circ}$C and 6 h reaction time.

Since water is the by-product throughout the esterification reactions, therefore the reaction activity can be suppressed by formation of water due to the competition between reactants and water in adsorption (Varhadi et al., 2013). Therefore, metal oxide catalysts can be easily deactivated by water albeit these catalysts showing high temperature stability. In addition, it was reported that tin oxide and metallic zinc have the tendency to form fatty acid metallic soaps in ester production. The formed metallic soaps require additional refining procedures such as a combination of hot water washing and bleaching earth filtration (Bondioli, 2004).

2.5.2.1 Sulfated zirconia

Zirconia is one valuable metal oxide, owing to its cost-effectiveness and commercial availability. It can be modified by sulfate ions to form a superacidic catalyst (Kiss, Dimian, & Rothenberg, 2007). (Oh et al., 2013a) investigated the esterification of polyols with OA in the presence of sulfated zirconia catalyst, SO_4^{2-}/ZrO_2 which was prepared through one-step sol-gel method. The effect of different zirconium precursors on catalytic performance was evaluated, and it was discovered that the catalyst which was prepared by zirconium propoxide precursor had the utmost physical property and catalytic activity. Zirconium precursors altered the tetragonal zirconia phase, pore texture, surface area and acidity of the catalyst. Therefore, 83.5 % conversion was obtained when reaction was performed at 140 °C, 5.6 wt% of catalyst, for 4 h reaction time and 1.2 molar ratio of trimethylpropane to OA. Despite high leaching possibility of SO_4/ZrO_2 by losing the sulfate ions, the elemental analysis of the catalysts indicated that

the sulfur content of catalyst is stable and no sulfur leaching was detected after five repeated reactions.

(a) **Acid supported on zirconia**

An efficient catalyst support can reduce the mass transfer limitation in liquid-solid phase reaction by providing higher surface area from the existence of pores (Zabeti, Wan Daud, & Aroua, 2009). The catalytic activity of zirconium phenyl phosphonate phosphite catalyst (ZrPP) was investigated in esterification of glycerol with OA (Varhadi, Kotwal, & Srinivas, 2013). This work compared the performance of ZrPP catalyst by evaluating different molar ratio of phosphorous acid/phenol phosphonic acid loaded on zirconium. They found a correlation between molar ratio of acid loaded on zirconium and hydrophobicity surface of the catalyst. Higher molar ratio of phosphorous acid-to-phenol phosphonic acid increases the hydrophobicity of ZrPP catalyst, whereas, hydrophobicity surface of the catalyst is the critical key in minimizing catalyst deactivation problem by water. In this study, ZrPP catalyst showed high di- and tri-ester selectivity (92.3 %) with conversion of 48.9 % at 180 $^{\circ}$C, 5 wt% catalyst, 4 molar ratio of OA to glycerol within 1 h reaction time. Operating reaction temperature of 180 $^{\circ}$C indicated that high thermal stability of ZrPP catalyst.

2.5.3   Zeolites

Zeolites are generally categorized as aluminosilicate minerals, which are applied as catalyst support for active species owing to their unique pore system, high surface area, and high stability. The example of zeolite systems include of ZSM-5, Zeolite-Beta, and USY. The catalytic esterification reaction over zeolite-based catalysts depends on their different crystal structure, Si/Al ratio, and proton exchange level; these properties allow the catalytic properties, such as pore size, hydrophobicity/hydrophilicity, Brønsted/Lewis acidity, and acid strength distribution, to be designed. The acidity of

zeolite can be tuned by altering their chemical composition (Si/Al ratio) and ion-exchange abilities. Theoretically, protonic zeolite consisting of bridging –OH groups (Al–(OH)–Si) is an active acid site that favors Brønsted acid-catalyzed esterification reactions (refer to Figure 2.6) (Shaikhutdinov & Freund, 2013). Zeolites exhibiting low Al framework are the most hydrophobic types.
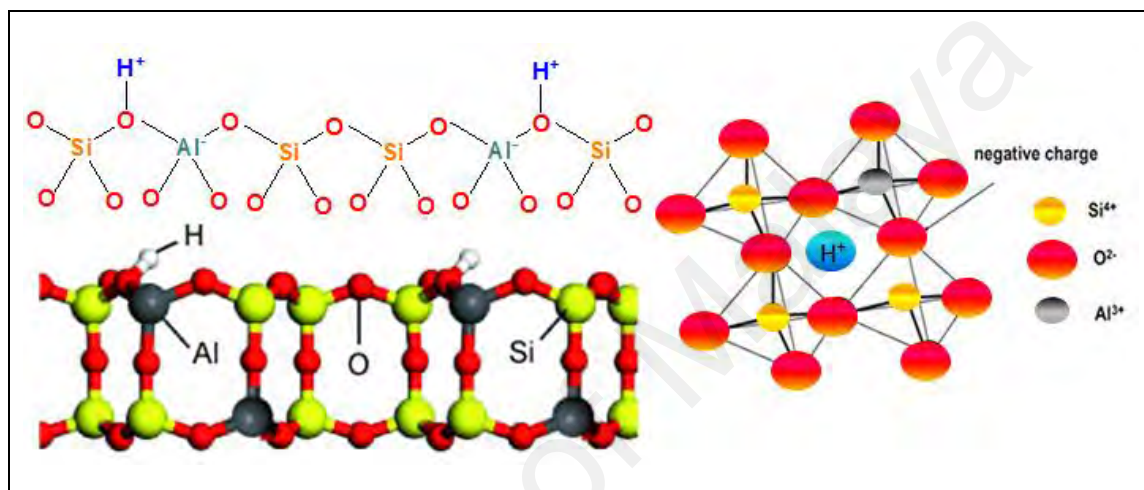
Figure 2.6: Existence of Si/Al in the structure zeolite catalyst

(redrawn from source of (Shaikhutdinov & Freund, 2013))

Nevertheless, small pore size of zeolite encounters poor reactivity as it hinders bulky molecules reaction. In this case, zeolite is not a good pore controlling catalyst as the external surface of zeolite produced undesirable di- and tri-ester (Márquez-Alvarez, Sastre, & Pérez-Pariente, 2004; C.-H. C. Zhou, Beltramini, Fan, & Lu, 2008). Despite of that, zeolite is known as a potential catalyst's support. Zinc oxide supported on β-zeolite with high silica content was studied in esterification of glycerol with OA by group Singh et al. (Singh et al., 2013). The intention was to utilize zeolite as a support to solve the leaching problem of conventionally used ZnO. Remarkably, a substantial reduction in leaching was observed when zeolite was used as catalyst support. The leaching value of ZnO/zeolite (663.05 ppm) was reduced when comparing to pure ZnO

(2986.86 ppm) under identical reaction environment. It was found that 25 % ZnO supported on zeolite demonstrated the highest catalytic activity, with approximately 85 % conversion and 70 % selectivity were achieved at 150 $^{\circ}$C, 4:1 glycerol to OA ratio, 2 wt% catalyst for 6 h reaction time. Moreover, addition of zeolite support increased the hydrophobicity nature of a catalyst. The promising yield and selectivity have shown that hydrophobic ZnO/zeolite catalyst is favorable in the immiscible OA-glycerol phase esterification reaction.

2.5.4 Heteropolyacids (HPAs)

HPAs, such as silicotungstic acid (HSiW), phosphotungstic acid (HPW), and phosphomolybdic acid (HPMo), are typical Brønsted acids containing a super-acid region that displays outstanding catalytic esterification activity both in homogeneous and heterogeneous phases. HPAs are complex proton acids that incorporate the Keggin-type polyoxometalate anions (heteropolyanions) containing metal–oxygen octahedra with a formula $XM_{12}O_{40}^{x-8}$, where X is the central atom (Si^{4+}/ P^{5+}), x is its oxidation state, and M is the metal ion (Mo^{6+}or W^{6+}) (Okuhara, 2002).

The acid strength of crystalline HPAs generally decreases in the following order: PW > SiW $\geq$ PMo > SiMo, which is identical to the dissociation constants presented in Table 2.5. Moreover, HPAs in solution are stronger than the usual mineral acids, such as H_2SO_4, HCl, and nitric acid (HNO_3) (Kozhevnikov, 1998). However, bulk HPAs exhibit low thermal stability, low surface area (1–10 m^2/g), and are highly soluble in polar media (water, short-chain alcohols, ketones, ethers or esters), which restricts their application as solid acid catalyst in esterification reaction. Thus, HPAs are often immobilized on strong supports such as metals and metal oxides to solve the problem of instability (Balaraju et al., 2010; Zhu et al., 2013).

Table 2.5: Dissociation constants of HPAs in Acetone at 25 $^{\circ}$C

HPAs	pK$_1$	pK$_2$	pK$_3$
H$_3$PW$_{12}$O$_{40}$	1.6	3.0	4.0
H$_4$PW$_{11}$VO$_{40}$	1.8	3.2	4.4
H$_4$SiW$_{12}$O$_{40}$	2.0	3.6	5.3
H$_3$PMo$_{12}$O$_{40}$	2.0	3.6	5.3
H$_4$SiMo$_{12}$O$_{40}$	2.1	3.9	5.9
H$_2$SO$_4$	6.6	-	-
HCl	4.3	-	-
HNO$_3$	9.4	-	-

The comparative study on catalytic-esterification of glycerol with OA between phosphotungstic acid supported on organic-tin catalyst (HPW/Cu$_3$(BTC))$_2$ and Sn-beta zeolite catalyst was performed by (L. Wee et al., 2013). It was found that Sn-beta zeolite suffers from poor performance (4 % conversion) and black product appearance. Quite the reverse, HPW/Cu$_3$(BTC)$_2$ showed better catalytic activity in the production of glycerol monooleate. Regrettably, HPW/Cu$_3$(BTC)$_2$ can be degraded by OA. Therefore, tert-butanol solvent was introduced for better process efficiency. This solvent esterification system produced 98 % of product selectivity, with total 40 % glycerol conversion at 150 $^{\circ}$C and 20 h operating conditions. This work revealed that microporous pore size of zeolite affects the reaction activity negatively in esterification of glycerol and OA.

2.5.5 Mesoporous silica

Mesoporous silica materials, such as MCM-41 and SBA-15, have attracted much attention as a catalyst support in heterogeneous catalysis owing to their high specific surface area (≥ 1000 m²/g), well-ordered mesoporous structure, and large pore sizes (2 nm $\leq$ size $\leq$ 20 nm) (Sánchez, Hernández, Moreno, Mondragón, & Fernández, 2011). Mesoporous ordered materials seem to be the most promising catalyst in chemical processes that involve bulky molecules. Figure 2.7 shows one of the possible preparation step of sulfonated silica, which was proposed by (Hasan, Yoon, & Jhung, 2014). The silica was prepared using tetraethyl orthosilicate (TEOS) precursor.
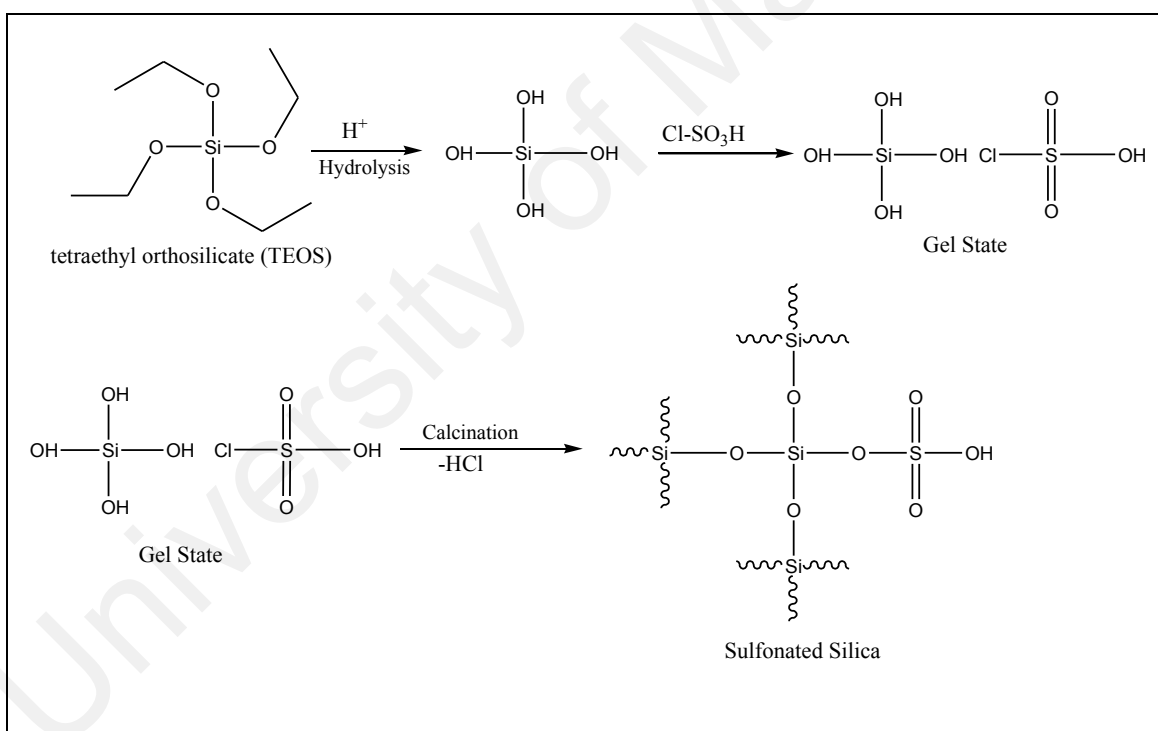
Figure 2.7: Preparation of sulfonated silica

(redrawn from the source of (Hasan et al., 2014))

2.5.5.1 Mobil Composition of Matter No. 41 (MCM-41)

The pore aperture of Mobil Composition of Matter No. 41 (MCM-41) is lying in the range of mesopores and exhibits hexagonal unidirectional channels along the *c* direction structure arrangement (Pérez-Pariente, Díaz, Mohino, & Sastre, 2003). MCM-41 anchored with different sulfonic acid groups was studied for esterification of glycerol with OA (Díaz et al., 2005). Chloromethyl, vinyl and methyl groups were incorporated with MCM-41 and it was revealed that incorporated methyl groups catalyst (HSO$_3$-methyl-MCM-41) had the highest catalytic activity due to the hydrophobic nature of pores surface. Moreover, the strength, nature and accessibility of MCM-41 were improved after the incorporation with methyl group. The conversion and selectivity of monoester for catalytic esterification of glycerol with OA was 90 % and 60 %, respectively, at reaction conditions of 120 $^{\circ}$C, 5 wt% catalyst, equimolar OA-to-glycerol ratio and 24 h reaction time.

2.5.5.2 Santa Barbara Amorphous (SBA)

The MCM-41 preparation work is complicated than SBA-15 as unstable nanoemulsions were formed during swelling agents dosing step (Galarneau et al., 2002). Therefore, SBA-12, SBA-15 and SBA-16 have been popularly investigated in the recent studies. The catalyst synthesis method for those silicates was relatively complicated. Table 2.6 demonstrates the textural properties of different blank silica catalyst support prepared by different structure directing, whereby TEOS was used as a precursor of silica.

Table 2.6: Textural properties of different mesoporous silica support

Catalyst support	Structure directing agent	Total surface area (m²/g)	Average pore diameter (nm)	Total pore volume (cm³/g)	References
SBA-12	Brij-76	672	5.4	0.64	(Kotwal, Kumar, & Darbha, 2013)
SBA-15	Pluronic P123	640	6.1	0.65	(Hoo & Abdullah, 2014)
SBA-16	Pluronic F127	800	3.6	0.67	(Kotwal et al., 2013)

Ti-SBA-12 and Ti-SBA-16 were compared towards esterification of glycerol with OA by (Kotwal et al., 2013). Brij-76 was used as a structure directing agent in the synthesis of Ti-SBA-12, whereas Ti-SBA-16 was prepared by Pluronic F127 block-copolymer. The results revealed that the conversion performance of Ti-SBA-16 was higher compared to Ti-SBA-12 due to the surface hydrophobicity of Ti-SBA-16. Surface hydrophobicity is important when glycerol is employed as starting material during esterification reaction. The polar nature glycerol can adhere on hydrophilic surfaces of catalyst which resulted in low activity. A similar statement was also prescribed by (Stephane Pariente, Tanchoux, & Fajula, 2009). The study concluded that hydrophobicity surface of the Ti-SBA-16 catalyst, Lewis acid Ti sites and mesoporosity structure of catalyst were ascribed to reaction activity. Consequently, 80.3 % conversion was obtained at catalyst content of 3 wt%, OA/glycerol molar ratio of 3, reaction temperature of 180 °C and 10 h reaction time.

(Hoo & Abdullah, 2014) studied the effect of loading amount of 12-tungstophosphorus acid (HPW) immobilized on SBA-15 material in esterification of

glycerol with short chain fatty acid, lauric acid. The ordered mesoporosity was observed in the pore system when 20 wt% of HPW was immobilized on SBA-15. Whereas, high HPW loading amount (30-40 wt%) resulted in the surface defects and encountered external deposition by HPW. Therefore, the study found that 20 wt% of HPW was the optimum immobilization amount. In this work, 70 % conversion and 50 % selectivity of mono-ester were obtained at 160 °C, 6 h, 2.5 wt% of catalyst and lauric acid to glycerol molar ratio of 1:4.

Aside from that, H_2SO_4 supported on silica was also studied by (Åkerman et al., 2011) in esterification of OA with polyols. 90 % conversion was achieved at reaction time of 24 h, 70 ^{o}C, 5 wt% SO_4^{2-}/silica catalyst and 3 OA/polyol molar ratio. The activity of Amberlyst 15 was compared under identical reaction conditions and slight increase of conversion (96 %) was observed. The activity of the Amberlyst 15 was correlated to its larger pore diameter (28.8 nm) although the acidity and specific surface area of SO_4^{2-}/silica catalyst (5.4 mequiv/g, 480 m^2/g) was much higher than Amberlyst 15 (4.7 mequiv/g, 42.5 m^2/g).

2.5.5.3 Silica-supported ionic liquid catalyst

A recent study on esterification of OA with glycerol over ionic liquid-silicotungstic acid-silica (STA-IL) catalyst was reported by (Wan N. R. W. Isahak et al., 2014). This STA-IL catalyst prepared by sol-gel method exhibits a reasonable surface area (88.36 m^2/g) and high acidity (63.5 mmol/g) due to the existence of nanoporous silica and silicotungstic acid. Ionic liquid of 1,2-dimethyl imidazolium tetrafluoroborate (DMIM·BF_4), was chosen in catalyst preparation due to its good behavior as reaction medium and phase transfer catalyst.

This study has shown the potential of ionic liquid as a promising medium in enhancing catalytic activity of esterification reaction. The insolubility of STA-IL in the product phase leads to an increase in reaction activity. The conversion of 96 % and selectivity of 90 % were attained at mild reaction conditions (100 $^{\circ}$C, molar ratio 1:6 of glycerol-to-OA, 7 wt% STA-IL for 9 h reaction). The temperature of reaction was operated at 100 $^{\circ}$C because higher temperature would shift the reaction equilibrium to more side products, prescribed by earlier work of (W. N. R. W. Isahak, Ismail, Nordin, Jahim, & Yarmo, 2011).

In brief, mesoporous ordered silica type catalysts have been popularly investigated by researchers as this material support offers an option to control pore size and pore diameter, which resulted in considerable activity and selectivity without facing pore-size limitation. (Stawicka, Trejda, & Ziolek, 2013) believed that mesoporous ordered silicate is a potential material for bulky reactant reaction process.

2.5.6 Double metal cyanide complexes (metal complex)

Double metal cyanide (DMC) is a low molecular weight complexing agent. The synthesis method for DMC catalyst is easy, where DMC precipitation is formed via mixing of metal salts and metal cyanide solution (Le-Khac, 1996). The formula for DMC catalyst is $M^1{}_a[M^2(CN)_b(A)_c]_d.$ $fM^1{}_gX_n.h(H_2O).eL$, where M^1 and M^2 can be different or identical (Grosch, Larbig, Lorenz, Junge, & Kammel, 2002). DMC exhibits micro-mesoporous structure which enables diffusion of molecules at interior pore (Sebastian & Srinivas, 2013).

The esterification of OA and glycerol over acidic solid Fe-Zn DMC complex was investigated by (Kotwal et al., 2011). The effect of catalyst preparation temperatures was studied which revealed that high-temperature prepared catalyst exhibits larger

surface area (50 °C, 165 m^2/g) than those prepared at room temperature (25 °C, 60 m^2/g). Moreover, the catalyst prepared at 50 °C demonstrated highest catalytic activity, with total conversion of 63.4 % and 67.3 % of GMO selectivity at 180 °C, 7 wt% of catalyst, 1:1 molar ratio of OA to glycerol and 8 h reaction time. They discovered that catalytic activity of Fe-Zn DMC relied heavily on acidity and surface area. In addition, Fe-Zn DMC was found to be very effective in the reaction although high polar glycerol was used due to the hydrophobic surface of DMC.

2.5.7 Hydrotalcite

Hydrotalcite is known as layered double hydroxide (LDH) and symbolized by $[M_{1-x}^{2+}M_x^{3+}(OH)_2]^{x+}X_{x/m}^{m-}\cdot nH_2O$. LDH is a complex layered material with ion-exchange capability and excellent biocompatibility. Therefore, LDHs have been widely employed in medicine, cosmetics and food industry (Choi, Oh, & Choy, 2008). Calcination of hydrotalcite material at 600 °C can transform the hydrotalcite into mixed Mg–Al oxides that consisted of Brønsted and Lewis acid and base sites. The thermal-treated hydrotalcite possesses acid-base property. For example, a sulphate modified Mg–Al hydrotalcite gave 0.0419 mmol/g acidity and 0.0018 mmol/g basicity. Therefore, calcined hydrotalcite is considered an acid-base catalyst with mild acidity (Kuśtrowski, Chmielarz, Bożek, Sawalha, & Roessner, 2004).

Complex Mg-Al-CO$_3$ LDH catalyst was selected by (Hamerski & Corazza, 2014) in esterification of lauric acid and glycerol and it was the first hydrotalcite material reported in esterification reaction. The intention of researchers for choosing Mg-Al-CO$_3$ LDH as catalyst was owing to its non-hazardous nature, as the produced mono- and di-ester are the emulsifiers that have been widely applied in food and cosmetic industries. Narrow pore size (11 nm) and larger surface area (106 m^2/g) of Mg-Al-CO$_3$ LDH was facilitated in the interaction between reagents and surface area during esterification. 99

% conversion and 90 % of mono- and dilaurine selectivity were obtained at operating temperature of 180 $^{\circ}$C, glycerol-to-lauric acid molar ratio (3:1) and 2 wt% of catalyst within 1 h reaction time.

2.5.8   Carbon-based acid catalyst

Mesoporous carbon has been actively studied as a catalyst support and/or acid-functionalized carbon for esterification reaction. The presence of surface oxide group in mesoporous carbon enables it to provide anchoring sites for active metals, which can tune the properties of carbon as a catalyst support material. Furthermore, the existence of unique properties, such as high thermal–mechanical stability with low metal leaching, as well as controllable textural and surface chemical properties, makes carbon a suitable catalyst support. Compared with mesoporous silica, mesoporous carbon is more resistant to structural changes caused by hydrolytic effects in aqueous environments. Acid-functionalized carbon, such as sulfonated-carbon via sulfonation by concentrated H_2SO_4 (formation of high density sulfonic acid group ($-SO_3H$)), has been extensively studied in esterification. Figure 2.8 shows the preparation of sulfonated carbon, (redrawn from the source (Konwar, Boro, & Deka, 2014; Okamura et al., 2006)).
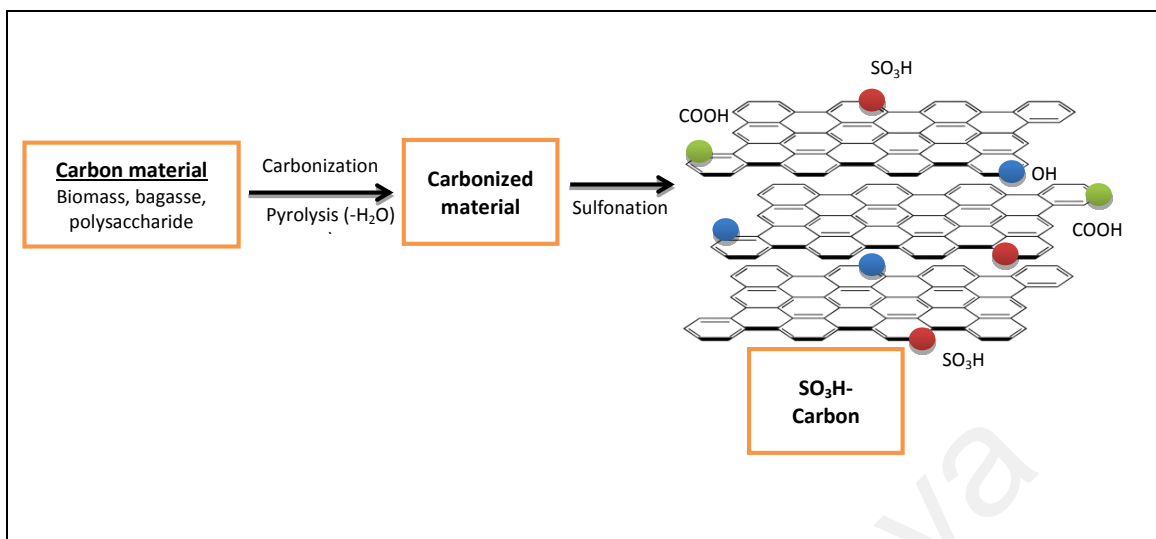
Figure 2.8: Preparation of SO₃H-carbon carbon

(redrawn from the source (Konwar et al., 2014; Okamura et al., 2006))

Esterification of glycerol with OA was recently investigated by (Konwar et al., 2016) in the presence of sulfonated mesoporous carbon catalyst (AC–SO₃H) at equimolar ratio of OA-to-glycerol, 5wt% catalyst concentration, temperature range from 100-150 $^{\circ}$C, and 7-24 h reaction time. The finding showed that the pore structure of catalyst (shape selectivity) and surface hydrophilicity affect product selectivity. The study concluded that conversion of 90 % and approximately 70 % of GMO selectivity (T= 150 $^{\circ}$C, 8 h reaction time and 5 wt% catalyst concentration, and equimolar ratio of glycerol and OA), were mainly influenced by acidic properties, pore structure of catalyst, and reaction temperature. Table 2.7 summarizes all the discussed acid heterogeneous catalysts for direct catalytic-esterification of glycerol with fatty acids (OA).

Table 2.7: Different heterogeneous acid catalysts for direct catalytic-esterification of glycerol with fatty acids (OA)

Catalysts	Feedstocks	Catalyst preparation method	Catalyst characterizations	Operating conditions	Performance	References
2.5.1 Ion-exchange resins						
Amberlyst 31	Glycerol; OA	Commercial available	Acidity= 4.8 mmeq/g Structure= gel Crosslinking degree= 4 %	T= 90 °C t= 24 h Gly:OA= 1:6 Catalyst= 7.4 wt%	C= 68% S_{GMO}= 17% S_{GDO}= 33%	(Pouilloux et al., 1999)
Amberlyst 16	Glycerol; OA	Commercial available	Acidity= 5.0 mmeq/g Structure= macroporous Crosslinking degree= 12% PD= 20 nm		C= 37% S_{GMO}= 83% S_{GDO}= 12%	

Table 2.7 continued

2.5.2 Metal oxides						
i. ZnO zinc oxide **ii. FeO** ferrous oxide **iii. SnO** stannous oxide	Glycerol; OA	The commercial available metal oxides were calcined at 550 °C for 5 h prior to use.	NA	T= 170 °C t= 6 h Gly:OA = 1:1 Catalyst= 0.8 wt%	C= 83.8%	(Dorin Bombos et al., 2010)
2.5.2.1 Sulfated zirconia						
SO_4^{2-}/ZrO_2 sulfated zirconia	Polyols; OA	<u>Sol-gel method preparation</u> Sulfated zirconia was prepared from zirconium propoxide $(Zr(OCH_2CH_2CH_3)_4)$ via one-step sol-gel method. 0.5 M H_2SO_4 was added dropwise to $Zr(OCH_2CH_2CH_3)_4$ for mixing of 6 h. <u>Drying</u> Solid was filtered, dried (100 °C) and calcined at 625 °C for 4 h.	Acidity = 0.614 mmol/g SSA= 80.4 m^2/g PV= 0.13 cm^3/g Sulfur content= 2.61 wt%	T= 140 °C t= 4 h Polyols/acid=1.2 Catalyst= 5.6 wt% Speed= 300 rpm	C= 83.5%	(Oh et al., 2013a)

Table 2.7 continued

2.5.2.1(a) Acid supported on zirconia						
PP/Zr zirconium phenyl phosphonate phosphite	Glycerol; OA	<u>Impregnation method</u> Phosphorous acid and phenyl phosphonic acid (3 molar ratio) were dissolved distilled water. Zirconium oxychloride ($ZrOCl_2 \cdot 8H_2O$) was added later and stirred until dryness at 90 °C. <u>Drying</u> The solid was recovering by water washing and dried overnight at 90 °C.	Acidity= 0.36 mmol/g SSA= 268 m^2/g	T= 180 °C t= 1 h Gly:OA = 1:4 Catalyst= 5 wt% of OA	C= 48.9% $S_{GDO+GTO}$= 92.3%	(Varhadi et al., 2013)
2.5.3 Zeolite						
Sn-beta zeolite	Glycerol; OA	NA	NA	T= 150 °C t= 20 h Gly:OA = 1:1 Catalyst=1 wt%	C= 4%	(L. Wee et al., 2013)

46

Table 2.7 continued

ZnO/zeolite Zinc oxide supported on zeolite	Glycerol; OA	<u>Hydrothermal impregnation precipitation</u> 1M solution of zinc nitrate was mixed with zeolite in a weight ratio of 1:3 (ZnO/zeolite). Urea (precipitating agent) was added to the mixture later. The mixture was stirred at 85 °C for 10 h in a autoclave. <u>Drying</u> The solid was filtered, dried (110 °C) for 14 h; it was calcined from 110 to 500 °C at a rate of 10 °C min^{-1} and was maintained at 500 °C for 3 h.	SSA= 327.71 m^2/g	T= 150 °C t= 6 h Gly:OA= 4:1 Catalyst= 2 wt%	C= 85% S_{GMO}= 70%	(Singh et al., 2013)
2.5.4 Heteropolyacids doped on tin framework						
HPW/Cu₃(BTC)₂ Tin-Organic Framework Catalyst	Glycerol; OA	<u>Hydrothermal preparation</u> $Cu_3(BTC)_2$ was encapsulated by Keggin phosphotungstic acid (HPW) and then mixed for 5 min. It was later heated to 110 °C under reflux condition for 24 h.. Solids were washed and dried at 60 °C in oven.	NA	T= 150 °C t= 20 h Gly:OA= 1:1 Catalyst= 1 wt% Reaction with tert-butanol solvent	C= 40 % S_{GMO}= 98%	(L. Wee et al., 2013)

Table 2.7 continued

2.5.5 Mesoporous silica						
MCM-41	Glycerol; OA	NA	Acidity= 0.89 mmeq/g	T= 150 °C Gly:OA= 1:1 t= 6 h	C= 88 %; S_{GMO}= 45%	(Díaz, Márquez-Alvarez, Mohino, Pérez-Pariente, & Sastre, 2000)
HSO$_3$-methyl-MCM-41	Glycerol; OA	<u>One-step hydrothermal synthesis</u> Mixture of organo-silane (VTES, ClTES or MTES) and TEOS was added to CTAB solution under continuous stirring. The produced gel is poured in autoclaves and heated at 95 °C for 24 h. <u>Drying</u> The solid was filtered, washed and dried at 65 °C for 24 h.	$T_{stability}$= 150 °C	T= 120 °C t= 24 h Gly:OA= 1:1 Catalyst= 5 wt%	C= 90 % S_{GMO}= 60%	(Díaz et al., 2005)

48

Table 2.7 continued

(i) silica- sulphuric acid **(ii) Amberlyst 15**	Polyols; OA	<u>One-step hydrothermal synthesis</u> Chlorosulfonic acid was added to silica gel (through constant flow dropping at room temperature and 30 min).	(i) Acidity= 5.4 mequiv./g SSA= 480 m^2/g PD= 6 nm PSD= 43-63 μm (ii) Acidity= 4.7 mequiv./g SSA= 42.5 m^2/g PD= 28.8 nm PSD= 300 μm	T= 70 °C t= 25 h OA: polyol= 3:1 Catalyst = 5 wt% Speed= 300 rpm	(i) C= 90% (ii) C= 96%	(Åkerman et al., 2011)
Ti-SBA-16 mesoporous titanosilicates (*more hydrophobic*)	Glycerol; OA	<u>Hydrothermal synthesis</u> Structure directing agent was dissolved in 2 M HCl solution stirred at 40 °C for 2 h. TEOS was then added drop-wise over 30 min and stirred for 4 h. The dissolved titanium iso-propoxide in isopropanol solution was added into mixture and stirred for 20 h. The material was treated thermally at 80 °C for 48 h. The solid was dried overnight at 100 °C and calcined in air at 550 °C for 8 h.	Acidity= 0.09 mmol/g SSA= 910 m^2/g PD= 3.8 nm PV= 0.86 cm^3/g PV_{meso}= 0.75 cm^3/g Si/Ti ratio= 50	T= 180 °C t= 3 h Gly:OA= 1:1 Catalyst= 3 wt% of OA	C= 72.8% S_{GMO}= 32.8% S_{GDO}= 57.9% S_{GTO}= 9.2%	(Kotwal et al., 2013)

Table 2.7 continued

Ti-SBA-12 mesoporous titanosilicates	Glycerol; OA	As above	Acidity= 0.12 mmol/g SSA= 460 m²/g PD= 5.5 nm PV= 0.64 cm³/g PV$_{meso}$= 0.62 cm³/g Si/Ti ratio= 40	Same as above (Ti-SBA-16)	C= 68% S$_{GMO}$= 52.9% S$_{GDO}$= 43.2% S$_{GTO}$= 3.9%	(Kotwal et al., 2013)
Ti-SBA-16			Same as above (Ti-SBA-16)	T= 180 °C t= 10 h Gly:OA = 1:3 Catalyst= 3 wt% of OA	C= 81.3 % S$_{GMO}$= 4.4% S$_{GDO}$= 51.3% S$_{GTO}$= 44.3%	
20 wt% HPW/SBA-15	Glycerol; Lauric acid	<u>Hydrothermal synthesis</u> Pluronic P123 was dissolved in HCl solution. HPW solution was then added into the polymer mixture drop-wise and kept under stirring at 60 °C for another 24 h. TEOS was added into the mixture under rapid stirring for 30 min then subjected to an aging at 80 °C under static condition (24 h).The solid was washed, dried and calcined in air at ramping temperature.	SSA= 368 m²/g PD= 4.5 nm PV= 0.2 cm³/g	T= 160 °C t= 6 h Gly:Lauric acid= 4:1 Catalyst= 2.5 wt%	C= 70 % S$_{GML}$= 50 %	(Hoo & Abdullah, 2014)

Table 2.7 continued

STA-SG silicotungstic acid -silica sol-gel	Glycerol; OA	<u>Sol-gel method</u> Water, 1-butanol, silicotungstic acid were added to tetraethyl orthosilicate (TEOS) 80 °C for 3 h. <u>Drying</u> The hydrogel was dehydrated at 80 °C for 1.5 h. It was extracted by Soxhlet method (methanol as a solvent) for 72 h and dried overnight at 100 °C.	SSA= 460 m^2/g	T= 100 °C t= 8 h Gly:OA = 1:6 Catalyst = 7 wt%	C= 94 % S_{GMO}= 95 %	(W. N. R. W. Isahak et al., 2011)
STA-IL silicotungstic acid-silica sol−gel ionic liquid template	Glycerol; OA	<u>Sol-gel method</u> Water, 1-butanol, silicotungstic acid, ionic liquid (DMIM·BF_4) were added to TEOS and stirred at 80 °C for 3 h. <u>Drying</u> The hydrogel was dehydrated at 80 °C for 1.5 h. It was extracted by Soxhlet method (methanol as a solvent) for 72 h and dried overnight at 100 °C.	Acidity= 63.5 mmol/g SSA= 88.36 m^2/g $T_{stability}$= 320 ^{o}C	T= 100 °C t= 9 h Gly:OA = 1:6 Catalyst = 7 wt%	C= 96 % S_{GMO}= 90 %	(Wan N. R. W. Isahak et al., 2014)

Table 2.7 continued

2.5.6 Double-metal cyanide (DMC)						
Fe–Zn DMC Fe–Zn double-metal cyanide (DMC) complex	Glycerol; OA	Precipitation method $K_4Fe(CN)_6 \cdot 3H_2O$ and $ZnCl_2$ were used as precursors while t-butanol was used as the complexing agent to prepare Fe-Zn DMC. The solids were filtered, washed with water and dried at 25 °C for several hours.	Acidity= 1.056 mmol/g SSA= 165 m^2/g PSD= 36.9 nm	T= 180 °C t= 8 h Gly:OA = 1:1 Catalyst= 7 wt% of OA	C= 63.4% S_{GMO}= 67.3% S_{GDO}= 31.7%	(Kotwal et al., 2011)
2.5.7 Hydrotalcite						
Mg–Al–CO₃ LDH layered double hydroxide	Glycerol; Lauric acid	Precipitation and hydrothermal synthesis Mixture DI water solution (contains $Mg(NO_3)_2 \cdot 6H_2O$ and $Al(NO_3)_3 \cdot 9H_2O$) was added dropwise into dissolved sodium carbonate solution. The precipitates were treated hydrothermally at 80 °C for 24 h. The solids were washed, filtered and dried at 80 °C for 48 h.	SSA= 106 m^2/g PV= 0.29 cm^3/g PD= 11 nm PSD= 1 to 50 μm Mesopores material	T= 180 °C t= 2 h Gly:Lauric acid= 1:3 Catalyst= 2 wt% Speed= 500 rpm	C= 99% $S_{GML+GDL}$= 90%	(Hamerski & Corazza, 2014)

Table 2.7 continued

2.5.8 Carbon-based acid catalyst						
AC–SO₃H	Glycerol; OA	<u>Sulfonation of activated carbon (AC)</u> Mesoporous AC was sulfonated with 4-benzenediazoniumsulfonate at 3-5 °C, in the presence of 120 mL aqueous H_3PO_2 (30–32%) solution as the reducing agent.	Acidity= 3.21 mmol/g SSA= 465 m²/g PV= 0.41 cm³/g PD= 4.7 nm $PV_{micropore}$= 0.22 cm³/g	T= 150 °C t= 8 h Gly:OA = 1:1 Catalyst= 5 wt%	C= 90% S_{GMO}= 70%	(Konwar et al., 2016)

2.6   Summary and proposition

The excess of glycerol produced from biodiesel production together with society's concerns on biodegradable resources have renewed the interests of researchers in catalytic esterification of glycerol. To date, direct-catalytic esterification of glycerol with OA to produce GMO, GDO and GTO is considered the more selective and cost-effective route compared to alkaline-glycerolysis of methyl oleate or GTO, as well as enzymatic glycerolysis process. Recent literature studies have indicated that mesoporous silica type catalysts are primarily investigated due to their ability in controlling pore size and diameter. This review revealed that catalyst surface structure and operating parameters play an important role in controlling the selectivity of products.

In terms of process parameters, the selectivity towards glycerol GMO and GDO is enhanced when using higher glycerol concentration, shorter reaction time and lower reaction temperature (1:4 molar ratio of oleic acid-to-glycerol; 3-6 h reaction time ; temperature < 180 °C). On the contrary, the formation of GTO can be achieved by increasing reaction time and operating temperature at higher oleic acid environment (3:1 molar ratio of OA-to-glycerol; reaction time > 10 h; temperature > 180 °C).

Overall, the hydrophobicity of the catalyst surface is one of the important criteria for developing reliable solid acid catalyst for water-sensitive esterification reaction. Aside from overcoming catalyst deactivation problem, hydrophobic catalyst could aid to minimize adhering of hydrophilic glycerol on catalyst surface. It has been shown that AC−SO$_3$H catalyst enabled highest conversion (90%) and GMO selectivity (70%) at mild operating conditions (T= 150 °C; t= 8 h; using equimolar glycerol-OA. Meanwhile, *sulfated zirconia (SO$_4^{2-}$/ZrO$_2$)* is found to be the most efficient catalyst in

GTO production (C= 83.5 %), mainly due to its tetragonal structural characteristic of zirconia phase, pore diameter and pore volume. Therefore, development of water-tolerant solid acid catalysts is investigated in this research in order to enhance water-sensitive esterification reaction rate and performance.

CHAPTER 3: METHODOLOGY

3.1   Catalyst preparations

Figure 3.1 shows the overall flow of the research activities for catalyst preparations, characterizations, and comparative catalytic activity studies. In this research, novel hydrophobic-enhanced catalyst (ZrO_2-SiO_2-Me&Et-$PhSO_3H$) preparation method was disclosed. In addition, three conventional SO_4^{2-}/ZrO_2 catalysts that synthesized from three different zirconium precursors were produced for catalyst structural correlation effect study.

All synthesized catalysts were characterized in order to study the relation between catalyst properties and conversion, esters yields and product selectivities. ZrO_2-SiO_2-Me&Et-$PhSO_3H$ catalysts with different hydrophobicity and acidity levels were first screened and then the most optimal designed catalyst was used to study the effects of process operating conditions. The last part of the experiments were devoted to the comparison of the performance of the best catalyst with three types of SO_4^{2-}/ZrO_2, Amberlyst 15 and Aquivion catalysts at the optimum conditions. The analytical methods to measure selectivities and yields of product are included herein.
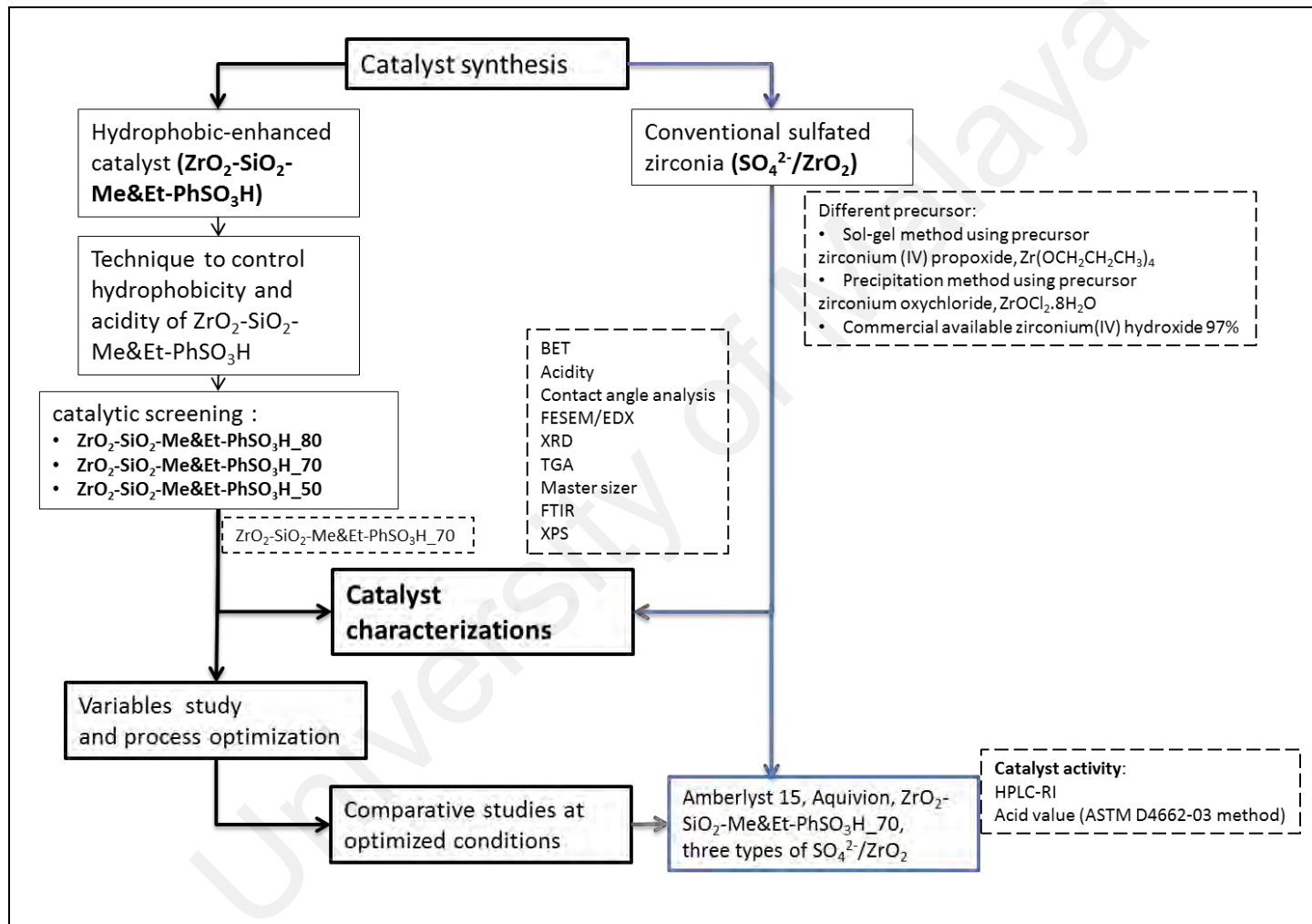
Figure 3.1: Schematic diagram of the catalyst preparations, characterizations and comparative catalytic activity studies

3.1.1 Preparation of hydrophobic-enhanced ZrO_2-SiO_2 catalyst

The coating of SiO_2 on ZrO_2 support was conducted using hydrolysis and co-condensation method. The commercial available zirconium hydroxide powder ($Zr(OH)_4$, 97% purity, Sigma-Aldrich) was first calcined at 625 ^{o}C for 4 h without any treatment, as it is a vital step to increase pore volume of ZrO_2 (Hongxia Zhao, Jiangang Chen, & Sun, 2003). 2 g of ZrO_2 powder was added into 100 ml of ethanol (99%, Sigma-Aldrich) under vigorous mixing condition at ambient temperature for 30 min. 12 ml of ammonia solution (NH_4OH, 25%, Sigma-Aldrich) and 4 ml of tetraethyl orthosilicate (TEOS, 98%, Sigma-Aldrich) were successively added slowly into the mixture. It can be observed that the clear solution gradually transformed to opaque because the addition of TEOS has generated white silica suspension environment. The resulted solution was continuously stirred for 24 h. The generated ZrO_2-SiO_2 powder was then filtered, rinsed with ethanol and dried overnight under vacuum at room temperature.

Modification of ZrO_2-SiO_2 surface to higher hydrophobicity level as well as functionalization of sulfonic acid group into ZrO_2-SiO_2 support was carried out using hydrophobic and surface initiating agents, known as trimethoxymethylsilane (TMMS, 98 %, Sigma-Aldrich) and 2-(4-chlorosulfonylphenyl)ethyltrimethoxysilane (CSPETS, 50% in dichloromethane, Fisher Scientific), respectively (Mobaraki et al., 2014). 0.2 g of CSPETS and 0.2 g of TMMS were added into 35 mL of dry toluene (99%, Sigma-Aldrich) that contained 1 g of SiO_2-ZrO_2. The mixture solution was continuously stirred for 24 h. The functionalized catalyst (ZrO_2-SiO_2-Me&Et-$PhSO_2Cl$) was then washed with toluene (2× 15 mL) and distilled water. Lastly, the modified solids were suspended in H_2SO_4 solution for 2 h (0.5 M, 5 ml). It was washed several times with water and dried overnight under vacuum at room temperature. The solid catalysts designed with

different TMMS amounts, ZrO_2-SiO_2-Me&Et-$PhSO_3H\_50$, ZrO_2-SiO_2-Me&Et-$PhSO_3H\_70$ and Me&Et-ZrO_2-SiO_2-Me&Et-$PhSO_3H\_80$ were produced and used for catalytic esterification reaction. The value of 80, 70 and 50 at the end of catalyst's symbol indicates the mol% of TMMS utilized in adjusting hydrophobicity level of the catalysts.

3.1.2 SO_4^{2-}/ZrO_2 catalyst prepared by using zirconium (IV) propoxide precursor

5 ml of zirconium (IV) propoxide, $Zr(OCH_2CH_2CH_3)_4$ (70 % in 1-propanol, Sigma-Aldrich) was first mixed with 6.6 ml of 1-propanol (99.7%, Sigma-Aldrich). Subsequently, 9.7 ml of 0.5 M aqueous H_2SO_4 was added dropwise into prepared mixed solution and stirred vigorously at ambient temperature for 6 h. The formed gels were filtered, dried (100 ^{o}C, overnight) and then calcined at temperature of 625 ^{o}C for 4 h.

3.1.3 SO_4^{2-}/ZrO_2 prepared by using zirconium oxychloride precursor

Zirconium oxychloride, $ZrOCl_2.8H_2O$ (99.5 %, Sigma-Aldrich) precursor was used to prepare SO_4^{2-}/ZrO_2 through precipitation method. At first, 21 ml of 1 M sodium hydroxide (NaOH) solution was added slowly into 5 ml of $ZrOCl_2.8H_2O$ under mild stirring at ambient temperature until the pH reached 8. The formed precipitates were washed thoroughly with distilled water, followed by filtration, and drying process at 100 ^{o}C (12 h). The $Zr(OH)_4$ (5.2 g) that had been prepared was mixed with 4.6 ml of 0.5 M H_2SO_4 at room temperature and stirred overnight. The final form SO_4^-/ZrO_2 was filtered, dried at 100 ^{o}C, and calcined at 625 ^{o}C for 4 h (Oh et al., 2013b).

3.1.4 SO_4^{2-}/ZrO_2 prepared by using commercial zirconia

The commercial available $Zr(OH)_4$ (5.2 g) from Sigma-Aldrich was mixed with 4.6 ml of 0.5 M H_2SO_4 at room temperature and stirred for overnight. Consequently, the SO_4^-/ZrO_2 catalyst was filtered, dried at 100 ^{o}C, and calcined at 625 ^{o}C for 4 h.

3.2 Catalyst characterizations

3.2.1 Brunauer, Emmett and Teller (BET)

N_2 physisorption measurement was performed using BELSORP-max analyzer (Japan) after the catalyst powders were outgassed under vacuum at 473 K for 5 h. The surface area of catalyst was calculated using Brunauer-Emmett-Teller (BET) method from the adsorption curve range at 0.04 to 0.2 relative pressures (P/P_o). While the pore size distribution curve was plotted using Barrett-Joyner-Halenda (BJH) desorption branch of isotherms, the average pore diameters were calculated according to the BJH method at 0.99 P/P_0.

3.2.2 Particle size distribution (PSD)

The particle size distribution of solid samples was measured by Malvern MS3000 particle sizer (dry) at pressure of 2 bars. The particle distribution size of the samples at each preparation step was measured.

3.2.3 Field Emission Scanning Electron Microscope (FESEM)

Field Emission Scanning Electron Microscope (FESEM) was performed on JSM-7100F to collect catalyst surface morphology at 1-30 kV acceleration voltage. The catalyst samples were degassed and coated with gold (Au) using Edwards Dirani S01 prior to EDX measurement.

3.2.4 Contact angle analysis

Hydrophobicity of the catalyst was measured by water contact angle method using KRUSS DSA100 instrument. The catalyst, in its powder form, was pressed in a pallet form using tablet press at 8 MPa prior to water angle measurement. Water was used as a solvent in the water contact angle measurement.

3.2.5 Acid-base titration

The acids exchange capacity of solid acid catalyst was determined by acid-base titration with 8.38×10^{-3} M NaOH solution (Chen et al., 2016). 40-50 mg of solid sample was degassed at 120 ^{o}C for 3 h. It was then suspended in 25 ml of NaCl (2 M) and stirred for 24 h at room temperature to reach equilibrium. The resulting suspension was titrated with NaOH solution and the acidity of acid solid catalyst was measured in mmol/g.

3.2.6 Fourier-transform infrared (FTIR)

Fourier-transform infrared (FTIR) spectra were obtained using Perkin Elmer, Spectrum BXII spectrometer in the range of 200-4000 cm^{-1}.

3.2.7 Thermogravimetric analysis (TGA)

Thermogravimetric analysis (TGA) techniques were performed to ascertain the thermal stability of the catalysts using Mettler Toledo system at a 10 ^{o}C/min rate to the maximum temperature of 900 ^{o}C.

3.2.8 X-ray photoelectron spectra (XPS)

X-ray photoelectron spectra (XPS) were performed using a Thermoscientific Kalpha device. The photoelectron emission spectra were recorded using Al–Kα radiation (hν = 1486.6 eV) from a monochromatized source. The X spot size was 400 μm. The pass energy was fixed at 30 eV for narrow scans (and 160 eV for the survey). Flood Gun was used for the charge effects measurement. The spectrometer energy was calibrated using Au $4f_{7/2}$ (83.9 ± 0.1 eV) and Cu $2p_{3/2}$ (932.8 ± 0.1 eV) photoelectron lines. XPS spectra were recorded in direct N(Ec). The background signal was removed using the Shirley method. The atomic concentrations were determined with an accuracy of 10% from photoelectron peak areas using the atomic sensitivity factors reported by Scofield,

taking into account the transmission function of the analyser. This function was calculated at different pass energies from Ag 3d and Ag MNN peaks collected for a silver reference sample, inside the system. The binding energy scale was established by referencing the C 1s value of adventitious carbon (284.7 ± 0.1 eV). The photoelectron peaks were analysed by Lorentzian/Gaussian (L/G = 30) peak fitting. The samples were analysed at about 5×10^{-9} Pa.

3.2.9 Powder X-ray diffraction (XRD)

The spectra were referenced with respect to the C 1s line at 284.5 eV. Powder X-ray diffraction (XRD) patterns were recorded using a Rigaku RINT 2000 X-ray diffractometer with Cu K$_\lambda$ radiation (λ = 1.54056 Å) over the 2Θ range from 10° to 80°.

3.3 Catalytic reaction and analysis of samples

The catalytic esterification reaction of glycerol ($\geq$ 99.5%, Sigma-Aldrich) with OA (90% technical grade, Sigma-Aldrich) was performed in a 250 ml batch reactor equipped with a thermometer to measure the temperature of the mixture; the reactor was connected to a condenser and a vacuum system to remove water during the reaction. The reaction was performed at 100 °C for 8 h using three catalysts designed with different hydrophobicity levels, ZrO$_2$-SiO$_2$-Me&Et-PhSO$_3$H_50, ZrO$_2$-SiO$_2$-Me&Et-PhSO$_3$H_70 and ZrO$_2$-SiO$_2$-Me&Et-PhSO$_3$H_80. During the running test, samples of 500 μL volume were withdrawn periodically and the samples were analysed by high performance liquid chromatography coupled to refractive index detection (HPLC-RI). The reliability of the procedure was confirmed by repeating the experiments at least twice. ZrO$_2$-SiO$_2$-Me&Et-PhSO$_3$H_70 catalyst was chosen as optimal catalyst for process variables study at temperature ranging from 100, 120, 140 to 160 °C, glycerol

to OA molar ratios (1:1, 2:1, 3:1, and 1:3), catalyst concentration with respect to mass of OA (3, 5 and 8 wt%) and different interval reaction times.

The separation and quantitative determination of the samples were conducted using HPLC-RI through an isocratic method, equipped with Gemini C18 11OA column (100 mm × 2 mm × 3 μm). All the analytical standard reagents such as GMO (≥ 99%), GDO (≥ 99%) and GTO (≥ 99%) were purchased from Sigma-Aldrich for qualitative and quantitative purpose. The analytical grade solvents such as acetonitrile (ACN), methanol (MeOH) and tetrahydrofuran (THF) which were purchased from Sigma-Aldrich were utilized as mobile phase while trifluoroacetic acid (TFA) was used as mobile phase additive due to its high resolving power. The OA and GMO groups of the sample were separated using a mobile phase consisted of ACN/water (80:20 v/v) with 0.1% TFA (v/v of total mobile phase). Meanwhile, GDO and GTO groups were separated using ACN/MeOH/THF (40:40:20 v/v/v) (Kathy Wai Yu, Christopher J. H., & Ben J., 2013). The injection volume was 10 μL and the diluted samples were eluted at a 220 μL/min flow rate. The column and RI detector temperatures were set at 40 °C.

The conversion, yield and selectivity of the products were calculated according to, Equation 3.1, 3.2 and 3.3, respectively using HPLC analysis. The conversion of OA was verified by using acid value determination according to ASTM D4662-03 method. The product mixtures were titrated by Metrohm auto-titrator with KOH-ethanol-solution (0.1 mol/L).

The conversion and yield were calculated according to the initial mole of OA instead of initial mole of glycerol is due to glycerol cannot be detected in the above-mentioned HPLC-RI analysis method. In addition, OA is the limiting reactant in optimization study. Therefore, initial mole of OA was used for conversion and yield calculation in

this study. The obtained chromatogram peaks for groups (OA and GMO) and (GDO and GTO) are presented in Appendix B.

$$\text{Conversion} = \frac{mol_{OA_{consumed}}}{mol_{OA_{initial}}} \times 100 \%$$ (3.1)

$$\text{Yield}_{total\ GMO,GDO,GTO} = \frac{mol_{total\ esters}}{mol_{OA_{initial}}} \times 100 \%$$ (3.2)

$$\text{Selectivity}_{GMO} = \frac{mol_{GMO}}{mol_{total\ GMO+GDO+GTO}} \times 100 \%$$ (3.3)

CHAPTER 4: RESULTS AND DISCUSSION

4.1   PART 1: Preparation and characterization of hydrophobic catalyst

In this part, the physicochemical and textural properties of the prepared hydrophobic ZrO_2–SiO_2 catalyst through four modification steps (ZrO_2, ZrO_2–SiO_2, ZrO_2–SiO_2–Me&Et–$PhSO_2Cl$ and ZrO_2–SiO_2–Me&Et–$PhSO_3H$) are presented and discussed. The novel technique used to control the acidity and hydrophobicity levels of the designed catalyst is described in this work. In addition, the effects of the loading amount of hydrophobic agent (TMMS) on the hydrophobicity level of the catalyst were investigated. Subsequently, the mechanism of catalyst formation was proposed on the basis of the comprehensive catalyst characterization results.

4.1.1   Physicochemical and textural properties of catalysts

N_2 physisorption was utilised to measure surface area, pore size distribution and porosity of the catalysts. Figure 4.1(a) shows the N_2 adsorption–desorption isotherm plots for ZrO_2 support. ZrO_2 showed a superposition of type IV isotherm with hysteresis loop at relative pressure range of 0.5–1.0. This result indicated that the pore size distributions are given by nonrigid aggregates of plate-like particles and mainly composed of mesoporous and minority of macroporous (Matthias et al., 2015). Results also confirmed that the ZrO_2 used in this study possessed meso–macropore pore sizes, with pore size ranging from 10.57 nm to 120 nm. The sintering process occurred at high calcination temperature, which resulted in the removal of OH^- from ZiO_2 and formation of large pore size for ZrO_2. The obtained result is similar to that reported by (Hongxia Zhao et al., 2003); they indicated that the surface area of a solid material decreases, and its average pore diameter increases with increased calcination temperature.

Figure 4.1(b) displays a sharp increase in the loading of the ZrO_2–SiO_2 catalyst at low values of P/P_0, which suggested a high surface. The presence of hysteresis type IV isotherm in this plot showed that the obtained pore size distribution was consistent, with small pore size within the mesoporous range. SiO_2 was mainly adsorbed on the inner wall and fitted inside the ZrO_2 support, which significantly reduced the average pore diameter of ZrO_2–SiO_2 from 120 nm to 3.71 nm. Therefore, the SiO_2 active species were well-deposited on the support, which was evidenced by its pore size distribution curve. The increased surface area of ZrO_2–SiO_2 can be explained by the adherence of new SiO_2 phase on the ZrO_2 support, which led to the formation of rough, heterogeneous and well-deposited small particles on the catalyst support.

The N_2 adsorption isotherms of the catalyst functionalised with TMMS and CSPETS, that is, ZrO_2–SiO_2–Me&Et–$PhSO_2Cl$, are presented in Figure 4.1(c). The obtained hysteresis plot of the ZrO_2–SiO_2–Me&Et–$PhSO_2Cl$ catalyst indicated a low-porosity adsorbent because the adsorbent–adsorbate interactions were relatively weak. Unlike the ZrO_2 support or ZrO_2–SiO_2, the average pore diameter for the ZrO_2–SiO_2– Me&Et–$PhSO_2Cl$ catalyst was determined using the NLDFT/GCMC method due to its incompatibility to the BJH model. Notably, the average pore diameter of the prepared catalyst in the 3rd step (ZrO_2–SiO_2–Me&Et–$PhSO_2Cl$, 2.24 nm) was slightly smaller than that of ZrO_2–SiO_2 (3.77 nm), which suggested the grafting of agents on the surface of ZrO_2–SiO_2. The TMMS–CSPETS hypothesis was proposed, and the functionalised ZrO_2–SiO_2 support was proven in this characterization analysis.

The acidification of functionalised catalyst (ZrO_2–SiO_2–Me&Et–$PhSO_3H$) exhibited hysteresis loop at a relative pressure range of 0.3–0.8, as shown in Figure 4.1(d). The hysteresis loop of the ZrO_2–SiO_2–Me&Et–$PhSO_3H$ catalyst ranged between those of

ZrO$_2$–SiO$_2$–Me&Et–PhSO$_2$Cl and ZrO$_2$–SiO$_2$. This result indicated that sulphonation removed some of the agents of ZrO$_2$–SiO$_2$–Me&Et–PhSO$_2$Cl. Comparison of the hysteresis curve and pore diameter plot of ZrO$_2$–SiO$_2$–Me&Et–PhSO$_3$H to ZrO$_2$–SiO$_2$ hysteresis loop (Figure 4.1(b)) confirmed that ZrO$_2$–SiO$_2$–Me&Et–PhSO$_3$H is a mesoporous catalyst.
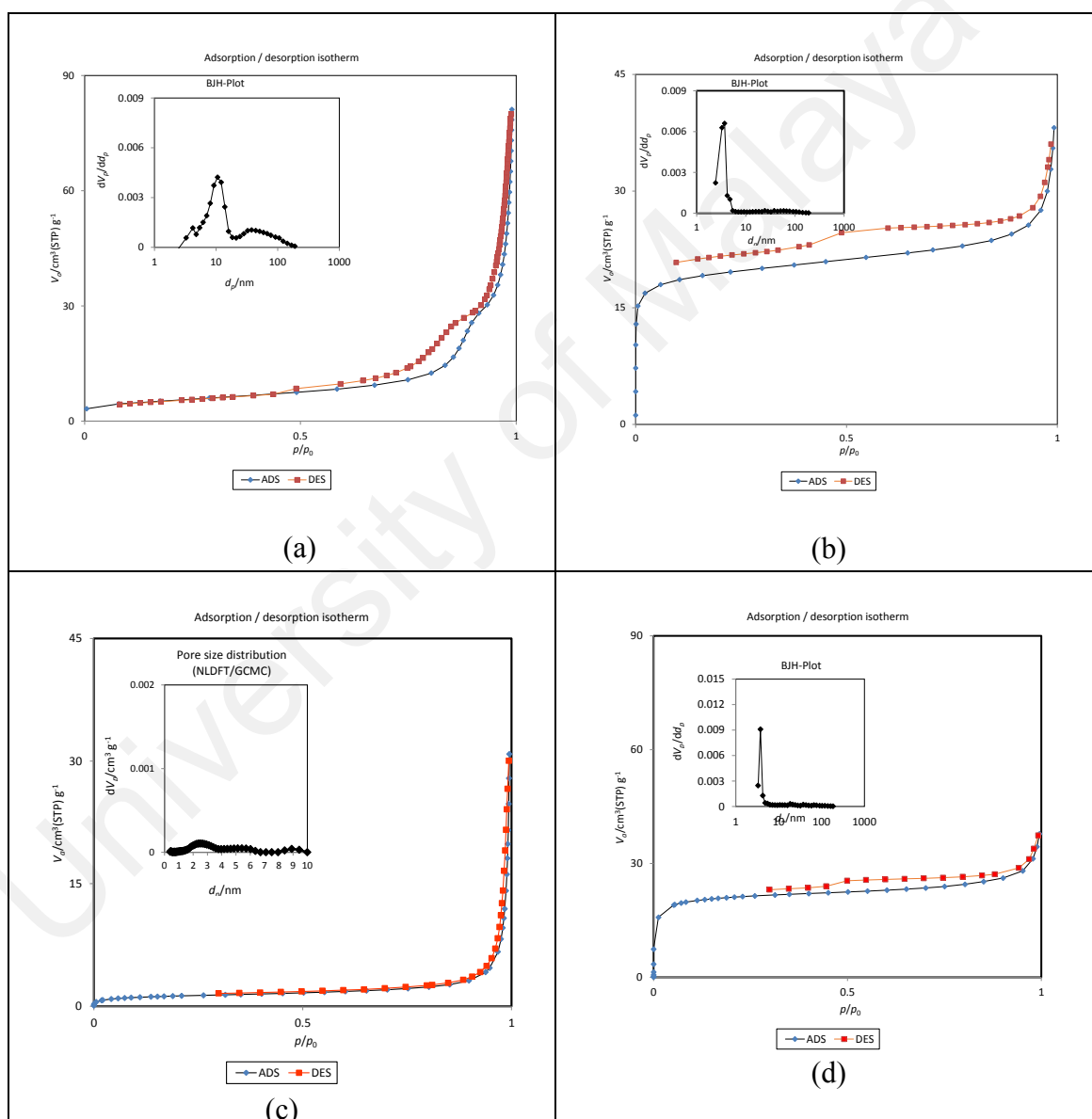
Figure 4.1: N$_2$ adsorption–desorption isotherms and BJH plots for ZrO$_2$ (a), ZrO$_2$–SiO$_2$ (b), ZrO$_2$–SiO$_2$–Me&Et–PhSO$_2$Cl (c) and ZrO$_2$–SiO$_2$–Me&Et–PhSO$_3$H (d)

4.1.1.1 Particle size distribution

The particle size distribution curves of the catalysts prepared at four different modification steps are shown in Figure 4.2. Results revealed that coating the ZrO_2 support with SiO_2 altered the particle size distribution range from a broad wide range to a narrow range and bell shaped distribution. This result may be attributed to the incorporation of Si atom into the Zr support. Nevertheless, this work indicated that functionalization of hydrophobic agent and sulphonation process exerted no effect on the particle size distribution of the catalysts. Moreover, the particle size distributions of ZrO_2–SiO_2, ZrO_2–SiO2–Me&Et-$PhSO_2Cl$ and ZrO_2–SiO_2–Me&Et–$PhSO_3H$ were identical.
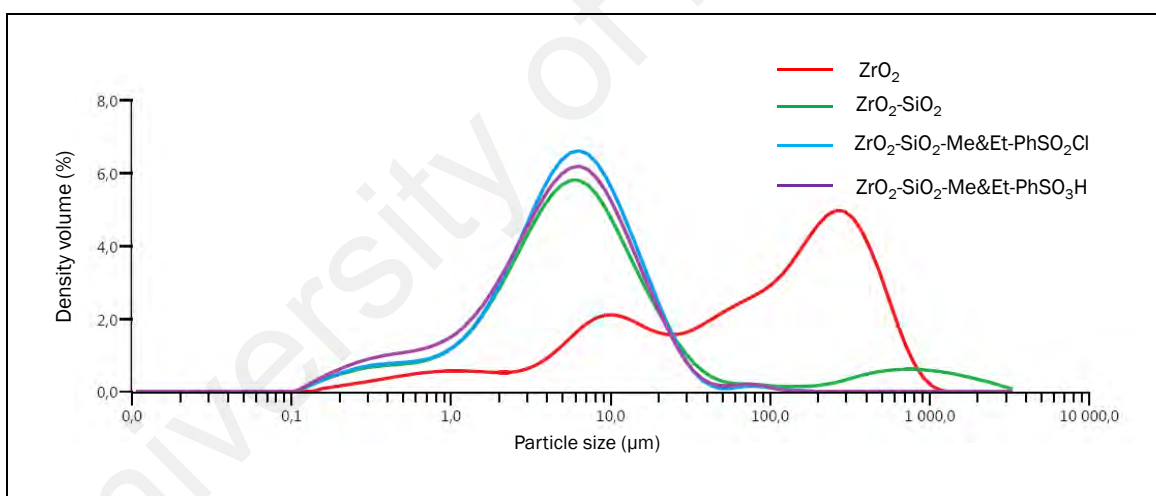
Figure 4.2: Particle size distribution curves for ZrO_2, ZrO_2–SiO_2, ZrO_2–SiO_2–Me&Et–$PhSO_2Cl$ and ZrO_2–SiO_2–Me&Et–$PhSO_3H$

4.1.1.2 Acidity

The catalyst acidity at four different modification steps was measured. Table 4.1 summarises the physicochemical and textural properties of the functionalised catalyst in each modification step. The original ZrO_2 showed low acidity value (0.18 mmol/g) because ZrO_2 is naturally a Brønsted base. Notably, the silication step reduced the ZrO_2 acidity from 0.18 mmol/g to 0.00 mmol/g. This effect can be explained by the fact that the NH_4OH used to catalyse the hydrolysis and condensation reaction in the silication step changed the surface acidity of original ZrO_2 due to neutralization and silicate coating. The zero acidity of SiO_2–ZrO_2 indicates that SiO_2 was well-coated on the ZrO_2 support. The acidity of the 3rd step-prepared SiO_2–Me&Et–$PhSO_2Cl$ catalyst was 0.16 mmol/g. The acidity of the ZrO_2–SiO_2–Me&Et–$PhSO_3H$ catalyst was increased to 0.62 mmol/g after the acidification step.

Table 4.1: Physicochemical property of functionalised catalysts in each modification step

Catalysts	Specific surface area [a] (m^2/g)	Pore volume [b] (cm^3/g)	Average pore diameter [b] (nm)	Average particle diameter [c] (μm)	Acidity (mmol/g)
ZrO_2	18.77	0.126	10.70-120	100	0.18
ZrO_2-SiO_2	73.05	0.0296	3.77	5.87	0.00
ZrO_2-SiO_2-Me&Et-$PhSO_2Cl$ [d]	-	0.0316	2.24	5.39	0.16
ZrO_2-SiO_2-Me&Et-$PhSO_3H$	79.75	0.0247	3.77	5.01	0.62

[a] Total surface area was determined using BET equation; [b] pore volume and average pore diameter were determined using BJH method; [c] particle diameter was measured by mastersizer; [d] pore volume and average pore diameter were determined using NLDFT/GCMC method.

4.1.2   Surface morphology characterization

4.1.2.1   Field emission scanning electron microscope (FESEM)

Images of the different development stages of the catalyst captured by using high-resolution FESEM are displayed in Figure 4.3. ZrO_2 presented typical rough, meso–macropore space and irregular surface morphology (Figure 4.3(a)). The uneven ZrO_2 surface can be associated with material sintering during drying and calcination processes. Nevertheless, the presence of silica-like-substance on ZrO_2 support was supported by the latter modified ZrO_2–SiO_2 (Figure 4.3(b)). The hydrolysis and condensation processes used in the silica coating in this work were according to the modified Stöber method. The base-catalysed hydrolysis and successive condensation of TEOS result in the formation of monodispersed spherical silica particle (Rahman & Padavettan, 2012). The spherical shape particles evolve when the chemical bond and Van der Waals forces generate elastic and plastic deformations between two oligomers; eventually, two oligomers engulf each other to maintain the spherical shape (X.-D. Wang et al., 2010).

The addition of both TMMS and CSPETS agents resulted in no modification on the surface morphology of ZrO_2–SiO_2–Me&Et–$PhSO_2Cl$. However, smearing of the silica-like-substance was observed (Figure 4.3(c)). ZrO_2–SiO_2–Me&Et–$PhSO_3H$ catalyst (Figure 4.3(d)) significantly displayed uniform and smooth spherical particles with consistent sizes. The pore diameter of a single silica sphere was approximately 400 nm. The overnight aging in the silication process and washing of ZrO_2–SiO_2 using excessively ethanol hence produce porosity-type particles; as the hydrolysis of alkoxy groups, condensation and re-esterification of silanol groups upon re-immersion in ethanol result in the formation of micro–mesoporous silica (Bazuła et al., 2014). Thus, the morphology images are correlated with the aforementioned BET results.
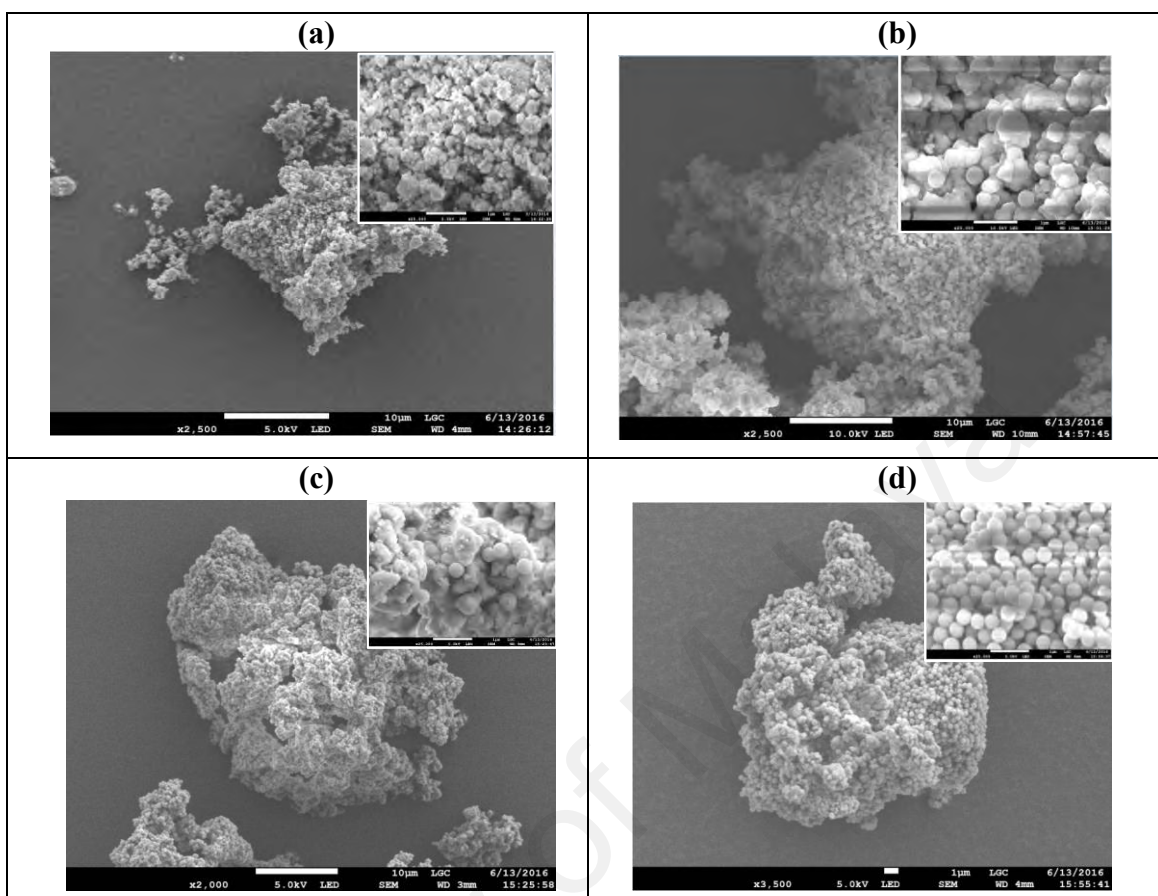
Figure 4.3: FESEM morphologies of ZrO₂ (a), ZrO₂–SiO₂ (b), ZrO₂–SiO₂–Me&Et–PhSO₂Cl (c) and ZrO₂–SiO₂–Me&Et–PhSO₃H (d)

4.1.3 Hydrophobicity measurement

4.1.3.1 Contact angle analysis

The hydrophobicity of the developed catalyst should be measured when developing highly hydrophobic and heterogeneous acid catalyst. The hydrophobicity level of each developed catalyst was determined by contact angle measurements. The results are presented in Figure 4.4. The water contact angle of the catalysts was increased in the order of ZrO₂–SiO₂–Me&Et–PhSO₃H > ZrO₂–SiO₂–Me&Et–PhSO₂Cl > ZrO₂–SiO₂ > ZrO₂. Noticeably, the lowest hydrophobicity was shown by the original ZrO₂ support. Hydrophobicity was enhanced through coating ZrO₂ support with SiO₂; this effect was

attributed to that the siliceous material improved the hydrophobic environment because Si atom can increase the hydrophobicity of a compound. With the addition of hydrophobic organosilica moiety, TMMS considerably increased the hydrophobicity of the catalyst surface. Superhydrophobic film chemical sensor and hydrophobic polyester fabrics are successfully constructed by TMMS (Li, Li, Dong, & Zhang, 2016). As expected the presence of methyl groups on the silica surface caused the decrease in surface hydrophilicity. The hydrophobicity of the ZrO_2–SiO_2–Me&Et–$PhSO_3H$ catalyst was also slightly improved with the incorporation of sulphonic acid groups.
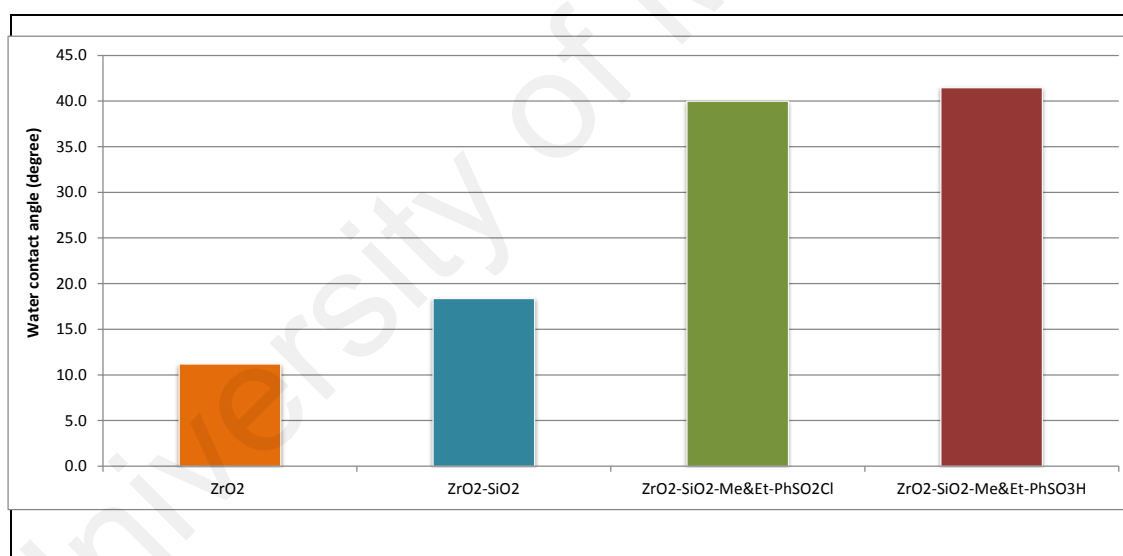
Figure 4.4: Hydrophobicity levels of ZrO_2, ZrO_2–SiO_2, ZrO_2–SiO_2–Me&EtPhSO_2Cl and ZrO_2–SiO_2–Me&Et–$PhSO_3H$ based on water contact angle analysis

4.1.4 Thermal stability analysis

4.1.4.1 Thermal gravimetric analysis (TGA)

The TGA curves of ZrO_2, ZrO_2–SiO_2, ZrO_2–SiO_2–Me&Et–$PhSO_2Cl$ and ZrO_2–SiO_2–Me&Et–$PhSO_3H$ are shown in Figure 4.5. A weight loss occurred in the ZrO_2–SiO_2–Me&Et–$PhSO_3H$ catalyst at a temperature range of 260 °C–300 °C. This weight loss was 4 wt% in ZrO_2–SiO_2–Me&Et–$PhSO_3H$ compared with the 3rd step-prepared ZrO_2–SiO_2–Me&Et–$PhSO_2Cl$, which indicated the decomposition of sulphate moiety (Fang et al., 2015). The second weight loss zone was observed at 560 °C–570 °C for ZrO_2–SiO_2, ZrO_2–SiO_2–Me&Et–$PhSO_2Cl$ and ZrO_2–SiO_2–Me&Et–$PhSO_3H$; this loss was attributed to the decomposition of SiO_2 material (Estevez et al., 2016). These weight losses were significant, especially for functionalised ZrO_2–SiO_2–Me&Et–$PhSO_2Cl$ and ZrO_2–SiO_2–Me&Et–$PhSO_3H$. TGA analysis showed that ZrO_2 support possessed good thermal stability. Therefore, the catalytic reaction is within the thermal stability range of catalyst for the reaction temperature of approximately 250 °C.
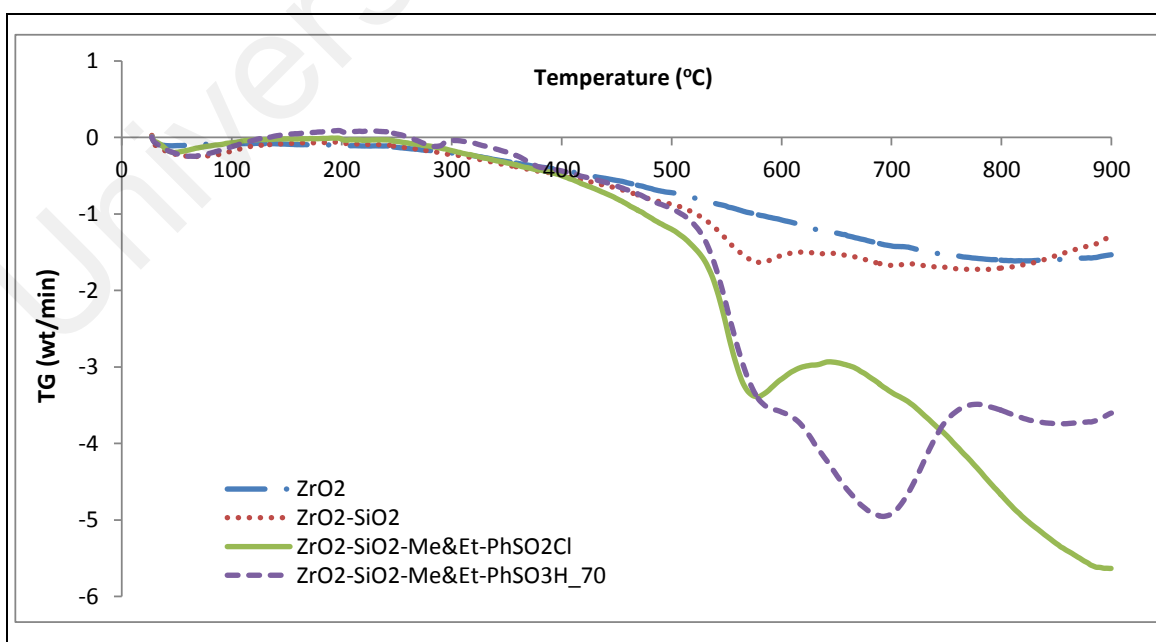
Figure 4.5: TGA curves for ZrO_2 (a), ZrO_2–SiO_2 (b), ZrO_2–SiO_2–Me&Et–$PhSO_2Cl$ (c) and ZrO_2–SiO_2–Me&Et–$PhSO_3H$ (d) on the basis of the weight loss rate

4.1.5 Chemical surface analysis

4.1.5.1 Fourier transform infrared spectroscopy (FT-IR)

The FT-IR spectra of the ZrO_2–SiO_2 catalyst are shown in Figure 4.6 and they provided evidence for the formation of SiO_2 (red spectra). The significant bands at 1061 and 576 cm^{-1} are assigned to the Si–O–Si asymmetric stretching vibrations (Chen et al., 2016; Saravanan, Tyagi, & Bajaj, 2016). Nonetheless, these bands did not appear at the spectra of blank ZrO_2. The band at 1061 cm^{-1} was attributed to the asymmetric stretching vibrations, such as those of Si–O and Si–O–Zr. The bands at approximately 791 and 730 cm^{-1} are associated with the formation of a condensed silica network (Faria et al., 2009; P. Wang, Liu, Niu, Li, & Ma, 2014). The band located around 950 cm^{-1} is given by the stretching vibrations of the Si–O bond (Faria et al., 2009). The FTIR results confirmed the successful coating of SiO_2.
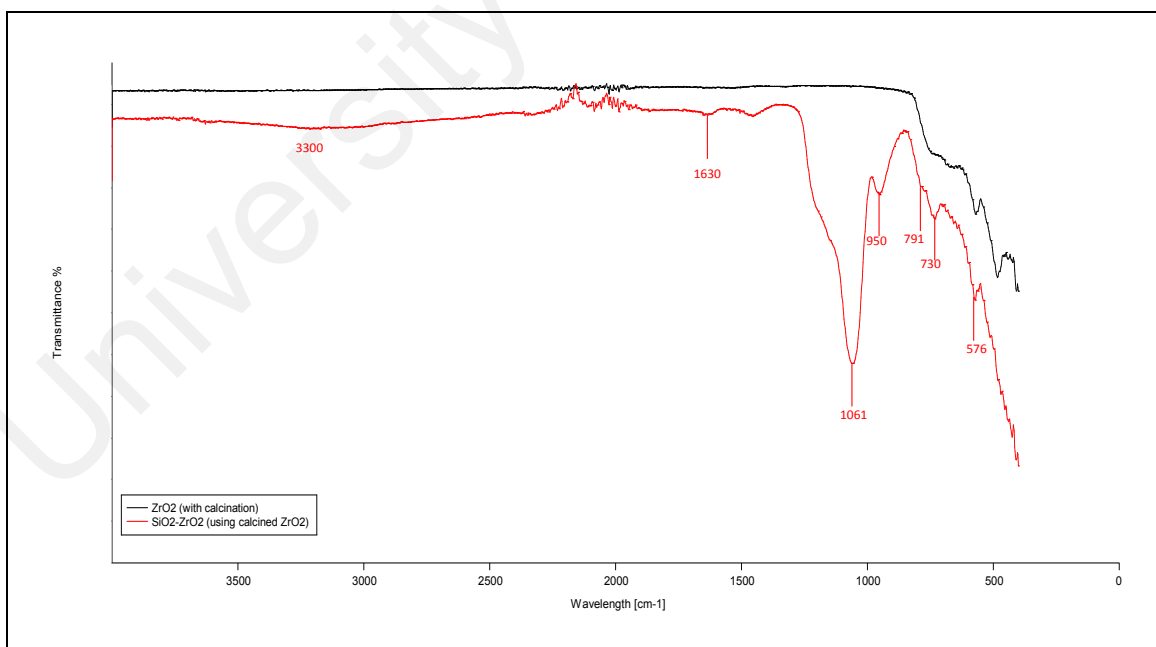
Figure 4.6: Fourier transform infrared spectroscopy (FT-IR) spectrum of ZrO_2–SiO_2 (black: ZrO_2 vs red: ZrO_2–SiO_2)

4.1.5.2 Energy-dispersive X-ray spectroscopy (EDX) analysis

EDX analysis was performed to identify the surface composition change in each modification step of the catalyst. As shown in Figure 4.7(a), ZrO_2 support displayed Zr and O peaks, with averaged mass percentages of 74.2% Zr and 25.8% O. In ZrO_2–SiO_2, the silica-coated ZrO_2 consisted of additional Si peak, as shown in Figure 4.7(b). The averaged mass percentages of Zr, O and Si are 42.7%, 42.8% and 14.5%, respectively. The increase in the O compound was in agreement with the adherence of SiO_2 to the support.

The surface composition of ZrO_2–SiO_2–Me&Et–$PhSO_2Cl$ and ZrO_2–SiO_2–Me&Et–$PhSO_3H$ showed no significant change. The averaged surface composition of ZrO_2–SiO_2–Me&Et–$PhSO_2Cl$ comprised 39.77% Zr, 42.2% O and 18.06% Si (Figure 4.7(c)). The Si content of ZrO_2–SiO_2–Me&Et–$PhSO_2Cl$ was 3.5% higher than that of ZrO_2–SiO_2. The discrepancy may be attributed to the ZrO_2–SiO_2 functionalised with TMMS and CSPETS. The ZrO_2–SiO_2–Me&Et–$PhSO_3H$ peaks with 44.7% Zr, 38.9% O and 16.4% Si are presented in Figure 4.7(d). The sulphonated surface of the ZrO_2–SiO_2–Me&Et–$PhSO_3H$ catalyst showed 1.66% lesser Si content than that of ZrO_2–SiO_2Me&Et–$PhSO_2Cl$.
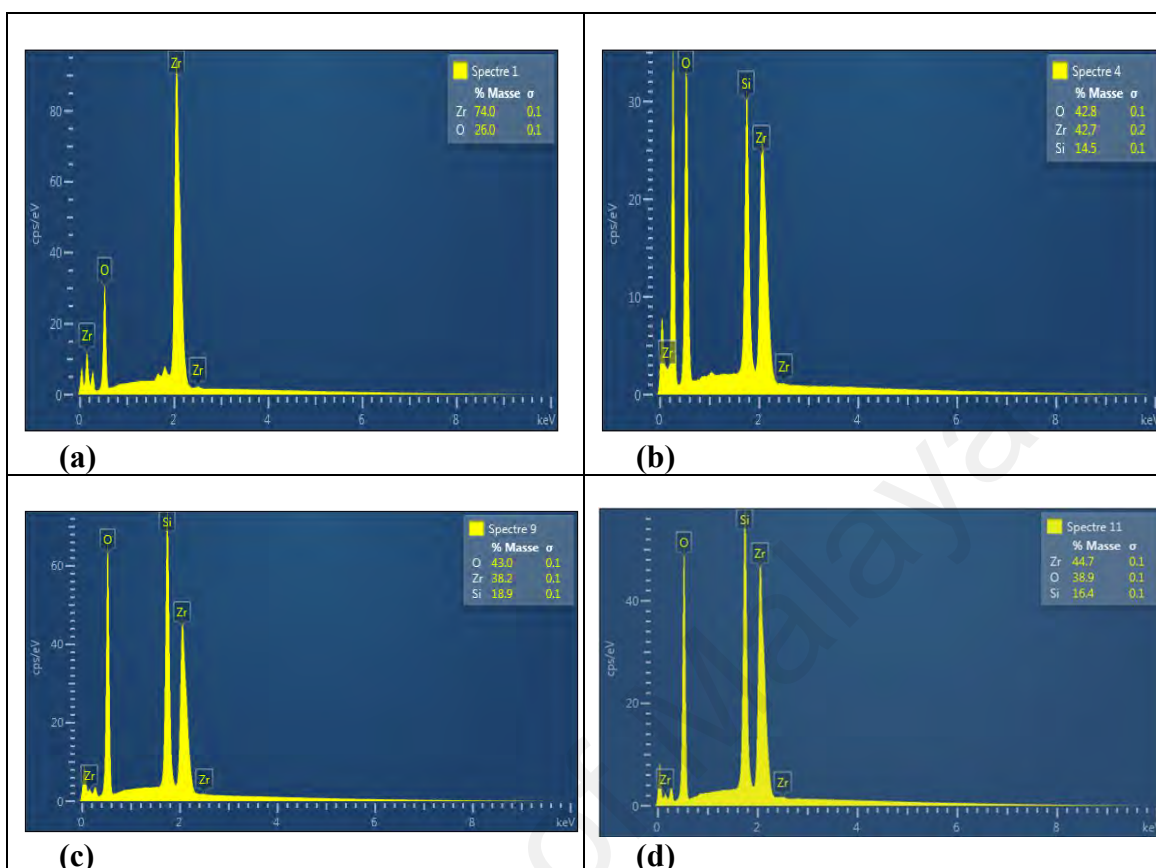
Figure 4.7: Energy-dispersive X-ray spectroscopy peaks of ZrO$_2$ (a), ZrO$_2$–SiO$_2$ (b), ZrO$_2$–SiO$_2$–Me&Et–PhSO$_2$Cl (c) and ZrO$_2$–SiO$_2$–Me&Et–PhSO$_3$H (d)

4.1.5.3 X-ray photoelectron spectroscopy (XPS)

XPS allows further insight analysis on the surface composition of each catalyst. Different from FTIR spectra, majority of the bands cannot be well distinguished in different composites due to the presence of broad and overlapping bands of silica with the sulphonated group. Therefore, the surface composition of each modified catalyst was investigated using XPS, and results are presented in Figure 4.8.

The binding energy in the interval ranged of 178–188 eV (Figure 4.8(a)) indicated that the ZrO$_2$ material belonged to Zr–O (182 and 185 ± 0.1 eV), Zr–Ox or Zr–OH groups (181 and 184 ± 0.1eV). In the ZrO$_2$–SiO$_2$ support (Figure 4.8(b)), the mainly

detected compound appeared at the peak corresponding to the interval of 530 –537 eV, which was attributed to the presence of SiO_2. The large peak at 533.1 ± 0.1 eV suggested a high-majority ratio mixture of SiO_2 with two different environments: Si–O–Si (at 533.0 ± 0.1 eV) and Si–O–Zr (at 531.0 ± 0.1 eV) (Rodríguez-Castellón et al., 2003). Moreover, different composites were observed for ZrO_2–SiO_2 support at a broad peak ranging from 100 eV to 105 eV. This result can be attributed to the presence of $Si(-O)_4$ species (103.7 ± 0.1 eV) and Si–O–Zr units (102.8 ± 0.1 eV).

As shown in (Figure 4.8(c)), the peak in the area ranging from 160 eV to 170 eV was assigned to C–SH (163–164 ± 0.1 eV), C–$S(O)_2$–Cl (168–169 ± 0.1 eV) and sulphate groups (168.5 ± 0.1 eV). This result can be attributed to the functionalised CSPETS and TMMS agents for ZrO_2–SiO_2–Me&Et–$PhSO_2Cl$. Nevertheless, in correspondence to the peak at 160–170 eV, limited percentage of the sulphonic group (silica composites of the SO_3H group) was detected at 168.5 ± 0.1 eV for ZrO_2–SiO_2–Me&Et–$PhSO_3H$ (Figure 4.8(d)) (Fang et al., 2015). This result may be obtained because the detection limit of XPS (approximately 10 nm) was inaccessible to a single mesoporous–monosphere particle with an approximate diameter of 400 nm. These results suggested that the sulphonic acid sites for the ZrO_2–SiO_2–Me&Et–$PhSO_3H$ catalyst were mainly distributed in the nanosphere pores. The sulphonic acid groups diffused into the mesopore of the silica shell during treatment. This finding is similar to that of the previous work, which reported that most of the acidic sites for silica-prepared catalysts are buried in the bulk polymer beads (Chen et al., 2016).
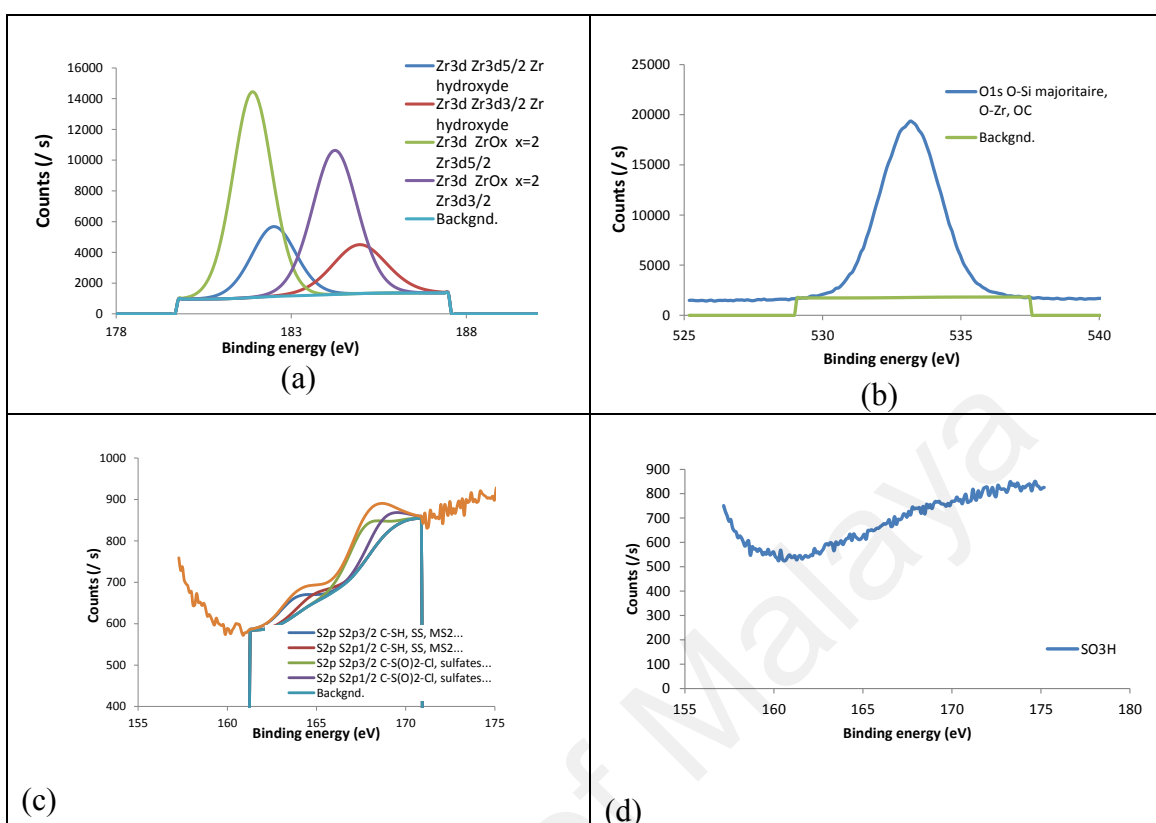
Figure 4.8: X-ray photoelectron spectroscopy spectra for ZrO_2 (a), ZrO_2–SiO_2 (b), ZrO_2–SiO_2–Me&Et–$PhSO_2Cl$ (c) and ZrO_2–SiO_2–Me&Et–$PhSO_3H$ (d)

4.1.6 Structural characterization

4.1.6.1 X-ray powder diffraction (XRD)

The catalyst crystallite structure can be measured by using XRD. Figure 4.9 shows the XRD patterns of catalyst in four different modification steps. The amorphous nature of ZrO_2 was transformed to relatively crystalline character during the calcination of monoclinic (M) and tetragonal (T) phase diffraction (Figure 4.9(a)). The main diffraction in the profile appeared at approximately 16°, 26°, 28°, 32°, 42°, 46°, 54° and 56° and corresponded to the stable M phase. Minor distribution of the metastable T phase is also observed at 2θ ca. 30°, 35°, 50° and 60° diffraction (Alcañiz-Monge, Bakkali, Trautwein, & Reinoso, 2018). The crystallinity structures at four different

78

modification steps (ZrO_2, ZrO_2–SiO_2, ZrO_2–SiO_2–Me&Et–$PhSO_2Cl$ and ZrO_2–SiO_2–Me&Et–$PhSO_3H$) were almost identical. Loading of ZrO_2–SiO_2 with TMMS and CSPETS caused no improvement on the crystallinity of the catalyst. Nevertheless, the intensity of ZrO_2–SiO_2–Me&Et–$PhSO_3H$ was slightly sharpened at 28° after sulphonation (Figure 4.9 (b)).
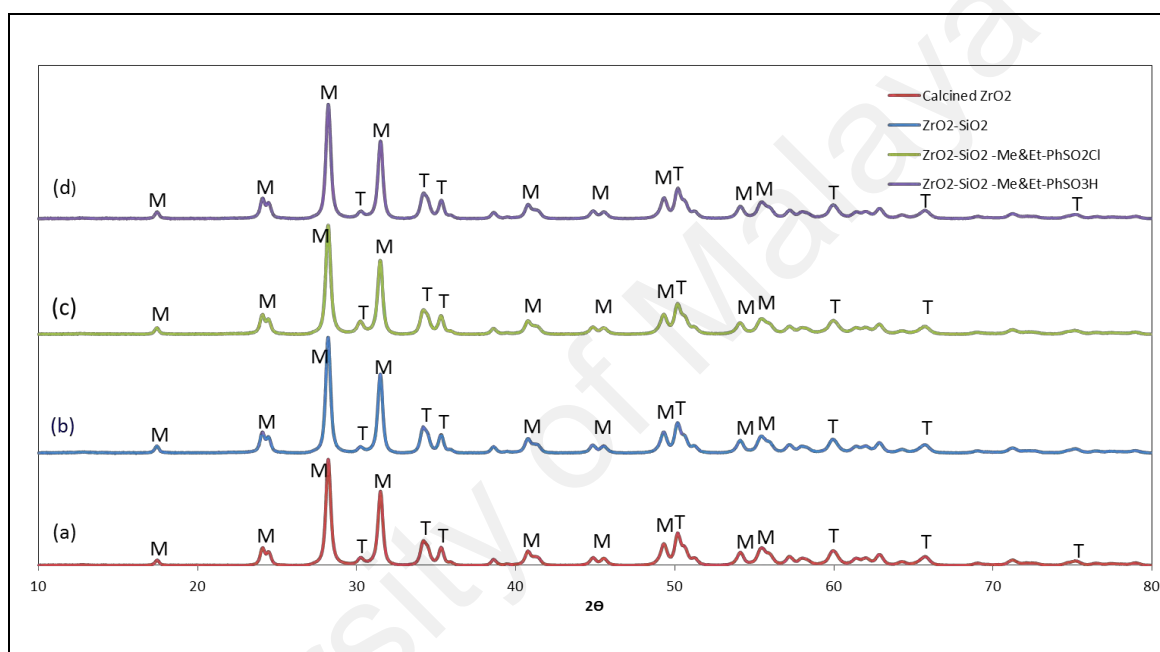
Figure 4.9: X-ray diffraction (XRD) profiles of ZrO_2 (a), ZrO_2–SiO_2 (b), ZrO_2–SiO_2–Me&Et–$PhSO_2Cl$ (c) and ZrO_2–SiO_2–Me&Et–$PhSO_3H$ (d)

4.2   PART 2: Control of the hydrophobicity and acidity of the catalyst

This part investigated the effect of the loading amount of TMMS-CSPETS on ZrO_2-SiO_2 support towards the hydrophobicity level of the catalyst. The total loading amount of both activation agents, which was expressed as the molar ratio of TMMS-CSPETS to ZrO_2-SiO_2, was optimised in the presence of a constant concentration of TMMS (80 mol%) to obtain the most suitable hydrophobicity level of the catalyst. Subsequently, the optimised ratio of CSPETS-TMMS to ZrO_2-SiO_2 was used to adjust the ratio of TMMS hydrophobic agent in mol%. Solid catalysts designed with different TMMS amounts, namely, ZrO_2-SiO_2-Me&Et-$PhSO_3H$_50, ZrO_2-SiO_2-Me&Et-$PhSO_3H$_70 and ZrO_2-SiO_2-Me&Et-$PhSO_3H$_80, were produced and applied in catalytic activity screening. The values of 80, 70 and 50 at the end of the catalysts' symbols indicate the mol% of TMMS utilised in adjusting the hydrophobicity level of the catalyst.

4.2.1   Effects of the loading amount of TMMS-CSPETS on the catalyst hydrophobicity

Table 4.2 presents the loading amounts of CSPETS and TMMS on ZrO_2-SiO_2. The effects of the amount of functionalisation agents (TMMS-CSPETS) must be investigated to obtain the highest possible hydrophobicity level of the designed catalyst. The molar ratio of activation agents to the ZrO_2-SiO_2 support was initially optimised at a constant concentration (80 mol%) of TMMS. Afterwards, the suitable CSPETS:TMMS ratio was optimised to obtain the most suitable catalyst acidity and hydrophobicity. In this study, the loading weights of TMMS-CSPETS ranged from 0.2 g to 1.2 g to functionalise 1 g of ZrO_2-SiO_2.

Table 4.2: Loading amounts of functionalisation agents (TMMS and CSPETS)
in ZrO$_2$-SiO$_2$ support

Catalysts	[a] Molar ratio SiO$_2$:total agents	[b] TMMS (mol%)	TMMS (g)	CSPETS (g)	TMMS (mmol)	CSPETS (mmol)
ZrO$_2$-SiO$_2$-Me&Et-PhSO$_2$Cl (3, 80)	3:1	80	0.2	0.2	1.47	0.31
ZrO$_2$-SiO$_2$-Me&Et-PhSO$_2$Cl (2.5, 80)	2.5:1	80	0.250	0.262	1.84	0.40
ZrO$_2$-SiO$_2$-Me&Et-PhSO$_2$Cl (2, 80)	2:1	80	0.313	0.328	2.30	0.50
ZrO$_2$-SiO$_2$-Me&Et-PhSO$_2$Cl (1, 80)	1:1	80	0.6255	0.655	4.59	1.01
ZrO$_2$-SiO$_2$-Me&Et-PhSO$_2$Cl (0.4, 80)	1:2.5	80	1.609	1.621	11.81	2.49

[a] Molar ratio SiO$_2$:total agent; [b] mol %of hydrophobic ratio= [(TMMS mmol)/ (TMMS mmol + CSPETS mmol)]; values in the parentheses represent molar ratio SiO$_2$:total reagent and TMMS mol%

The effects of the loading amount of TMMS on the hydrophobicity level of the designed catalysts are illustrated in Figure 4.10. Results revealed that the 2.5:1 molar ratio of SiO$_2$ to TMMS-CSPETS (ZrO$_2$-SiO$_2$-Me&Et-PhSO$_2$Cl [2.5, 80]) achieved the highest performance amongst the designed catalysts because it exhibited the highest hydrophobicity level. The experimental work also proved that the hydrophobicity level of the catalyst was unaltered by loading an excessive amount of total agents. For instance, the corresponding 1.6 g of CEPETS and 1.6 g of TMMS were loaded excessively to 1 g of SiO$_2$-ZrO$_2$ to gain a highly hydrophobic surface catalyst in designing the ZrO$_2$-SiO$_2$-Me&Et-PhSO$_2$Cl (0.4, 80) catalyst, but the highest hydrophobicity was not achieved. This work evidenced that further increase in the loading amount of CSPETS and TMMS will not improve the catalyst hydrophobicity. Furthermore, no direct relation existed between the amount of CSPETS and TMMS

loading and the hydrophobicity level. This study confirmed that the best molar ratio of SiO_2 to the total agents was 2.5:1, and the catalyst with the highest hydrophobicity was ZrO_2-SiO_2-Me&Et-$PhSO_2Cl$ (2.5, 80).
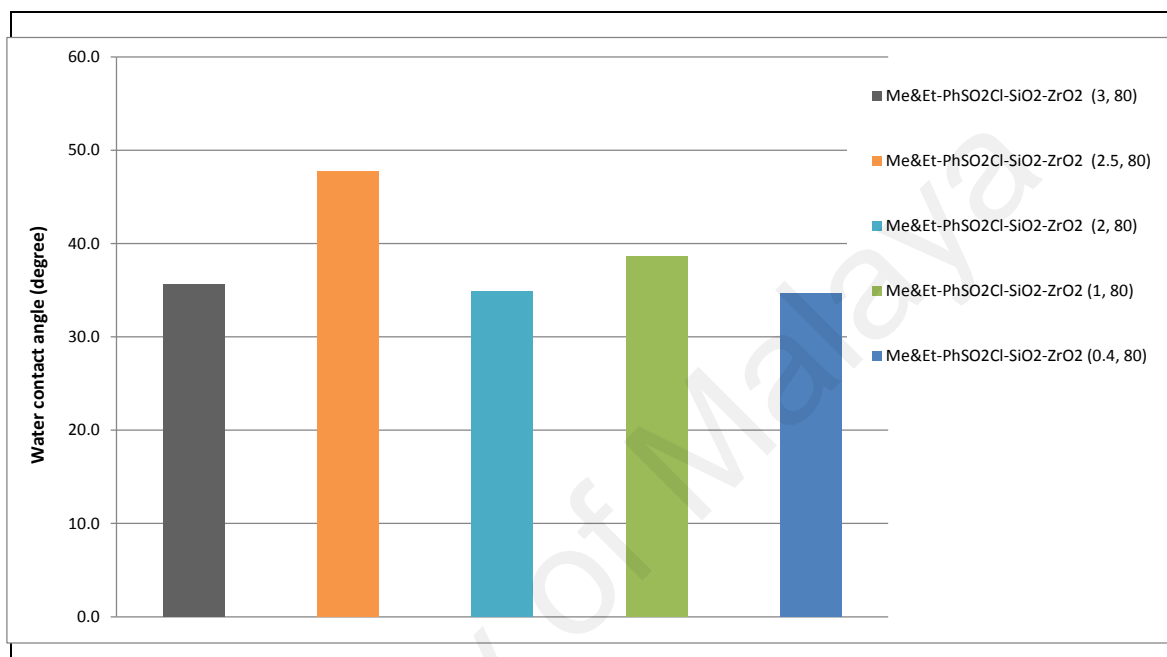
Figure 4.10: Effects of the loading amount of TMMS-CSPETS on the hydrophobicity levels of the designed catalysts

4.2.2 Effects of TMMS loading on the catalyst acidity

The previous section identified 2.5:1 as the most suitable molar ratio of SiO_2 to the total agents. Different mole percentages of TMMS were used to investigate the hydrophobicity level of each designed catalyst at a constant molar ratio of SiO_2:TMMS-CSPETS (2.5:1). Table 4.3 reveals the mole percentages of TMMS utilised to adjust the hydrophobicity level of the designed catalysts, which were ZrO_2-SiO_2-Me&Et-$PhSO_3H$_80, ZrO_2-SiO_2-Me&Et-$PhSO_3H$_70 and ZrO_2-SiO_2-Me&Et-$PhSO_3H$_50. The values (80, 70 and 50) at the end of catalysts' symbols indicate the mol% of TMMS utilised in adjusting the hydrophobicity levels of the catalysts.

With consideration of the hydrophobicity and exchangeable capacity of CSPETS of the catalyst, this study used no TMMS ratio that is less than 50 mol% in preparing acid catalyst with good hydrophobicity at more than 40° in contact angle analysis. Results confirmed that the ZrO_2-SiO_2-Me&Et-PhSO$_3$H_80 possessed a hydrophobicity level higher than those of ZrO_2-SiO_2-Me&Et-PhSO$_3$H_70 and ZrO_2-SiO_2-Me&Et-PhSO$_3$H_50, which reasonably agreed with the relative amount of TMMS (i.e., the highest TMMS amount was utilised for ZrO_2-SiO_2-Me&Et-PhSO$_3$H_80) (Table 4.3). The experimental results also showed that the loading amount of TMMS affected the acidity of the designed catalyst. The relationship of the acidity and hydrophobicity of the designed catalysts is illustrated in Figure 4.11; increasing the catalyst hydrophobicity can decrease the catalyst acidity.

Table 4.3: Loading amounts of TMMS and CSPETS in designing different acidities of catalysts

Catalysts	[a] Molar ratio SiO_2 : total reagents	[b] TMMS (mol%)	TMMS (g)	CSPETS (g)	TMMS (mmol)	CSPETS (mmol)	Acidity (mmol/g)
ZrO_2-SiO_2-Me&Et-PhSO$_3$H (2.5, 80)	2.5:1	80	0.250	0.262	1.84	0.403	0.33
ZrO_2-SiO_2-Me&Et-PhSO$_3$H (2.5, 70)	2.5:1	70	0.2	0.4	1.47	0.62	0.62
ZrO_2-SiO_2-Me&Et-PhSO$_3$H (2.5, 50)	2.5:1	50	0.153	0.7276	1.12	1.12	0.72

[a] Molar ratio SiO_2:total agent; [b] mol% of hydrophobic ratio= [(TMMS mmol)/ (TMMS mmol + CSPETS mmol)]; values in the parentheses represent molar ratio SiO_2:total reagent and TMMS mol%
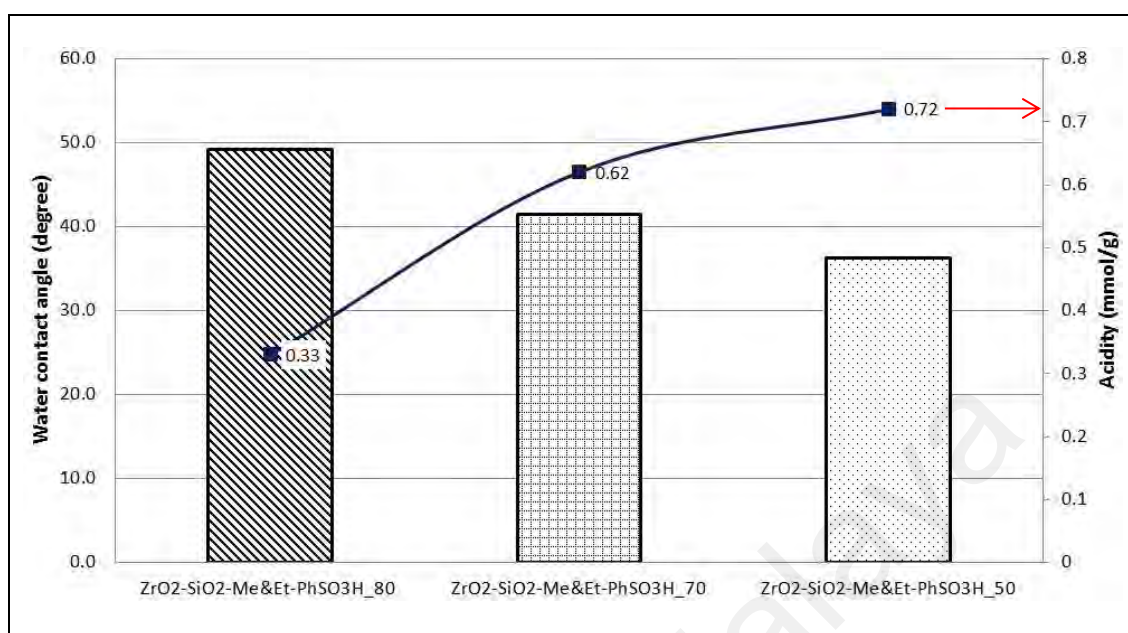
Figure 4.11: Relationship of hydrophobicity level and acidity of the designed catalysts

4.2.3 Effects of hydrophobicity and acidity of the designed catalysts on the catalytic activities

The designed catalysts with different hydrophobicity and acidity levels (ZrO_2-SiO_2-Me&EtPhSO$_3$H_80, ZrO_2-SiO_2-Me&EtPhSO$_3$H_70 and ZrO_2-SiO_2-Me&EtPhSO$_3$H_50) were used in comparative studies on glycerol esterification with OA. All the reactions were conducted at an equimolar OA-to-glycerol ratio, 100 °C reaction temperature, 3 wt% catalyst concentration with respect to the OA weight and solvent-less reaction conditions for 8 h. Figure 4.12 shows the catalytic activities of the designed catalysts, which were also compared with the results in the absence of catalyst.
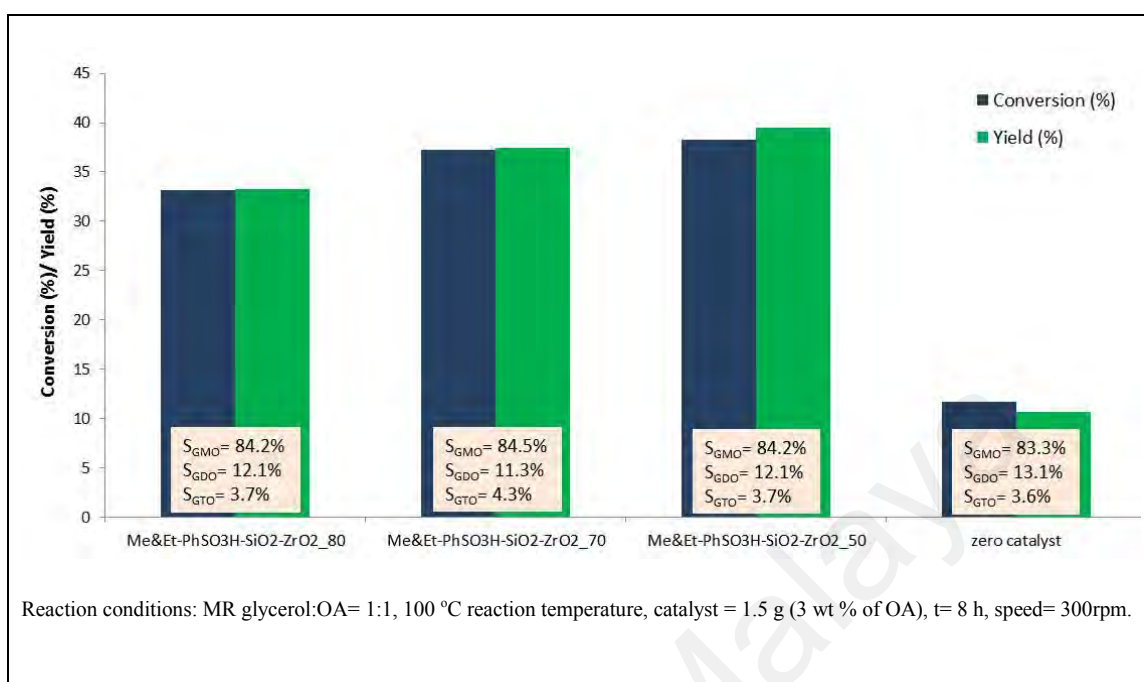
Figure 4.12: Performance evaluation of the designed catalysts

The obtained results demonstrated that the acidity of the catalyst significantly affected the conversion and yield. Results showed that catalytic activity increased with increased catalyst acidity, following the order of ZrO_2-SiO_2-$Me\&EtPhSO_3H\_50$ (acidity: 0.72 mmol/g; yield: 39.5%) > ZrO_2-SiO_2-$Me\&EtPhSO_3H\_70$ (acidity: 0.62 mmol/g; yield: 37.4%) > ZrO_2-SiO_2-$Me\&EtPhSO_3H\_80$ (acidity: 0.33 mmol/g; yield: 33.3%). Nevertheless, the yield difference between ZrO_2-SiO_2-$Me\&EtPhSO_3H\_50$ and ZrO_2-SiO_2-$Me\&EtPhSO_3H\_70$ was only 2%. With consideration of the amount of CSPETS used in catalyst development and the insignificant difference in the yield obtained between ZrO_2-SiO_2-$Me\&EtPhSO_3H\_50$ and ZrO_2-SiO_2-$Me\&EtPhSO_3H\_70$, this study suggested that ZrO_2-SiO_2-$Me\&EtPhSO_3H\_70$ catalyst is the best catalyst for this reaction.

4.2.4 Catalytic activity: role of hydrophobicity in GMO production

The role of hydrophobicity in the catalytic glycerol esterification with OA at a constant catalyst acidity level must be evaluated to eliminate the effect of catalyst acidity in this investigation. Hence, ZrO_2-SiO_2-Me&EtPhSO$_3$H_50h was synthesised by using a 50% lower amount of TMMS at constant CSPETS loading than that of the high-performing ZrO_2-SiO_2-Me&EtPhSO$_3$H_70 catalyst (Table 4.4). ZrO_2-SiO_2-Me&EtPhSO$_3$H_50h and ZrO_2-SiO_2-Me&EtPhSO$_3$H_70 catalysts possessed identical acidity levels (0.62 mmol/g).

This comparative study demonstrated the role of the hydrophobicity of acid catalyst in increasing the reaction yield (37.4% vs. 28.9%) at identical reaction conditions. Moreover, this study confirmed that the hydrophobicity of acid catalysts enhanced the formation rate of GMO, which is well illustrated in Figure 4.13. The plot revealed that the reaction rate of ZrO_2-SiO_2-Me&EtPhSO$_3$H_70 was faster than that of ZrO_2-SiO_2-Me&EtPhSO$_3$H_50h. This result reasonably agreed with that reported by (Jérôme et al., 2008); they observed that the hydrophobic interactions improve the diffusion of fatty acids within the silica pores because the reduced hydrophobic amount of ZrO_2-SiO_2-Me&EtPhSO$_3$H_50h achieves a low yield. ZrO_2-SiO_2-Me&EtPhSO$_3$H_70 increased the product yield.

Table 4.4: Designed catalysts with different TMMS loading amounts

Catalysts	Acidity (mmol/g)	TMMS (g)	CSPETS (g)	Contact angle analysis (°)	Yield (%)	Selectivity (%)
ZrO_2-SiO_2-Me&EtPhSO$_3$H_70	0.62	0.2	0.4	42	37.4	S_{GMO}= 84.5% S_{GDO}= 11.2% S_{GTO}= 4.3%
ZrO_2-SiO_2-Me&EtPhSO$_3$H_50h	0.62	0.1	0.4	30.7	28.9	S_{GMO}= 90.1% S_{GDO}= 9.2% S_{GTO}= 0.7%

The yield was obtained using HPLC analysis. Reaction conditions: MR Gly:OA= 1:1, 100 ºC reaction temperature, catalyst = 1.5 g (3 wt % of OA), t= 8 h, speed= 300rpm
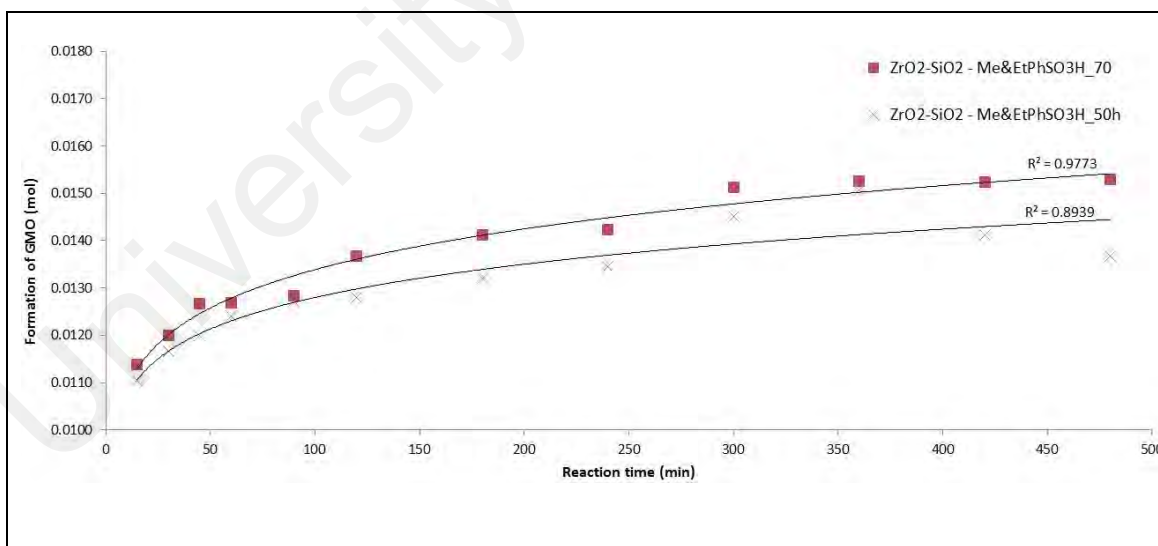
Figure 4.13: Effects of the catalyst hydrophobicity on the formation rate of GMO in the presence of ZrO_2-SiO_2-Me&EtPhSO$_3$H_70 and ZrO_2-SiO_2-Me&EtPhSO$_3$H_50h catalysts

A comparison of catalytic activity between ZrO_2-SiO_2-Me&EtPhSO$_3$H_70 and several other catalysts reported in literature is summarised in Table 4.5. All the reactions were conducted at an equimolar glycerol-to-OA ratio. The conversion (40%) for ZrO_2-SiO_2-Me&EtPhSO$_3$H_70 catalyst at 100 °C reaction temperature was lower than that of the MCM-4-methyl-SO$_3$H catalyst (89%) at 120 °C. This discrepancy was mainly attributed to the acidity (1.7 mmol/g) of the MCM-4-methyl-SO$_3$H catalyst. However, the GMO selectivity for MCM-4-methyl-SO$_3$H was 40%, which is two times lower than that of ZrO_2-SiO_2-Me&EtPhSO$_3$H_70. The catalyst developed in this work showed a better performance than that of the tin–organic framework (HPW/Cu$_3$(BTC)$_2$ catalyst with conversions of 45% and 62% of GMO selectivity at 120 °C.

Nonetheless, the catalyst activity of ZrO_2-SiO_2-Me&EtPhSO$_3$H_70 (40% conversion) was considered remarkable compared with that of the Fe–Zn DMC complex subjected to a high reaction temperature (Table 4.5). The Fe–Zn DMC complex obtained a conversions of 63.4% and 67.3% of GMO selectivity despite being operated at a high reaction temperature (180 °C) and high loading catalyst concentration (8 wt%). The hydrophobicity enhanced titanium silicate-type catalyst (Ti-SBA-16) achieved a conversion of 72.8% at 180 °C and short reaction time (3 h) and showed the potential of ZrO_2-SiO_2-Me&EtPhSO$_3$H_70 to perform well at a long reaction time.

Table 4.5: Comparison of the catalytic activity between ZrO₂-SiO₂-Me&EtPhSO₃H_70 and several other catalysts reported in literature

Catalysts	Reaction parameters			Performance		References
	Temperature (^{o}C)	Catalyst concentration (wt%)	Time (h)	Conversion (%)	Selectivity (%)	
ZrO₂-SiO₂-Me&EtPhSO₃H_70 Acidity= 0.63 mmol/g	100	3	8	39	S_{GMO}= 84.5% S_{GDO}= 11.2% S_{GTO}= 4.3%	This work
MCM-4-methyl-SO₃H Acidity= 1.7 mmol/g	120	5	8	89	S_{GMO}= 40%	(Díaz, Mohino, Pérez-Pariente, & Sastre, 2003)
HPW/Cu₃(BTC)₂ Tin-organic framework Acidity= NA	120	1	8	45	S_{GMO}= 62%	(L. H. Wee et al., 2013)
Fe–Zn DMC complex Acidity= 1.06 mmol/g	180	8	8	63.4	S_{GMO}= 67.3 % S_{GDO}= 31.7 %	(Kotwal et al., 2011)
Ti-SBA-16 Acidity= 0.09 mmol/g	180	3	3	72.8	S_{GMO}= 32.8 S_{GDO}= 57.9% S_{GTO}= 9.2%	(Kotwal et al., 2013)

All the reactions were conducted at equimolar ratio of glycerol to OA, catalyst concentration was with respect to OA, and solventless conditions.

4.3   Schematic of catalyst synthesis

Figure 4.14 shows the schematic illustration for the synthesis of the mesoporous ZrO_2-SiO_2-Me&Et-$PhSO_3H$ catalyst. BET, FESEM, FTIR, EDX and XPS results proved the successful coating of SiO_2 on ZrO_2 support. The strong adherence of SiO_2 to ZrO_2 support was mainly contributed by the OH^- group of NH_4OH because the suspension of static repulsion against Van der Waals attractive forces stabilises the bonding of ZrO_2-SiO_2 (X.-D. Wang et al., 2010). In addition, the mass of adhered SiO_2 can be measured from the mass difference between ZrO_2 and SiO_2-ZrO_2. This study revealed that ZrO_2 support gained approximately 1 g of SiO_2 through this silica-coating process and confirmed the presence of SiO_2.
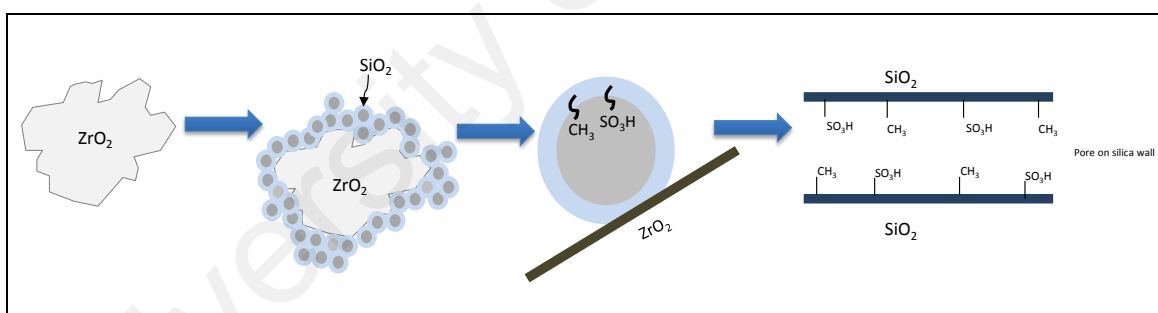
Figure 4.14: Synthesis diagram for the surface functionalisation on the ZrO_2-SiO_2 support

The hydrophobic organosilica moiety TMMS was utilised to increase the hydrophobic surface of the catalysts. The formation of covalent bonds on the ZrO_2-SiO_2 surface transformed the hydrophilic character to hydrophobic as proven by the contact angle analysis, BET and XPS. This observation was also reported by Markovska et al. (Markovska, Yovkova, Minov, Rusev, & Lyubchev, 2013) in a previous work on

changing the surface property of ceramics through TMMS grafting. Hydrophobisation involved the attachment of methyl groups from TMMS to a silicon atom; similarly, the CSPETS was used to initiate the conversion of the silica surface to sulfonic moieties by exchanging Cl$^-$ with OH$^-$ during sulphonation. Sulfonic acid site is considerably important for catalysis. XPS and BET results suggested that SO$_3$H was mainly distributed in the mesopore of the nanospheres. Figure 4.15 illustrates the mechanism of TMMS and CSPETS in functionalising ZrO$_2$-SiO$_2$.
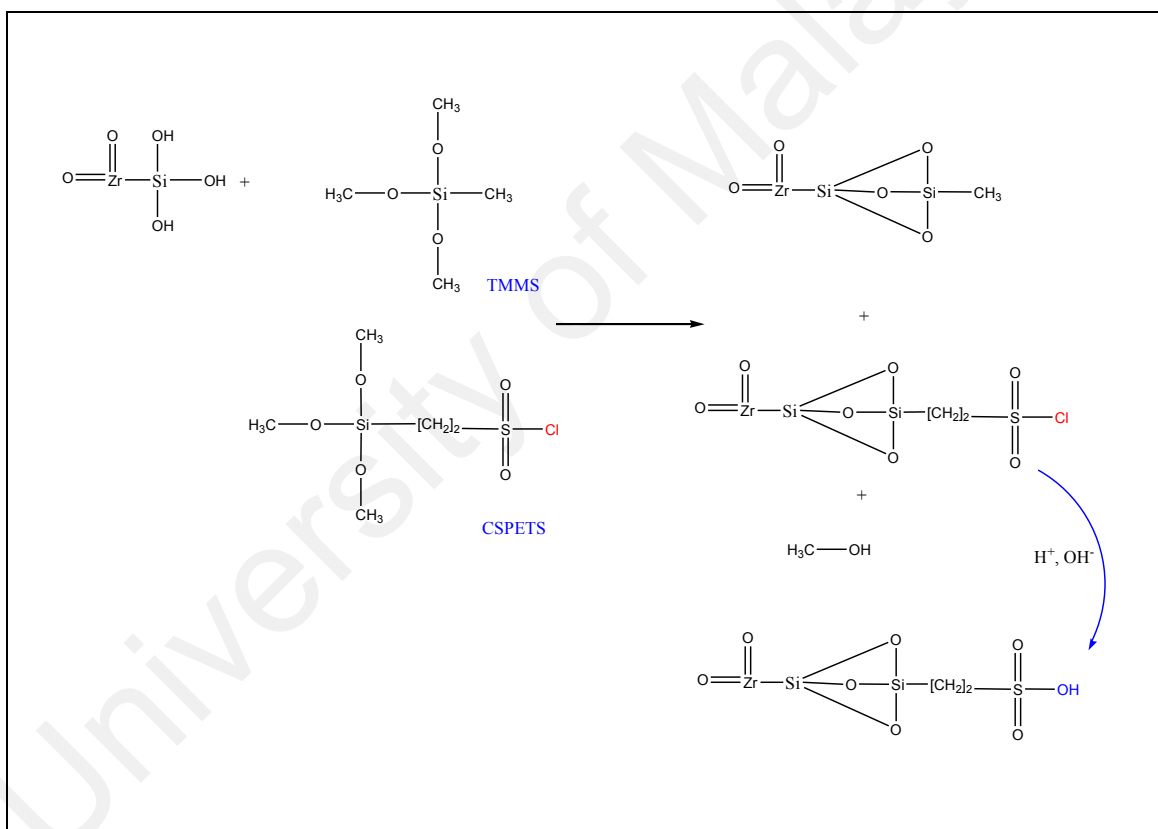
Figure 4.15: Mechanism for the synthesis of hydrophobicity-enhanced ZrO$_2$-SiO$_2$-Me&Et-PhSO$_3$H catalyst

4.4 Catalytic activity studies

The hydrophobicity-enhanced ZrO_2-SiO_2-Me&EtPhSO$_3$H_70 catalyst was selected to study the effect of process operating parameters. The influences of reaction temperature, catalyst concentration, glycerol-to-OA molar ratio and reaction time on the catalytic glycerol esterification with OA were investigated. The mass transfer limitation was evaluated prior to investigating the process variables to ensure that the esterification process was reaction controlled. The stability of the designed catalyst ZrO_2-SiO_2-Me&EtPhSO$_3$H_70 was also evaluated.

4.4.1 Effects of mass transfer

Mass transfer limitation was assessed at the reaction temperature of 100 °C prior to temperature optimisation. The experiments were carried out at an equimolar OA-to-glycerol ratio, 100 °C reaction temperature, 480 min and 3 wt% catalyst concentration with respect to the OA weight and solvent-less reaction conditions during mass transfer limitation study. Figure 4.16 demonstrates the reaction yield and selectivity by using ZrO_2-SiO_2-Me&EtPhSO$_3$H_70 catalyst under two different stirring speeds (300 and 650 rpm).The high stirring speed 650 rpm resulted in a slightly increased yield (from 35.3% to 37.4%) compared with the 300 rpm reaction speed. The selectivity of GDO and GTO also slightly increased compared with the reaction at 300 rpm, but the difference was insignificant. Therefore, the maximum stirring speed of 650 rpm was proposed for further testing of process variables in the presence of ZrO_2-SiO_2-Me&EtPhSO$_3$H_70 catalyst to eliminate the external mass transfer resistance. External mass transfer resistance can be completely eliminated when a high stirring speed is applied, and external diffusion negligibly affects the overall reaction rate (Nanda et al., 2014).
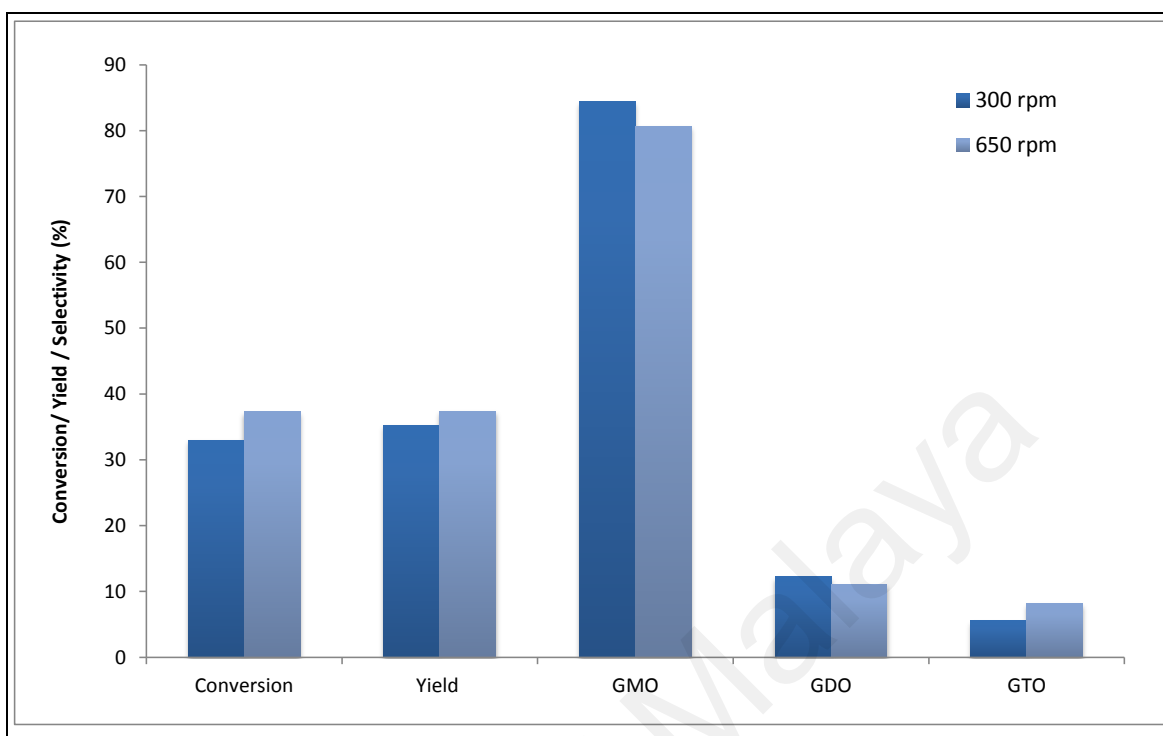
Figure 4.16: Effects of stirring speed on yield and selectivity using the ZrO$_2$-SiO$_2$-Me&EtPhSO$_3$H_70 catalyst at identical reaction conditions

4.4.2 Effects of reaction temperature

ZrO$_2$-SiO$_2$-Me&EtPhSO$_3$H_70 catalyst was used to study the effects of reaction temperature. Various temperatures (100 °C, 120 °C, 140 °C and 160 °C) were utilised under the stirring speed of 650 rpm, equimolar OA-to-glycerol ratio, 3 wt% catalyst concentration with respect to the OA weight and solvent-less reaction conditions.

Figure 4.17 presents the effects of reaction temperatures on the catalytic esterification of glycerol with OA. Results indicated that the conversion increased with increased reaction temperature because high temperature favours a high equilibrium product yield in a typical endothermic reaction (Trinh, Yusup, & Uemura, 2018). The initial rate of esterification also increased with increased reaction temperature. The reaction temperature of 160 °C yielded the highest conversion level (86.7%) in this

study. On the contrary, relatively low activities were observed at the beginning of reaction at 100 °C and 120 °C. The activation energy required for successful conversion is difficult to exceed at low temperatures because the energy possessed by the reactant molecules is low; consequently, the effective collision is decreased because the kinetic energy in the reactant molecules and potential energy of molecules are decreased (Hoo & Abdullah, 2014).
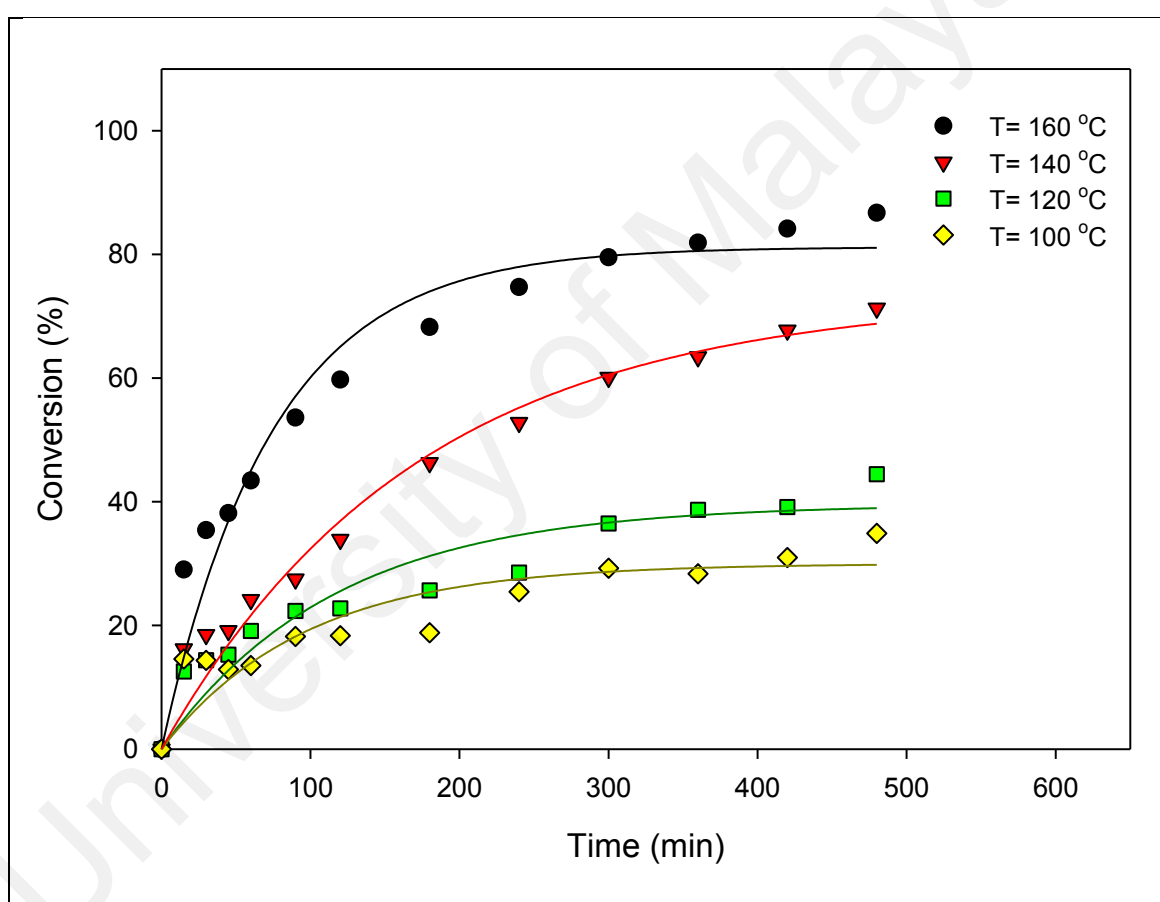
Figure 4.17: Effects of reaction temperature on the catalytic esterification of glycerol with OA using ZrO$_2$-SiO$_2$-Me&EtPhSO$_3$H_70 catalyst

The effects of reaction temperature on the selectivity of GMO, GDO and GTO are shown in Figure 4.18. The selectivity trends of GMO, GDO and GTO followed a similar order at their respective reaction temperatures of 100 °C, 120 °C, 140 °C and 160 °C. The GMO selectivity decreased by increasing the reaction temperature but increased the selectivity for GDO and GTO. Notably, the selectivity percentage at 140 °C and 160 °C were much alike, particularly at more than 360 min because approximately 60% of GMO and 36% of GDO were obtained. Therefore, 160 °C was suggested as the optimal reaction temperature by considering the obtained conversion and selectivity under the ZrO_2-SiO_2-Me&EtPhSO$_3$H_70-catalysed esterification reaction of glycerol with OA.
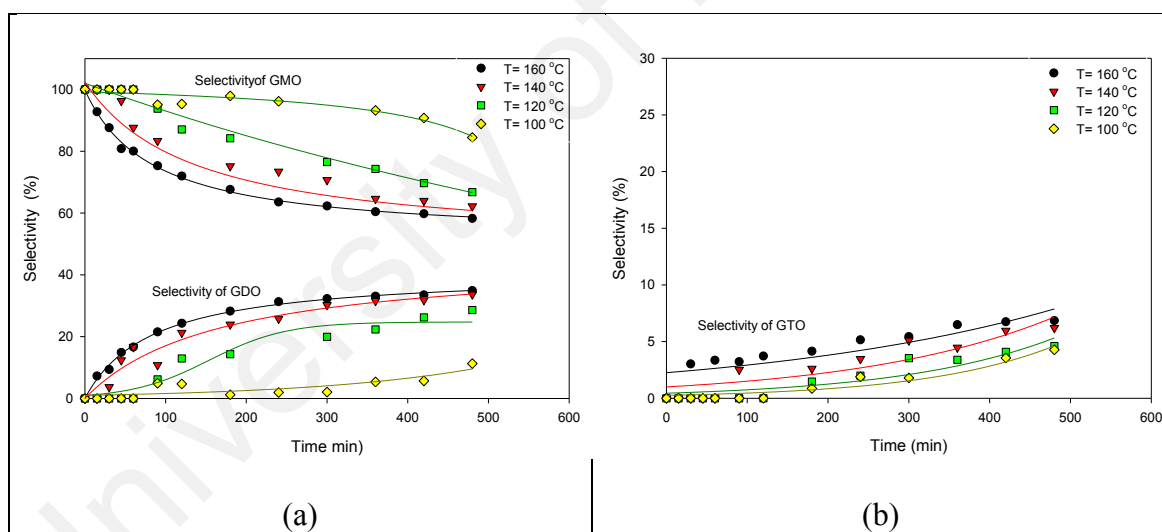
Figure 4.18: Effects of reaction temperature on the selectivities of GMO, GDO and GTO

The performance of ZrO_2-SiO_2-Me&EtPhSO$_3$H catalyst was compared with those available in literature in Table 4.6. The conversion ZrO_2-SiO_2-Me&EtPhSO$_3$H catalyst (conversion = 44.5%; acidity = 0.62 mmol/g) was lower than that of MCM-41-Q$_3$H (conversion = 89%; acidity = 1.7 mmol/g) at 120 °C; the difference was mainly attributed to the decreased acidity of ZrO_2-SiO_2-Me&EtPhSO$_3$H catalyst in this work. However, the conversion of ZrO_2-SiO_2-Me&EtPhSO$_3$H catalyst at 160 °C (conversion = 89%; acidity = 0.62 mmol/g) was higher than that of Fe–Zn DMC (conversion = 63.4%; acidity = 1.06 mmol/g) at 180 °C, which indicated that the surface and textural properties of ZrO_2-SiO_2-Me&EtPhSO$_3$H catalyst are both key influencing factors on the rate of conversion and GMO formation with the elimination of catalyst acidity factor.

Moreover, the hydrophobic-altered titanium-based catalyst (Ti-SBA-16) posed a relatively low catalyst acidity (0.09 mmol/g) but an improved catalytic performance (conversion = 72.8%) within 180 min. Given its considerably low GMO selectivity (32.8%), the designed catalyst ZrO_2-SiO_2-Me&EtPhSO$_3$H can produce products with increased GMO selectivity (59%). In conclusion, the performance of ZrO_2-SiO_2-Me&EtPhSO$_3$H (conversion = 86.7% at equimolar reactant, 3 wt% catalyst concentration and 160 °C) is significant compared with those from literature studies performed in the absence of catalyst (conversion = 20% at equimolar glycerol-to-OA ratio, 150 °C and 20 h reaction time) (L. H. Wee et al., 2013).

Table 4.6: Comparison of the catalytic activity between ZrO_2-SiO_2-Me&EtPhSO$_3$H_70 and available literature results

Catalysts	Reaction conditions			Performance		References
	Temperature (^{o}C)	Catalyst concentration (wt%)	Time (min)	Conversion (%)	Selectivity (%)	
ZrO_2-SiO_2-Me&EtPhSO$_3$H_70 Acidity= 0.62 mmol/g	100	3	480	39.0	S_{GMO}= 84.5% S_{GDO}= 11.2% S_{GTO}= 4.3%	This work
	120			44.5	S_{GMO}= 66.7% S_{GDO}= 28.6% S_{GTO}= 4.6%	
	140			70.7	S_{GMO}= 60.1% S_{GDO}= 33.7% S_{GTO}= 6.2%	
	160			86.7	S_{GMO}= 58.4% S_{GDO}= 34.5% S_{GTO}= 7.1%	
MCM-41-Q$_3$H Acidity= 1.7 mmol/g	120	5	480	89	S_{GMO}= 40%	(Díaz et al., 2003)

Table 4.6 continued

Fe–Zn DMC Acidity= 1.06 mmol/g	180	7	840	63.4	S_{GMO}= 67.3% S_{GDO}= 31.7 %	(Kotwal et al., 2011)
Ti-SBA-16 Acidity= 0.09 mmol/g	180	3	180	72.8	S_{GMO}= 32.8 S_{GDO}= 57.9% S_{GTO} = 9.2%	(Kotwal et al., 2013)

All the reaction were conducted at MR Glycerol:OA= 1:1, catalyst concentration is with respect to mass of OA and solventless conditions.

4.4.2.1 Interaction effects of reaction temperature and reaction time

Figure 4.19 elucidates the interaction effects of reaction time and reaction temperature on the conversion and selectivity of GMO. Figure 4.19(a) indicates that the highest conversion was obtained at 160 °C after 480 min reaction time. The selectivity trend of GMO at various temperatures is shown in Figure 4.19(b). The selectivity of GMO decreased with time and temperature. Combining the plots in Figure 4.19(a) and (b) an intersection point corresponding to the highest conversion (74 %) and GMO selectivity (63.6 %) is obtained at 160 °C and after 240 min reaction time, at equimolar OA-and-glycerol ratio and 3 wt% catalyst concentration. It is worthy to note that under these conditions the GMO and GDO combined selectivity is 91.6%.
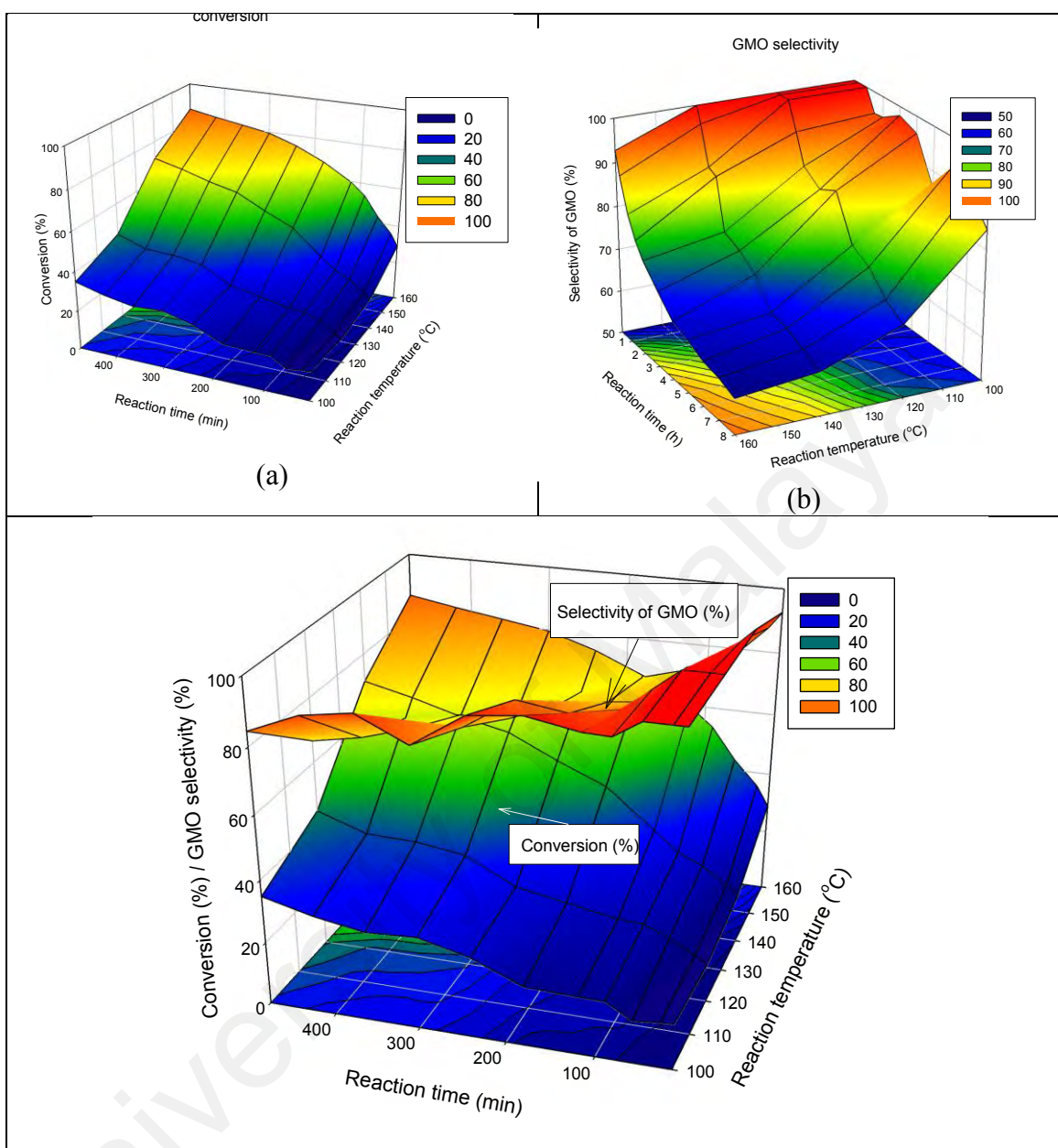
Figure 4.19: Interaction effects of reaction time and reaction temperature on the conversion and selectivity of GMO: (a) conversion, (b) selectivity of GMO and (c) combined interaction of conversion and selectivity

4.4.3 Effects of the oleic acid-to-glycerol molar ratio

The effects of excess glycerol on glycerol esterification with OA catalysed by ZrO_2-SiO_2-Me&EtPhSO$_3$H were investigated at the constant reaction temperature of 160 °C, catalyst concentration of 3 wt%, stirring speed of 650 rpm and solvent-less reaction conditions. Figure 4.20 shows the effects of excess glycerol under the OA-to-glycerol molar ratios of 1:1, 1:2 and 1:3 in 480 min. At this reaction time, the conversion increased slightly with increased glycerol amount in the following descending order: 91.6%, 89.0% and 87.5% for 1:3, 1:2 and 1:1 OA-to-glycerol molar ratios, respectively. According to Le Chatelier's principle, the glycerol esterification with OA will shift to improve products formation with increased reactant concentration.
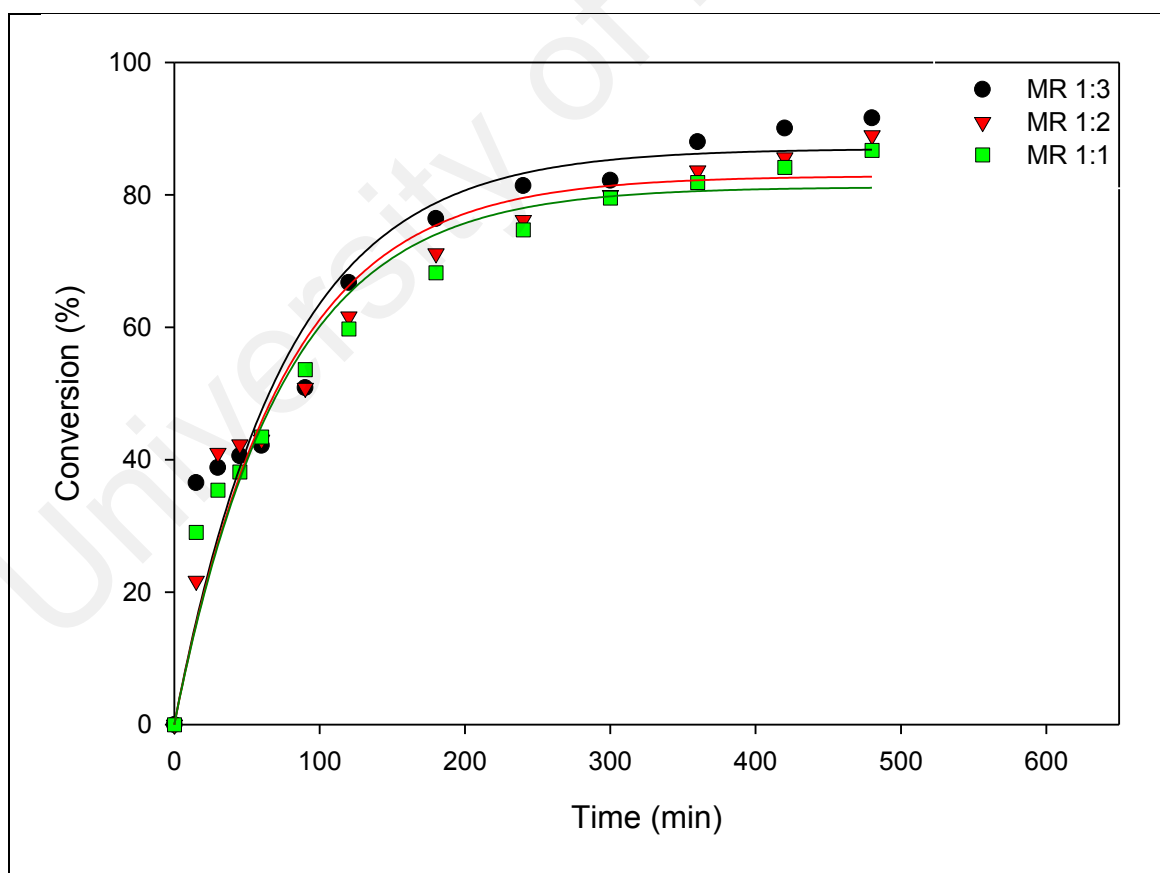
Figure 4.20: Effects of the OA-to-glycerol molar ratio on the conversion in ZrO_2-SiO_2-Me&EtPhSO$_3$H_70-catalysed glycerol esterification with OA

The conversion and selectivity of various mono-, di- and trioleates at reaction time are presented in Figure 4.21 to evaluate the effects of excess glycerol on conversion and selectivity. The conversion of 1:1 OA to glycerol (75%) was nearly close to the 1:2 molar ratio of OA to glycerol (76%). Results revealed that the 1:3 OA-to-glycerol molar ratio produced the highest conversion of about 82% at 240 min reaction time. Similarly, Singh et al. (Singh et al., 2013) stated that the significant reaction rate increases when the molar ratio increases from 1:2 (OA:glycerol) and insignificantly changes when excess glycerol is added at 1:6 OA-to-glycerol molar ratio.

The selectivity of GDO and GTO increased with the increased glycerol feeding ratio. Thus, the GMO selectivity was minimised by increasing the loading amount of glycerol in the catalytic esterification of glycerol with OA. It has been reported that unreacted glycerol removal is necessary despite of an equimolar OA-to-glycerol ratio of reactant was used in reaction (Konwar et al., 2016). Therefore, it can be concluded that equimolar OA-to-glycerol ratio can produce high GMO and GDO yield and equimolar ratio is suggested to obtain maximum GMO and GDO yield.
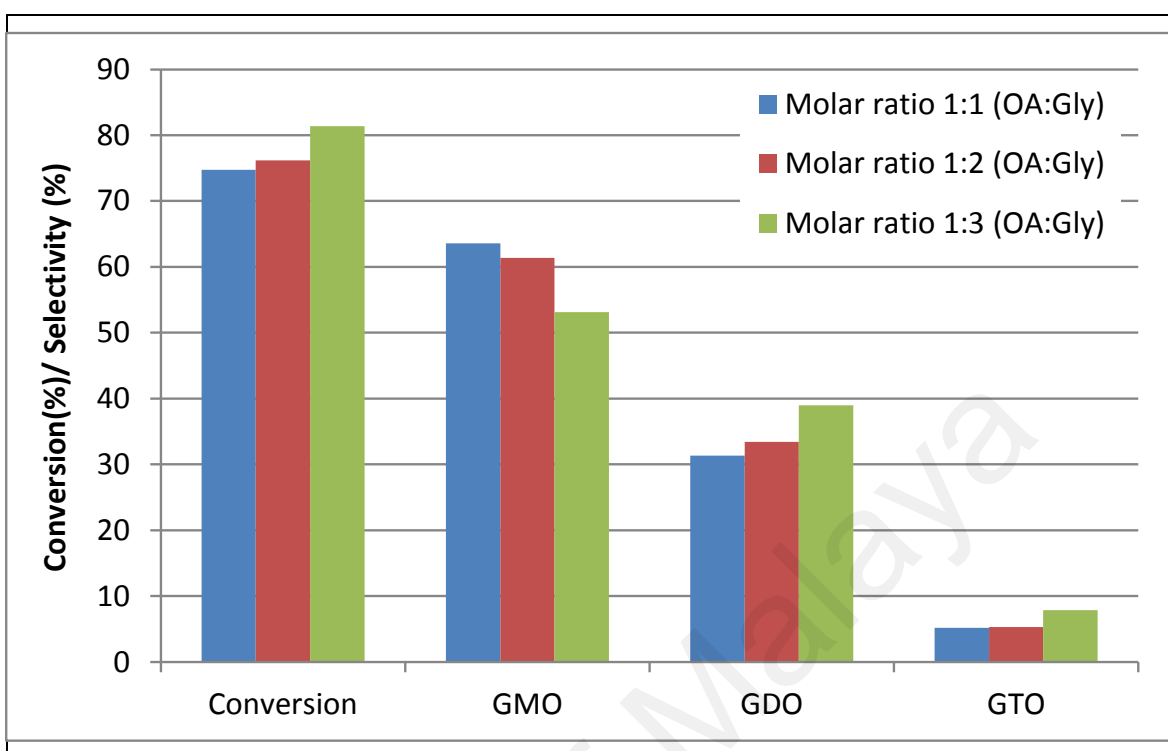
Figure 4.21: Effects of the OA-to-glycerol molar ratio on conversion and selectivity at 240 min reaction time. Conditions: catalyst concentration of OA, 3 wt%; reaction temperature, 160 °C and speed, 650 rpm

The GMO, GDO and GTO selectivities at different molar ratios are illustrated in Figure 4.22. The GMO selectivity decreased with increased glycerol ratio; by contrast, increased glycerol improved GDO and GTO selectivity. Significant GDO and GTO increments were also observed at more than 240 min reaction time. This work revealed that the selectivity profiles for the OA-to-glycerol molar ratios of 1:1 and 1:2 were similar, which demonstrated that no significant effect was observed for excess glycerol amount in the glycerol:OA molar ratio range of 1–2.
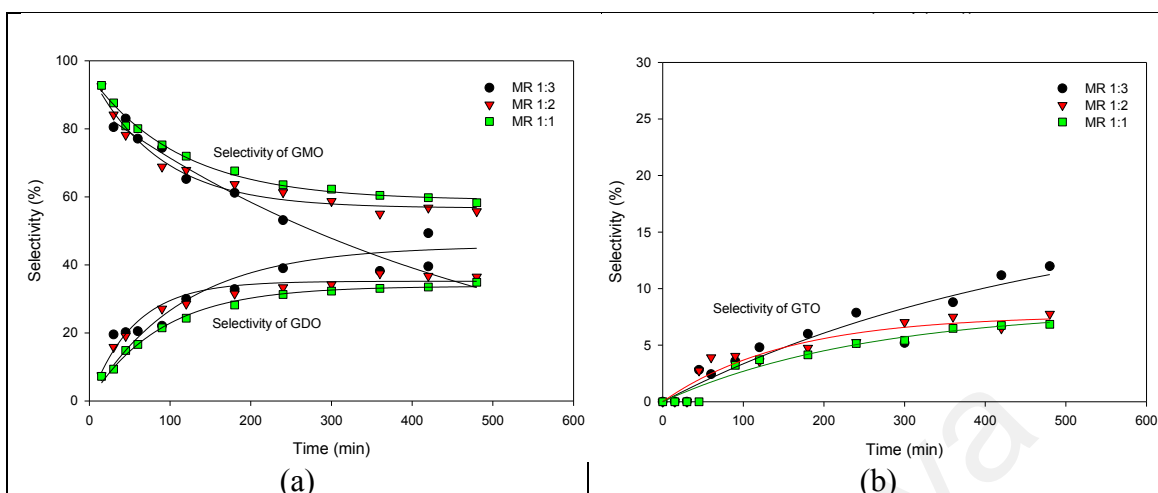
Figure 4.22: Effects of OA-to-glycerol molar ratios on the selectivities of GMO, GDO and GTO

Glycerol esterification with OA was conducted with excess OA to compare the different reaction behaviour in the OA-to-glycerol molar ratio of 3:1 at 160 °C and 3 wt% catalyst concentration of OA for 480 min. Figure 4.23 shows the conversion and selectivity obtained at the OA-to-glycerol molar ratio with excess glycerol (1:1, 1:2 and 1:3) and OA (3:1) conditions. This work showed that excess OA caused the high formation of GTO (selectivity = 40%) and GDO (selectivity = 50%) and relatively low GMO yield. This work also confirmed that an equimolar OA-to-glycerol ratio resulted in an optimum yield of GMO, with 93% combined selectivity of GMO and GDO.
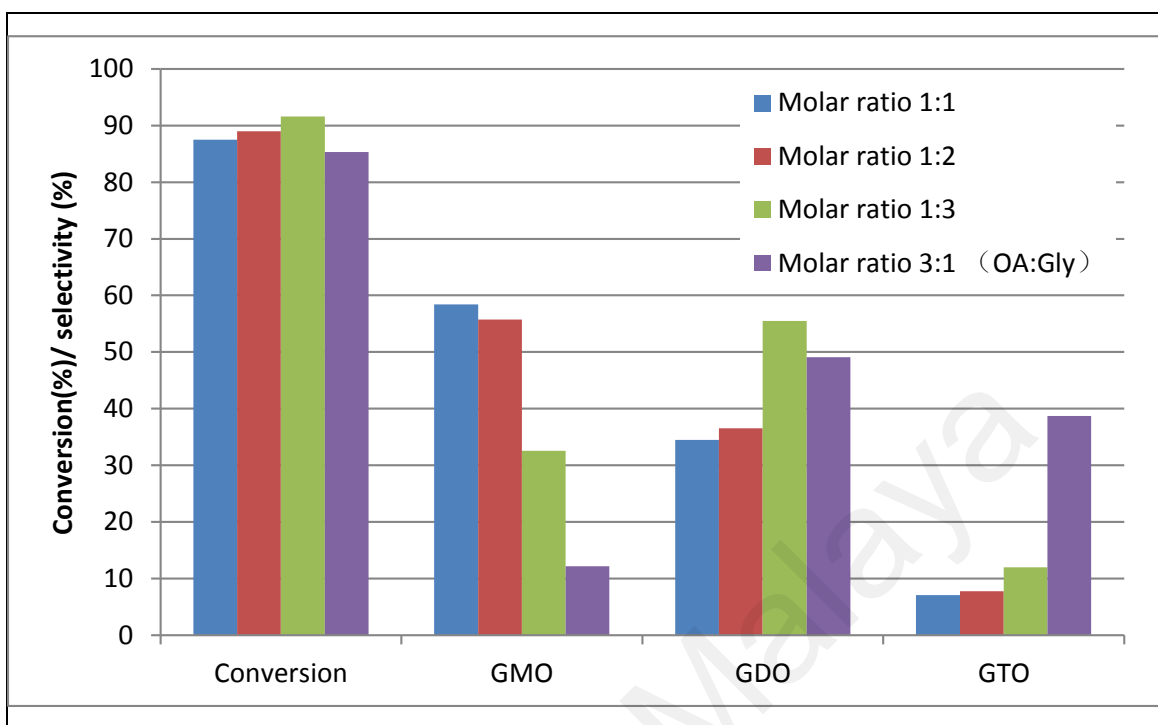
Figure 4.23: Effects of OA-to-glycerol molar ratios at 480 min reaction time. Conditions: catalyst concentration of OA, 3 wt%; reaction temperature, 160 °C and speed, 650 rpm

4.4.3.1 Interaction effects of molar ratio and reaction time

The interaction effects of glycerol-to-oleic acid molar ratio and reaction time on the conversion and selectivity of GMO are displayed in Figure 4.24. The diagram clearly indicated that reaction time exerted stronger influence on selectivity and conversion than the molar ratio.
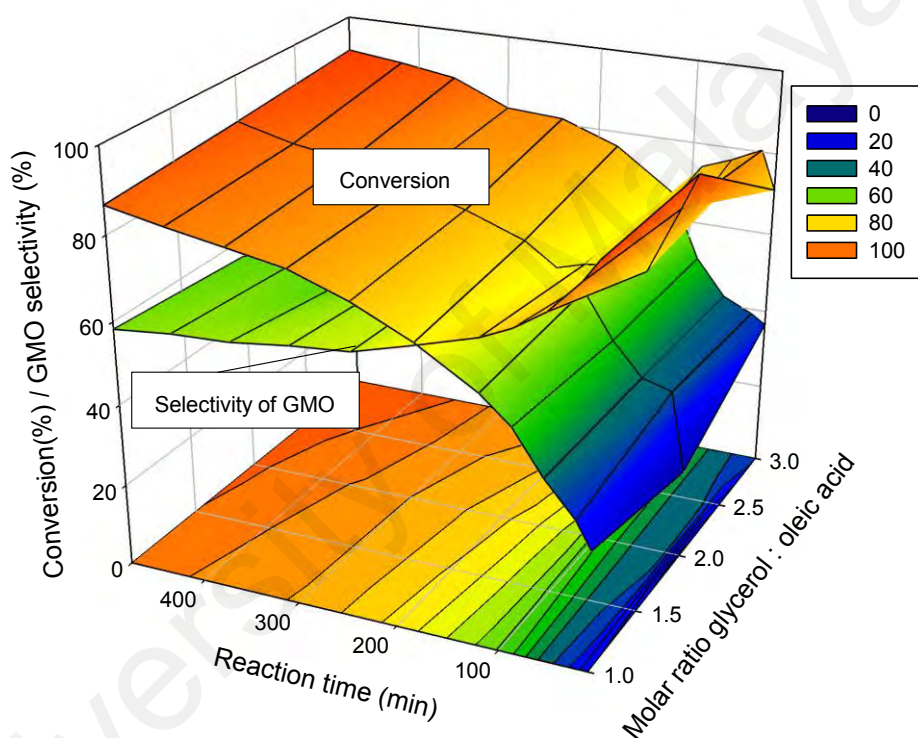
Figure 4.24: Interaction effects of glycerol-to-oleic acid molar ratio and reaction time on the conversion and selectivity of GMO

4.4.4 Effects of catalyst concentration

ZrO_2-SiO_2-Me&EtPhSO$_3$H_70 catalyst (3 wt%, 5 wt% and 8 wt%) was used to investigate the effects of catalyst concentration on the conversion and selectivity of the catalytic glycerol esterification with OA at the constant operation parameters of 160 °C, equimolar ratio and 650 rpm. Catalyst loading was calculated with respect to the weight of the limiting reactant OA. Figure 4.25 shows the conversion profile produced by using different concentrations of ZrO_2-SiO_2-Me&EtPhSO$_3$H_70 catalyst.

Catalyst concentrations 3 wt%, 8 wt% and 5 wt% achieved the slowest reaction rate in sequence. A significant initial reaction rate difference was observed for 3 wt% versus 5 wt% or 8 wt% catalyst concentration. The conversion profiles for the 5 wt% and 8 wt% catalyst concentrations were almost identical. At the end of reaction, generally after 420 min, a change in catalyst loading resulted in non-accelerated reaction rate. The conversion was insignificantly influenced with further increase in catalyst loading from 5 wt% to 8 wt% due to the equilibrium limit (Tao, Guan, Wang, Liu, & Louh, 2015).
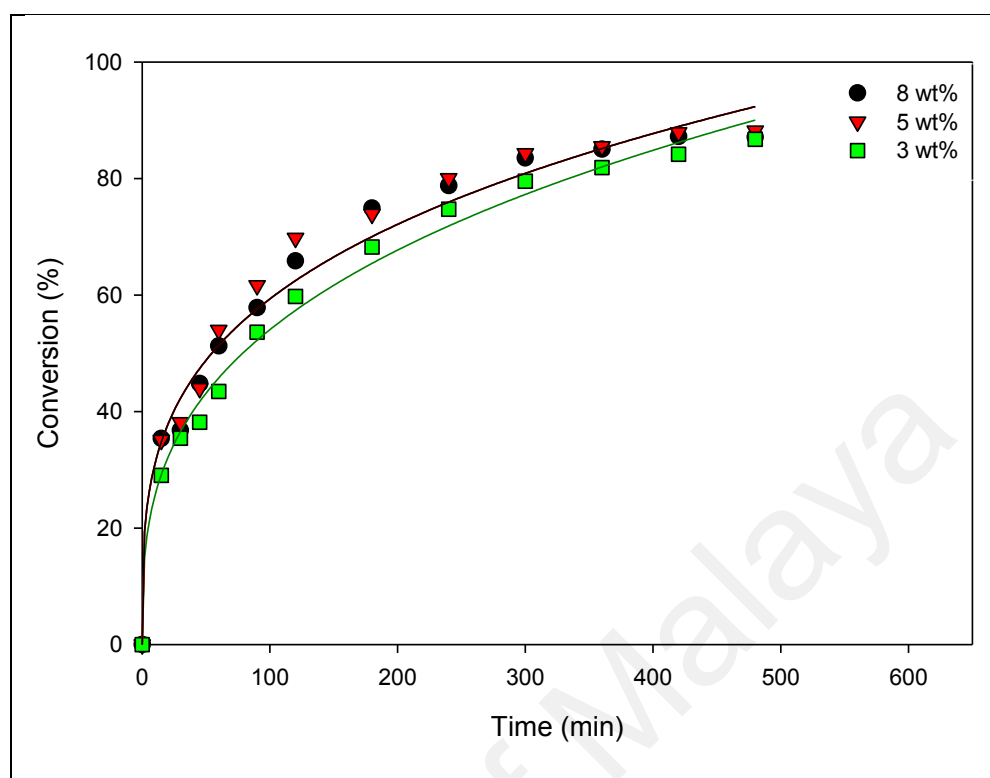
Figure 4.25: Effects of the ZrO$_2$-SiO$_2$-Me&EtPhSO$_3$H_70 catalyst concentration on the conversion during catalytic glycerol esterification with OA

A plot explained the effects of catalyst concentration on the conversion and selectivity at 240 min (Figure 4.26). At this reaction time, the obtained conversion was 74.7%, 80.0% and 78.8% for the catalyst concentrations of 3 wt%, 5 wt% and 8 wt%, respectively. These results proved that 5 wt% catalyst concentration was the optimal level for this catalytic study. Increasing the catalyst concentration at more than 5 wt% was not recommended because such increase does not improve the conversion. A similar trend was also reported in a previous work on glycerol esterification with palmitic acid; the conversion is unaffected beyond a certain amount of catalyst loading (Yusoff & Abdullah, 2016). Notably, the GMO selectivity trend decreased with increased catalyst concentration; the 3 wt%-produced selectivity was 64%, which was

higher than that of the 5 wt% (S_{GMO} = 61%) and 8 wt% (S_{GMO} = 53%). These findings clearly revealed that GMO was successfully converted to GDO and GTO. The increased effective interaction between the reactant molecules and GTO formation was highly attributed to the increased number of available acidic sites and acidity of the catalyst.
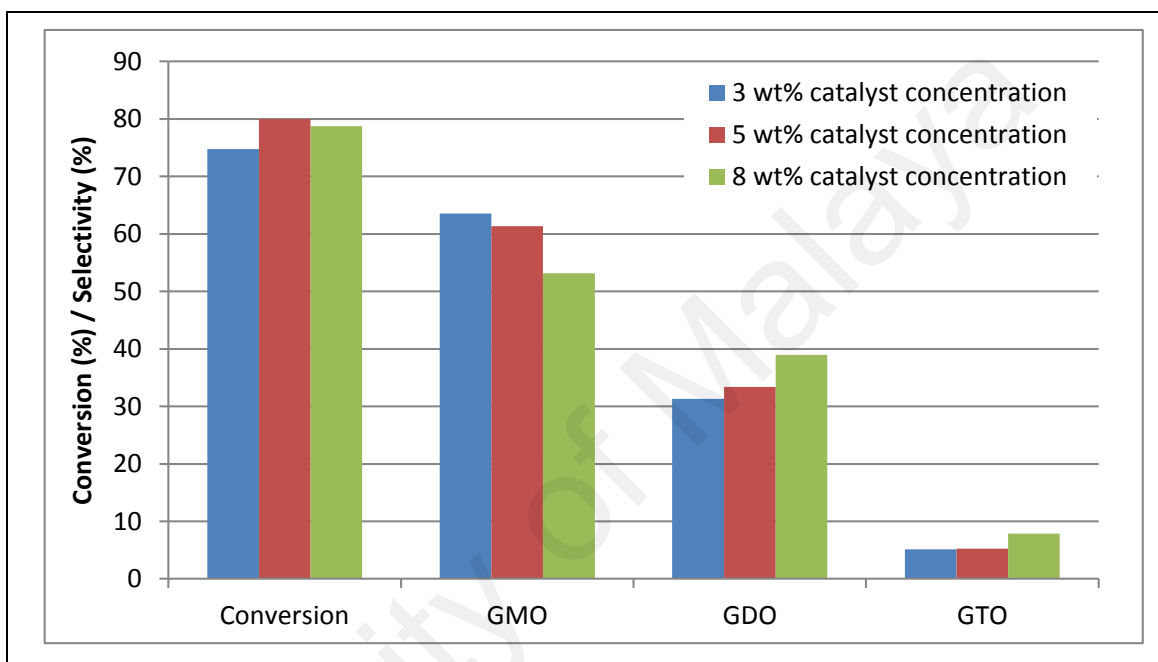
Figure 4.26: Effects of catalyst concentration on the conversion and selectivity at 240 min reaction time. Conditions: equimolar glycerol-to-OA ratio; reaction temperature, 160 °C and speed, 650 rpm

The influence of catalyst concentration on the formation trend of GMO, GDO and GTO in terms of selectivity is elaborated in Figure 4.27. The selectivity profile of GMO decreased with increased catalyst concentration. The GMO selectivity curve for the 8 wt% catalyst concentration markedly decreased, particularly from 15 min to 180 min. Moreover, 5 wt% and 8 wt% catalyst concentrations achieved high tendency to form GDO and GTO. However, the formation ratios in terms of selectivity were almost identical. In brief, the conversion acquired from ZrO_2-SiO_2-Me&EtPhSO$_3$H_70-

catalysed glycerol esterification with OA was 88.2% with 53.5% of GMO and 39.6% of GDO selectivity at 5 wt% catalyst concentration, 160 °C, equimolar reactant ratio and 480 min reaction time.
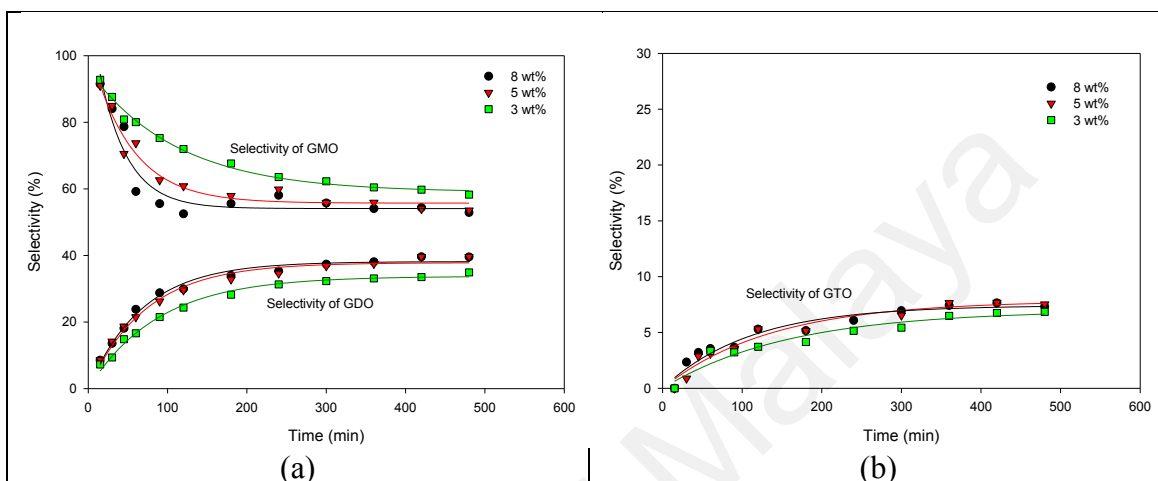
Figure 4.27: Effects of the catalyst concentration of ZrO_2-SiO_2-Me&EtPhSO$_3$H_70 on the selectivities of GMO, GDO and GTO

4.4.4.1 Interaction effects of catalyst concentration and reaction time

The interaction effects of catalyst concentration and reaction time on conversion and selectivity were also investigated. The aforementioned section reported that 3 wt% catalyst concentration, 240 min reaction time and an equimolar ratio of OA and glycerol resulted in 74% conversion and 63.6% of GMO selectivity (about 95% of combined selectivity of GMO and GDO).

The interaction plot in Figure 4.28 indicates that a short reaction time (180 min), 5 wt% catalyst concentration and an equimolar ratio of reactants realized a conversion of 74% and 62.5% selectivity of GMO (approximately 95.8% combined selectivity of GMO and GDO). Additionally, extending the reaction time to 240 min under the same reaction parameters (5 wt% catalyst concentration, equimolar ratio of OA to glycerol

and 650 rpm) achieved a conversion of 80% and about 60% selectivity of GMO, with a low combined GMO and GDO selectivity (94.8%). Consequently, 240 min reaction time was suggested for the catalytic esterification of glycerol with OA in the presence of 5 wt% of ZrO_2-SiO_2-Me&EtPhSO$_3$H_70 catalyst with the use of equimolar reactants.
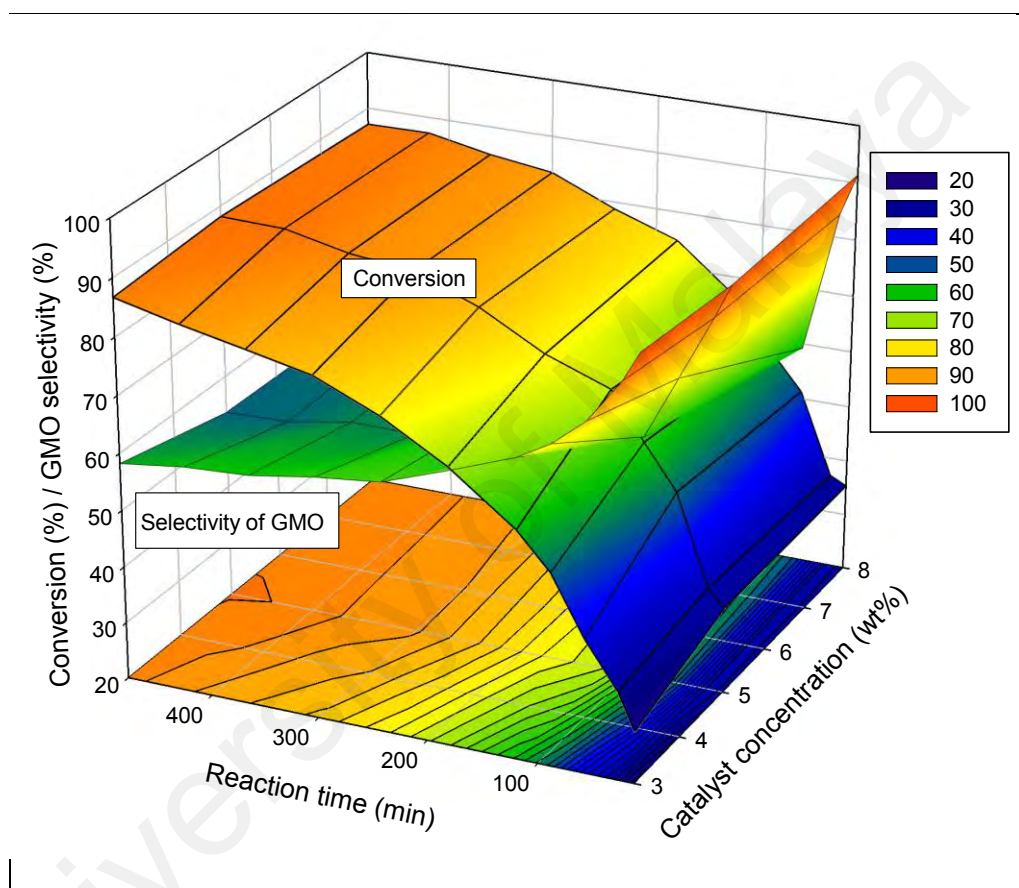
Figure 4.28: Interaction effects of catalyst concentration and reaction time on the conversion and GMO selectivity at an equimolar ratio of OA and glycerol, reaction temperature of 160 °C and speed of 650 rpm

4.4.4.2 Interaction effects of catalyst concentration and reaction temperature

The interaction effects of catalyst concentration and reaction temperature were studied comprehensively at 240 and 480 min in Figure 4.29(a) and (b), respectively. These two response surface diagrams display a similar relation curve but different

intersection points shown between the conversion and selectivity of GMO. At 240 and 480 min, the conversion can be increased in two ways: increasing the reaction temperature and the catalyst concentration. The effect of catalyst concentration was much significant at a short reaction time of 240 min.

An increased GMO selectivity can be obtained at a low reaction temperature and a high catalyst concentration. At 240 min, the GMO selectivity was highly dependent on the reaction temperature (an inclined curve was obtained). By contrast, the GMO selectivity was less dependent on the reaction temperature at a long reaction time. Figure 4.29(b) shows that at a low range of reaction temperature (100 °C–125 °C), the GMO selectivity was high when a high loading catalyst amount was used. In conclusion, a high conversion (more than 80%) and selectivity of GMO (about 60%) can be achieved at 480 min reaction time, equimolar reactant ratio, 160 °C and 650 rpm.
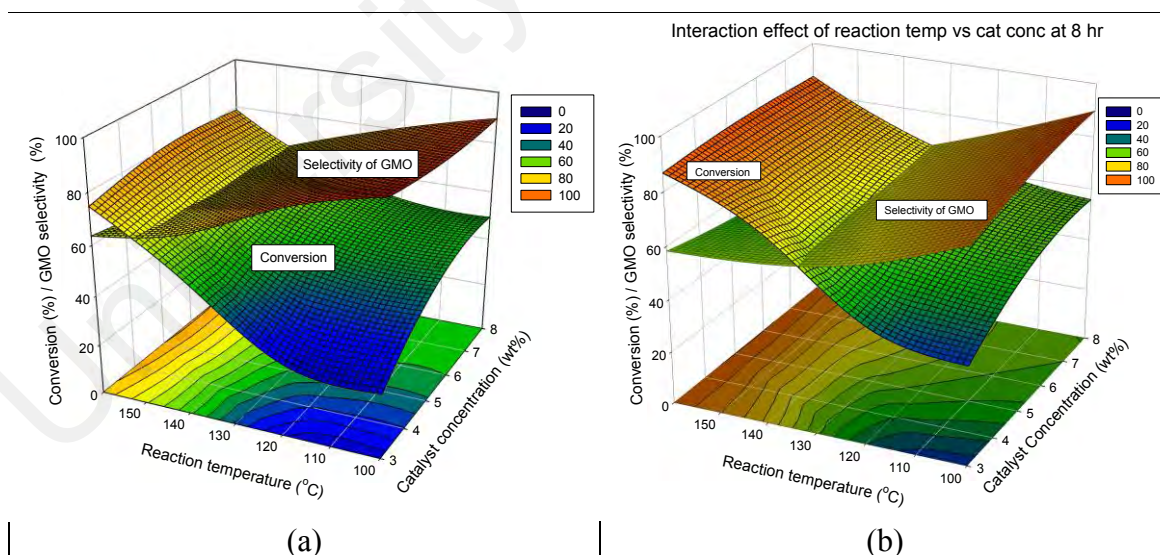

Figure 4.29: Interaction effects of catalyst concentration and reaction temperature on the conversion and GMO selectivity at (a) 240 and (b) 480 min reaction time, equimolar ratio of OA and glycerol, reaction temperature of 160 °C and speed of 650 rpm

4.4.4.3 Interaction effects of catalyst concentration and molar ratio

The interaction effects of catalyst concentration and molar ratio on the selectivity and product conversion should be studied. Figure 4.30 clearly illustrates that equimolar glycerol-to-OA ratio enhanced the production of high GMO yield; the GMO selectivity decreased by increasing glycerol feeding in reaction at 240 min reaction time and 160 °C reaction temperature. The plot also highlighted that the influence of molar ratio on conversion was insignificant compared with the significant effect of catalyst concentration. The increased catalyst concentration also resulted in an increased conversion. At constant molar ratio of reactants, low catalyst concentration was preferred in acquiring a high GMO selectivity.
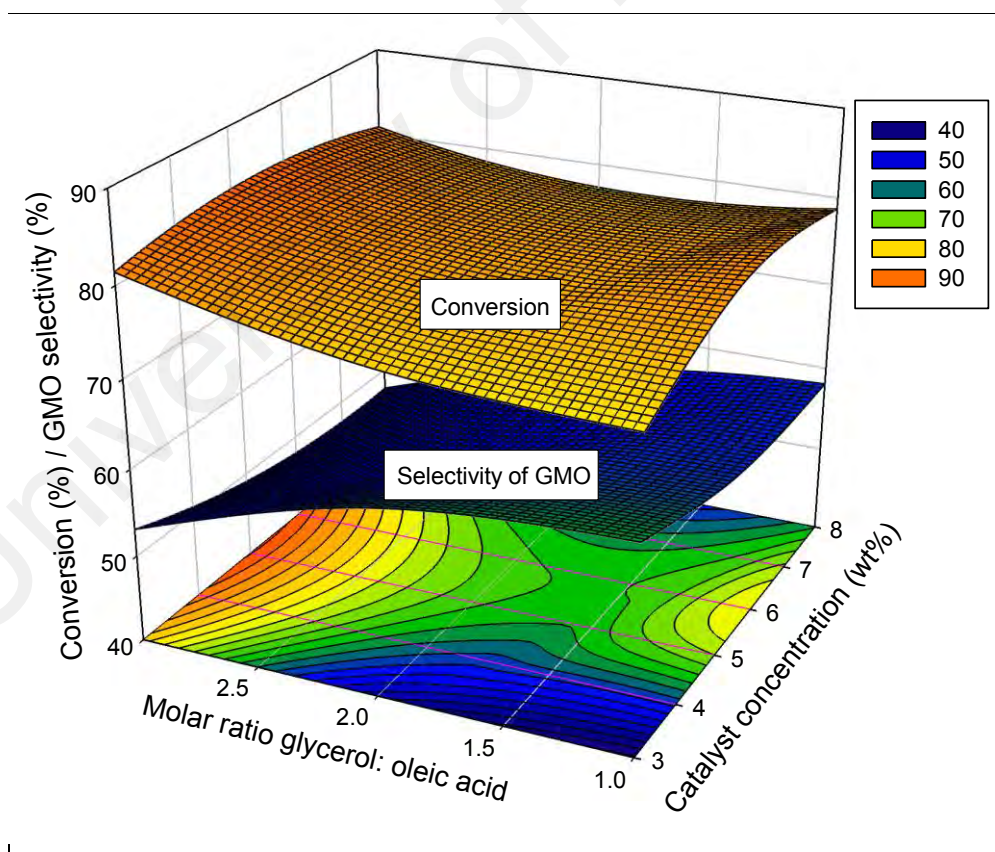
Figure 4.30: Interaction effects of the glycerol-to-oleic acid molar ratio and catalyst concentration on the conversion and GMO selectivity at reaction temperature of 160 °C, reaction time of 240 min and speed of 650 rpm

4.4.5 Catalyst stability studies

The stability of the ZrO_2-SiO_2-Me&EtPhSO$_3$H_70 catalyst was studied by separating the reaction mixture after reaction. The recovered catalyst was directly applied in the subsequent reaction cycle without any further treatment. The catalyst recyclability experiments were performed under the following optimised operating parameters: 160 °C, temperature; 5 wt%, catalyst concentration; equimolar glycerol-to-OA ratio; 650 rpm, stirring speed; and 480 min reaction time. Catalyst recyclability and stability experiment revealed that the yield decreased with the number of uses (Figure 4.31). The yield was reduced from 83%, 74% and 69% in accordance with the number of times of usage. Herein, yield refers to the total GMO, GDO and GTO in product mixtures, respectively. This trend may be attributed to that the GTO product blocks the active centres of the catalyst or the hydrophobic properties are lost (Zhang et al., 2017). The contact angle analysis result of the spent catalyst was inferior (31.9°) to that of the newly developed catalyst with 41.5° (Figure 4.32). The decreased yield also indicated the formation of the potential side products, such as acrolein, polyglycerol or polyglycerol esters (Jérôme et al., 2008). This result showed that the good hydrophobicity of a catalyst most probably minimised the undesirable side reaction.

The BJH plots and N_2 adsorption–desorption isotherms for the fresh and spent catalysts of ZrO_2-SiO_2-Me&EtPhSO$_3$H_70 are shown in Figure 4.33. The pore size distribution was unevenly distributed at the low surface area of the spent catalyst, which was most probably due to the existence of less-ordered structures of silica (Estevez et al., 2016) and the adherence of triglycerides/compounds within the pore of the spent samples (FESEM image of spent catalyst, Figure 4.34).
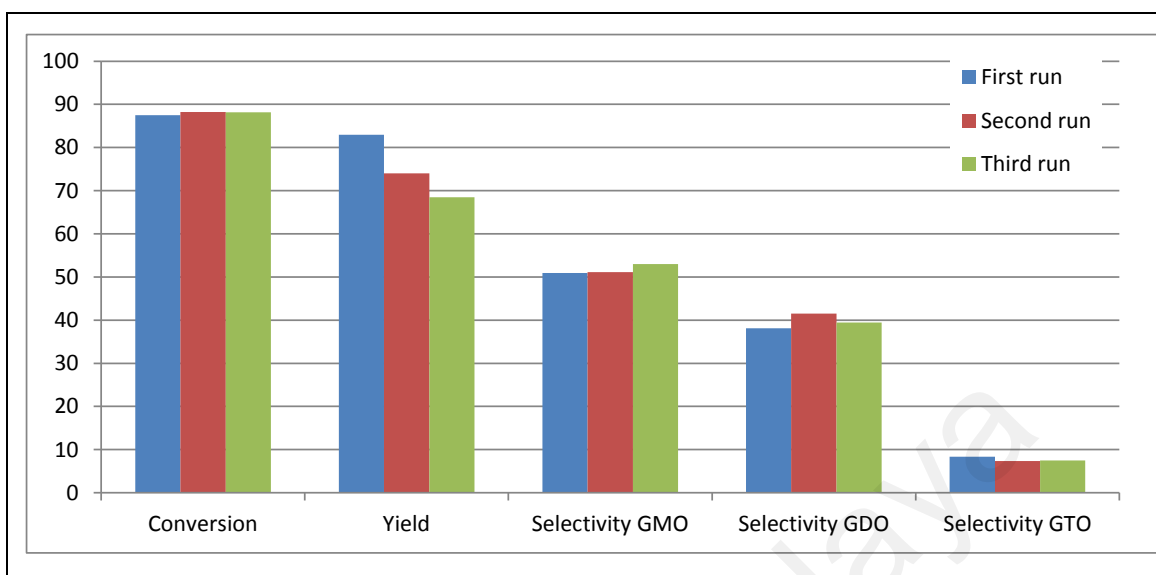
Figure 4.31: Catalyst stability study on the ZrO_2-SiO_2-Me&EtPhSO$_3$H_70 catalyst at an equimolar glycerol-to-oleic acid ratio, 5 wt% catalyst concentration of OA, 160 °C reaction temperature, 650 rpm speed and 480 min reaction time
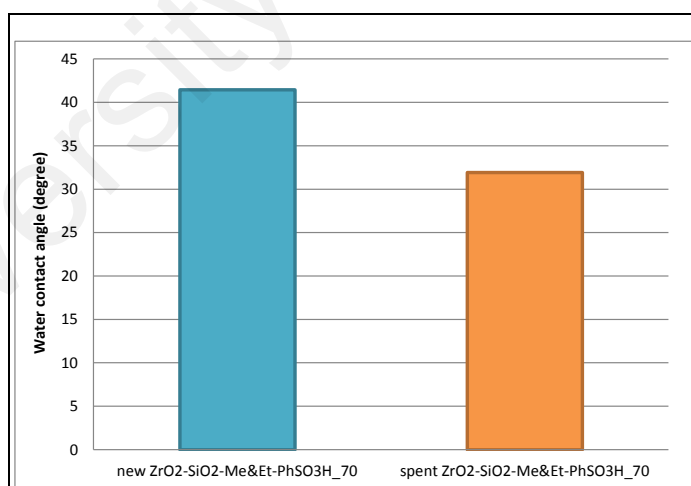
Figure 4.32: Water contact angle results for new and spent ZrO_2-SiO_2-Me&EtPhSO$_3$H_70 catalyst
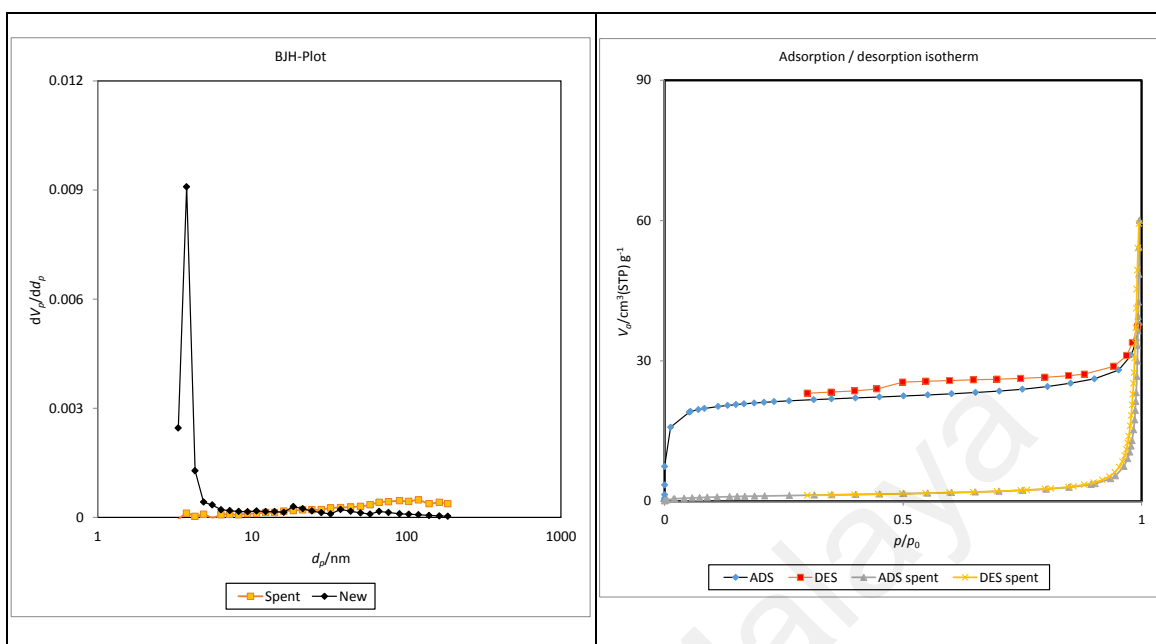
Figure 4.33: BJH plot and N$_2$ adsorption–desorption isotherms of new and spent ZrO$_2$-SiO$_2$-Me&EtPhSO$_3$H_70 catalyst
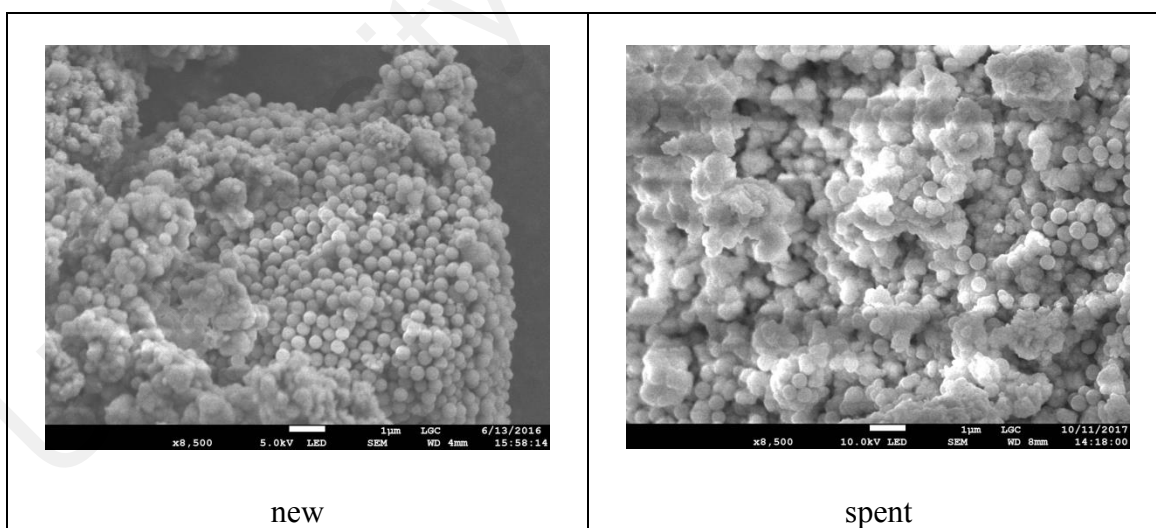
Figure 4.34: FESEM images of new and spent ZrO$_2$-SiO$_2$-Me&EtPhSO$_3$H_70 catalyst

4.5 Catalytic activity comparison of ZrO₂-SiO₂-Me&EtPhSO₃H_70 with conventional sulphated zirconia and commercial catalysts

This part investigated the comparative catalytic activity of ZrO_2-SiO_2-Me&Et-PhSO₃H_70 catalyst with three types of SO_4^{2-}/ZrO_2 catalysts, which were developed from three different zirconium precursors. The first SO_4^{2-}/ZrO_2 was prepared using a sol–gel method with a $Zr(OCH_2CH_3)_4$ precursor (labelled as SO_4^{2-}/ZrO_2 sol gel). Precipitation method was used to prepare SO_4^{2-}/ZrO_2 (SO_4^{2-}/ZrO_2 precipitation) by using $ZrOCl_2 \cdot 8H_2O$ precursor. SO_4^{2-}/ZrO_2 commercial was developed using a commercially available $Zr(OH)_4$. The reaction performance was related to the properties of each catalyst.

4.5.1 SO_4^{2-}/ZrO_2 catalyst characterisation and performance evaluation

The designed catalyst (ZrO_2-SiO_2-Me&Et-PhSO₃H_70) and three SO_4^{2-}/ZrO_2 catalysts were characterised by controlling the acidity amount at 1.55 mmol H^+ under optimised reaction conditions. The textural properties and hydrophobicity of each catalyst are summarised in Table 4.7. The acidity of SO_4^{2-}/ZrO_2 catalysts ranged from 0.35 mmol/g to 0.62 mmol/g. With regard to the influence of catalyst acidity on the reaction activity and selectivity, comparative studies were carried out at a constant concentration of 1.55 mmol H^+ to investigate the effect of textural property in a reaction performance. Factors affecting the total performance of catalyst, especially when studying the complex catalyst structure, should be determined (Ogino, Suzuki, & Mukai, 2017).

The surface areas of SO_4^{2-}/ZrO_2 catalysts prepared using different precursors (SO_4^{2-}/ZrO_2 sol gel, SO_4^{2-}/ZrO_2 precipitation and SO_4^{2-}/ZrO_2 commercial) were 85.29, 44.91 and 60.06 m²/g, respectively, and these results also agreed with those synthesised by (Oh et

al., 2013a). In addition, the hydrophobicity of each catalyst was examined. Result showed that all SO_4^{2-}/ZrO_2 catalysts, regardless of the presence of Zr precursors, were less hydrophobic (as the obtained contact angle degree was low) compared with that of the designed catalyst ZrO_2-SiO_2-Me&Et-PhSO$_3$H_70.

Table 4.7: Textural properties of the different types of SO_4^{2-}/ZrO_2 catalysts and ZrO_2-SiO_2-Me&EtPhSO$_3$H catalyst

Catalysts	BET			Acidity (mmol/g)	Particle size distribution (μm)	Contact angle analysis (degree)
	Area [a] (m²/g)	Pore volume [b] (cm³/g)	Average pore diameter [b] (nm)			
ZrO_2-SiO_2-Me&Et-PhSO$_3$H_70	79.75	0.0247	3.77	0.62	5.01	41.5
SO_4^{2-}/ZrO_2 sol gel	85.29	0.475	4.85	0.61	11.3	9.0
SO_4^{2-}/ZrO_2 precipitation	44.91	0.079	3.77	0.35	4.36	12.1
SO_4^{2-}/ZrO_2 commercial	60.06	0.240	3.77	0.44	125	10.8

[a] Total surface area was determined using BET equation; [b] pore volume and average pore diameter were determined using BJH method

Figure 4.35 shows the catalytic activities of ZrO_2-SiO_2-Me&Et-PhSO$_3$H_70 and SO_4^{2--}/ZrO_2 catalysts. Dissimilar to ZrO_2-SiO_2-Me&Et-PhSO$_3$H_70 catalyst, SO_4^{2-}/ZrO_2 sol gel-catalysed reaction produced considerably high conversion (93.0%) and selectivity of GDO; (61.3%) in a short reaction time of 240 min (Figure 4.35(a)), whereas further extending the reaction time to 480 min increased the GDO conversion and selectivity to approximately 75% and 20%, respectively (Figure 4.35(b)). SO_4^{2-}/ZrO_2 sol gel catalyst produced the highest amount of GDO and GTO at optimised

reaction conditions. The obtained selectivity for SO_4^{2-}/ZrO_2 $_{precipitation}$ (S_{GMO} = 59% and S_{GDO} = 36%) was comparable to that of ZrO_2-SiO_2-Me&Et-PhSO$_3$H_70 (S_{GMO} = 61% and S_{GDO} = 33%) at 240 min. A long reaction time (480 min) for SO_4^{2-}/ZrO_2 $_{precipitation}$ catalyst can obtain equal selectivities of GMO and GDO (both 46%). SO_4^{2-}/ZrO_2 $_{commercial}$ achieved a high conversion profile and GDO selectivity at 480 min, (C=93%, S_{GMO} = 17% and S_{GDO} = 66%), but its GDO selectivity was much lower than that of the SO_4^{2-}/ZrO_2 $_{sol\ gel}$ (S_{GDO} = 74.6%) at 480 min.

The resultant trends showed that the SO_4^{2-}/ZrO_2 catalysts generally presented better conversions than that of ZrO_2-SiO_2-Me&Et-PhSO$_3$H_70 but with a much lower yield. The high conversion (94%), low yield (39%) and high selectivity for GDO and GTO (S_{GDO}= 75% and S_{GTO}= 20%) at 480 min of the SO_4^{2-}/ZrO_2 $_{sol\ gel}$-catalysed reaction were highly attributed to the catalyst's pore volume or high accessibility of the organic reactants to the active sites (Kuwahara, Kaburagi, Nemoto, & Fujitani, 2014). The formation rates of the high-molecular-weight GDO and GTO were fast for the catalyst with high pore volume (SO_4^{2-}/ZrO_2 $_{sol\ gel}$, 0.475 m^2/g) and (SO_4^{2-}/ZrO_2 $_{commercial}$, 0.240 m^2/g), which may subsequently lead to undesirable product formation. Remarkably, the role of catalyst hydrophobicity was effective in obtaining a high product yield. Therefore, the correlation between the structure/property of catalysts and the catalytic performance was investigated in the following section. Understanding the correlation characteristics of catalyst to reaction is vital in developing effective catalysts (Diao, He, Yang, Wang, & Zhang, 2015).
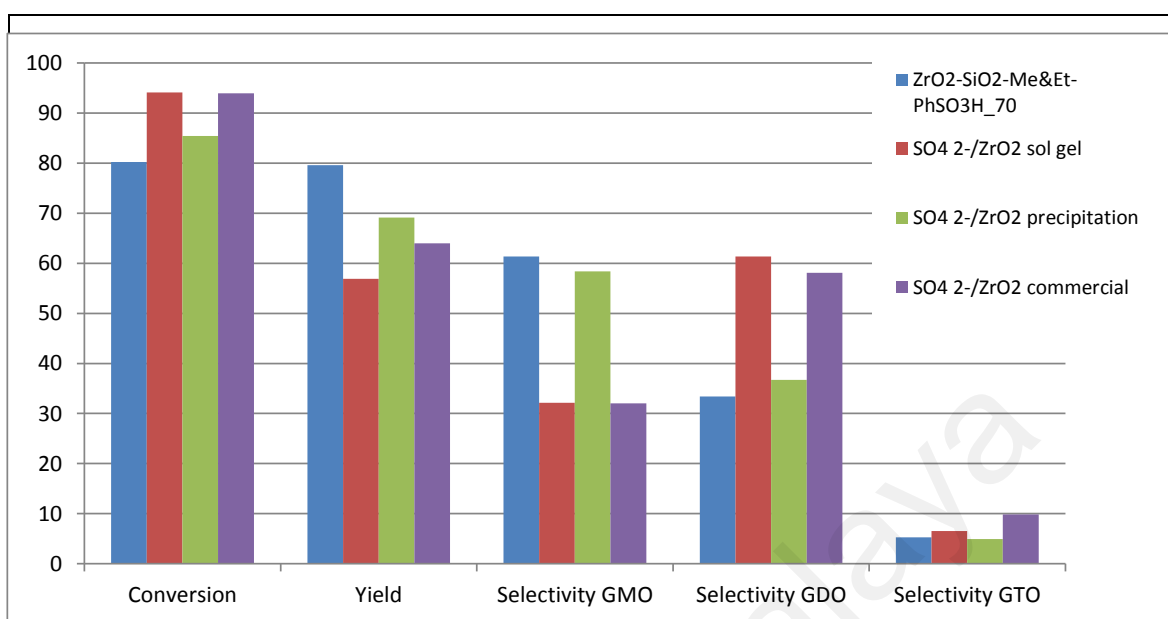
(a)
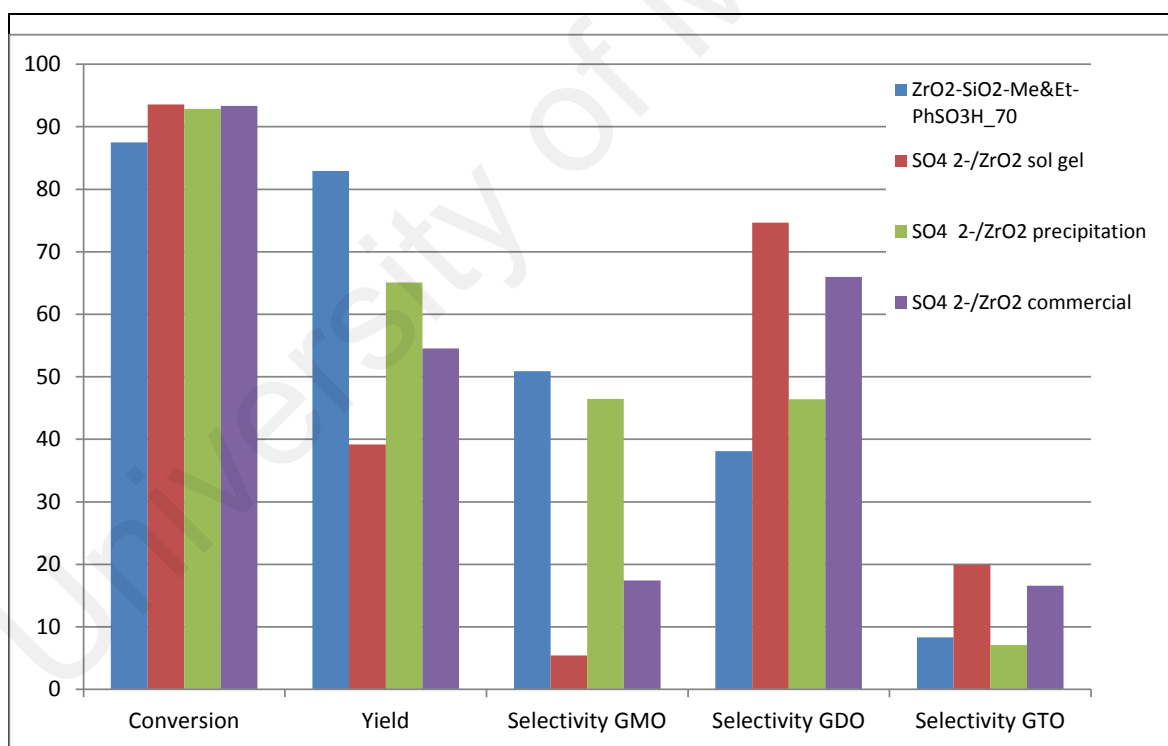
(b)

Figure 4.35: Comparison of the catalytic activities of various Zr-based catalysts. All reactions were conducted at constant amount of 1.55 mmol H$^+$, equimolar ratio of OA and glycerol, reaction temperature of 160 °C and 650 rpm stirring speed for 240 min (a) and 480 min (b)

4.5.2 Correlation between SO_4^{2-}/ZrO_2 catalyst properties and selectivities/activities

Two correlations were successfully established. Firstly, the correlation between structural properties and selectivity was made. The correlation of hydrophobicity with selectivity/initial reaction rate was also proven.

4.5.2.1 Correlation between structural properties and selectivity

The aforementioned XRD results indicated that ZrO_2-SiO_2-Me&Et-PhSO$_3$H catalyst mainly consisted of a monoclinic phase and a minor tetragonal phase. Comparison of the XRD results of different types of SO_4^{2-}/ZrO_2 catalysts with ZrO_2-SiO_2-Me&Et-PhSO$_3$H can provide correlation between the structural properties and the selectivities of product mixture.

Figure 4.36 demonstrates the XRD patterns for various catalysts. All SO_4^{2-}/ZrO_2 catalysts possessed highly tetragonal phase and less monoclinic phase. The acidic tetragonal phase may be stabilised by sulphated group (Oh et al., 2013a). XRD results also clearly revealed that ZrO_2-SiO_2-Me&Et-PhSO$_3$H catalyst was composed of a more thermodynamically stable monoclinic phase than those of other SO_4^{2-}/ZrO_2 catalysts. The monoclinic diffractions at 16°, 26°, 28° and 32° were more intense than those of SO_4^{2-}/ZrO_2 precipitation (c) and SO_4^{2-}/ZrO_2 commercial (d). Notably, no monoclinic peak was observed at SO_4^{2-}/ZrO_2 sol gel (b), but a crystalline tetragonal phase was mostly detected. This result reasonably agreed with the highest pore volume (0.475 cm^3/g) and pore size (4.85 nm) of SO_4^{2-}/ZrO_2 sol gel obtained in the BET results. The tetragonal phase was highly attributed to the different precursors used with identical calcination temperature and calcined time. Crystallinity was also proven affected with the type of zirconia precursor (Rashad & Baioumy, 2008).
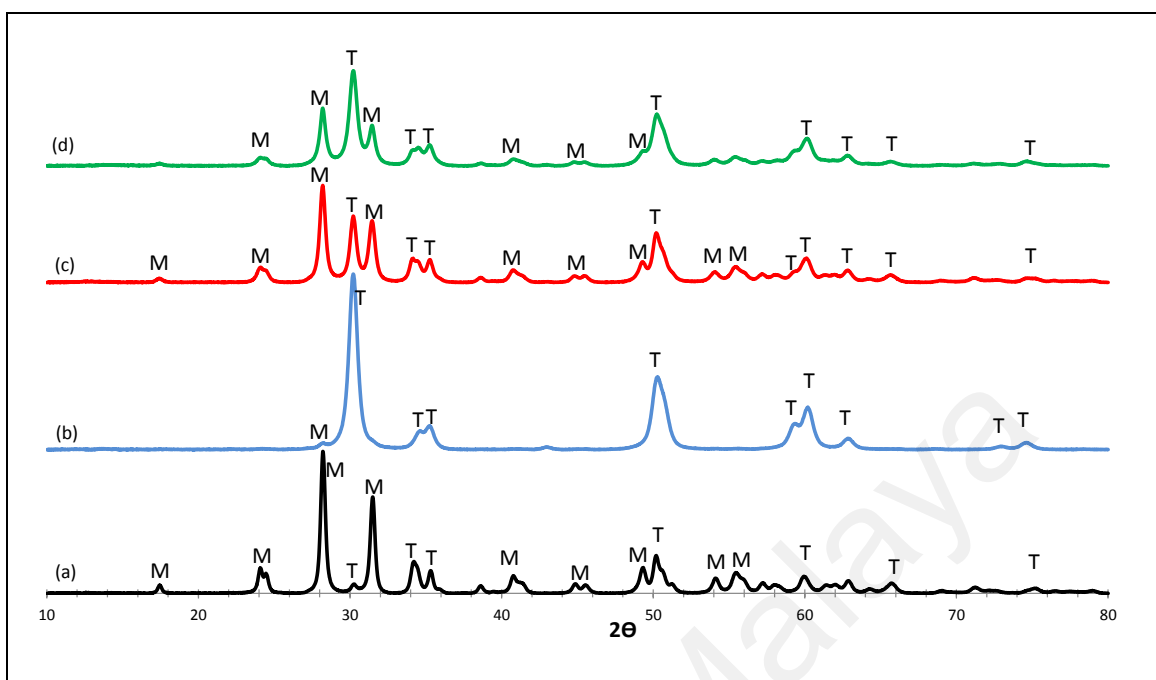
Figure 4.36: XRD patterns of (a) ZrO$_2$-SiO$_2$-Me&Et-PhSO$_3$H_70, (b) SO$_4^{2-}$/ZrO$_2$ sol gel, (c) SO$_4^{2-}$/ZrO$_2$ precipitation and (d) SO$_4^{2-}$/ZrO$_2$ commercial

Figure 4.37 displays the correlation between pore volume versus conversion and selectivity. The experimental results fitted with the curve representing selectivity and conversion. This work proved the importance of pore volume in controlling product selectivity. Notably, increasing the pore volume of a catalyst can increase the formation of GDO and GTO with large molecular sizes. Furthermore, GMO formation was unfavourable when catalysed by catalyst with a large pore volume. The conversion rate increased gradually with the increased catalyst pore volume.

The pore size (average pore diameter (nm); Table 4.7) was correlated with product selectivity, but the outcome was irrational because the obtained average pore diameter mostly ranged at the same peak (3.77 nm). Nevertheless, a remarkable phenomenon was observed in the BJH plot of different catalysts (Figure 4.38). The high selectivities of

GDO and GTO detected in the reaction mixtures using the SO_4^{2-}/ZrO_2 $_{sol}$ $_{gel}$ and SO_4^{2-}/ZrO_2 $_{commercial}$ catalysts were attributed to their macroporous sizes, which exceeded 50 nm, and mesoporous catalyst. Nonetheless, the pore sizes of ZrO_2-SiO_2-Me&Et-PhSO$_3$H_70 and SO_4^{2-}/ZrO_2 $_{precipitation}$ were highly uniform in less than 15 nm. The BJH plots of each catalyst clarified the influence of pore size on product selectivity. The FESEM images, FTIR profile and TGA curve of ZrO_2-SiO_2-Me&Et-PhSO$_3$H_70, SO_4^{2-}/ZrO_2 $_{sol}$ $_{gel}$, SO_4^{2-}/ZrO_2 $_{precipitation}$ and SO_4^{2-}/ZrO_2 $_{commercial}$ are presented in Appendix A.
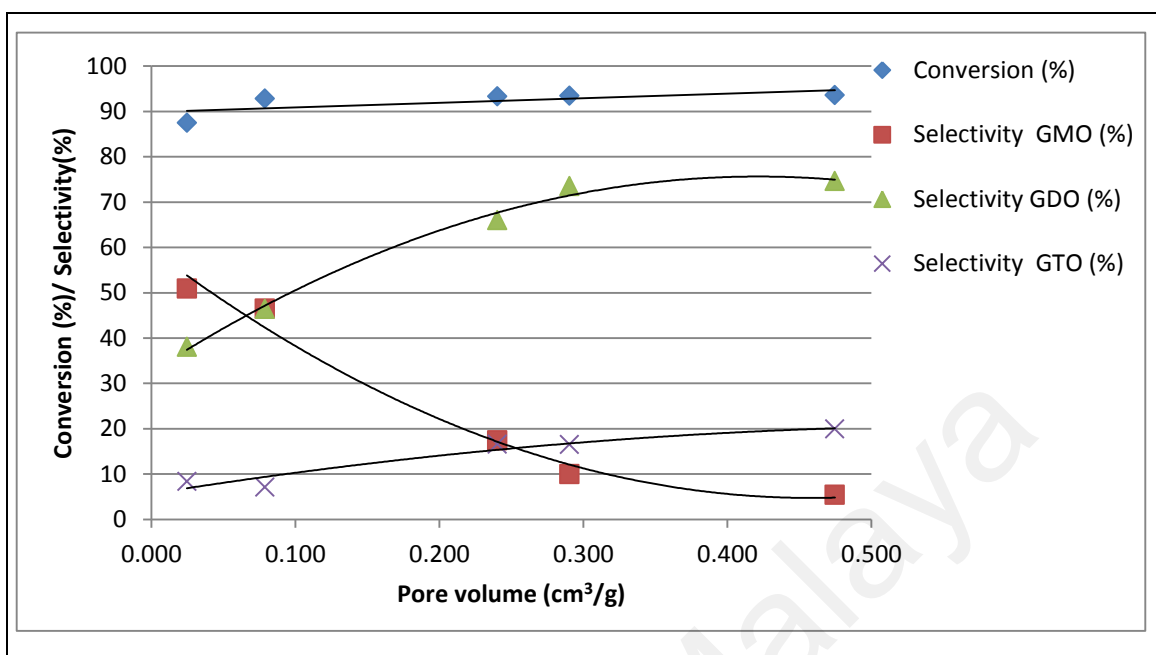
Figure 4.37: Correlation of pore volume with conversion and selectivity at the constant acidity of 1.55 mmol H$^+$ and other operating parameters
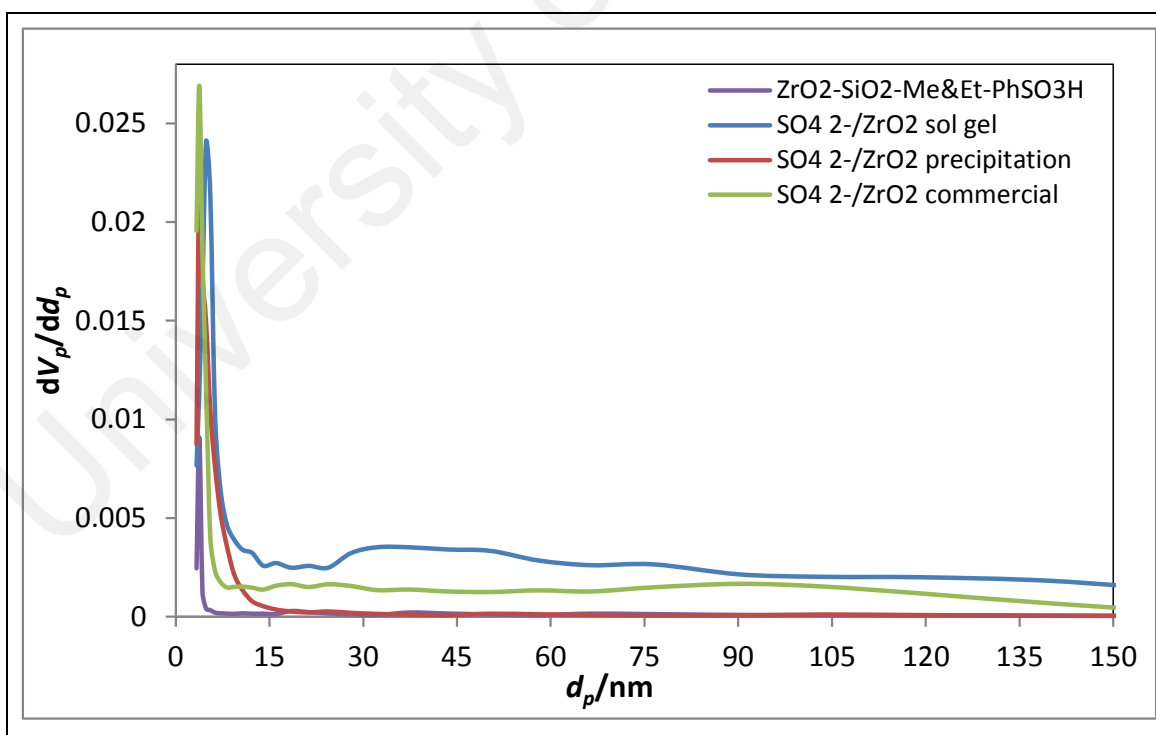
Figure 4.38: BJH plots of (a) ZrO$_2$-SiO$_2$-Me&Et-PhSO$_3$H_70, (b) SO$_4^{2-}$/ZrO$_2$ $_{sol}$ $_{gel}$, (c) SO$_4^{2-}$/ZrO$_2$ $_{precipitation}$ and (d) SO$_4^{2-}$/ZrO$_2$ $_{commercial}$

124

4.5.2.2 Correlation between hydrophobicity and selectivity/initial reaction rate

The correlation of catalyst hydrophobicity with the selectivity of reactions was evaluated. Figure 4.39 demonstrates that the increased hydrophobicity of a catalyst decreased the conversion rate. Unlike the pore textural properties, the increased hydrophobicity enhanced the GMO formation. However, the GDO and GTO selectivities decreased with improved hydrophobicity. Despite the decreased hydrophobicity and the total conversion of reaction at 8 h, the initial reaction rate or turnover frequency, which was calculated during the first 15 min reaction time, indicated that a catalyst with improved hydrophobicity displayed an increased turnover frequency value (Table 4.8). Surface hydrophobicity plays an important role in esterification reactions with polyols (glycerol) (Kotwal et al., 2013).
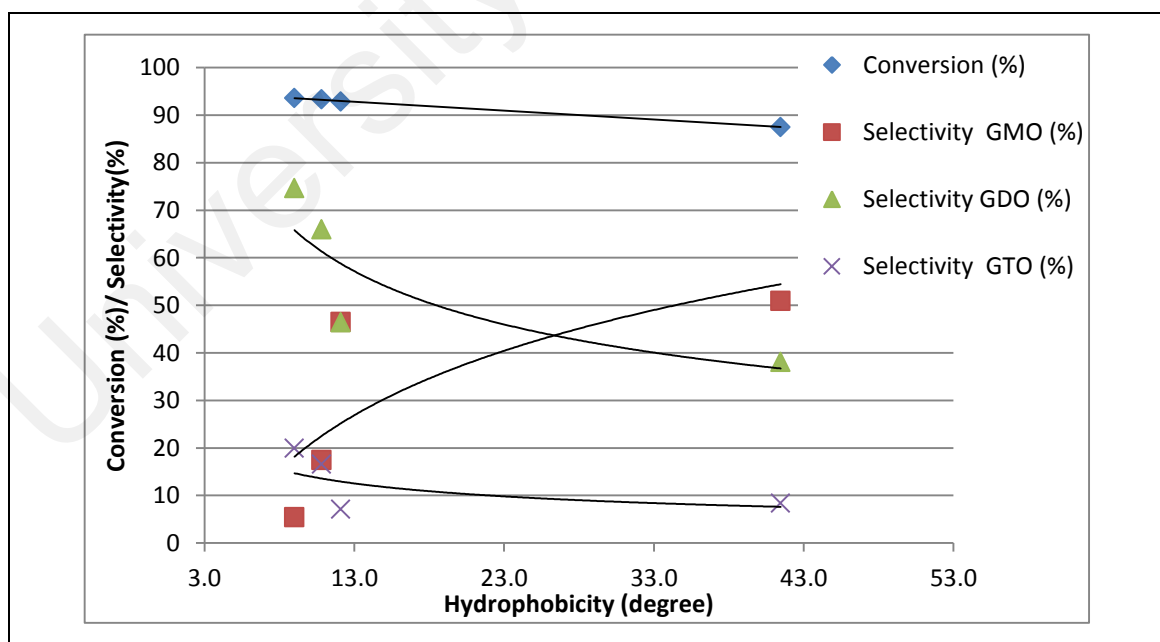
Figure 4.39: Correlation between hydrophobicity and the conversion and selectivity at the constant acidity of 1.55 mmol H$^+$ and operating parameters

Table 4.8: Turnover frequency of each catalyst during the first 15 min of reaction

Entry	Catalyst	TOF (h^{-1})^{a}
1	ZrO_2-SiO_2-Me&Et-$PhSO_3H$_70	61.4
2	SO_4^{2-}/ZrO_2 sol gel	48.7
3	SO_4^{2-}/ZrO_2 precipitation	47.9
4	SO_4^{2-}/ZrO_2 commercial	57.5

^{a}Turnover Frequency (TOF)= total number of moles transformed into the desired product by one mole of active site per initial 15 min of reaction time

4.5.3 Commercial Amberlyst 15 and Aquivion characterisations and performance evaluations

A comparative study between ZrO_2-SiO_2-Me&Et-$PhSO_3H$_70 and the commercially available Amberlyst 15 and polymeric perfluorosulfonic acid (PFSA) Aquivion was performed under optimised operating reaction conditions in the glycerol esterification with OA. Aquivion PFSA is a copolymer based on tetrafluoroethylene and the sulfonyl fluoride vinyl ether catalyst from Solvay Specialty Polymers. Aquivion is a perfluorosulfonic superacid resin with a relatively high acid strength, high thermal stability and approximately −12 Hammett acidity (comparable to the acid strength of H_2SO_4) (Fang et al., 2016). Amberlyst 15 is a conventional macroporous sulphonic ion exchange resin with 120 °C thermal stability (Kong et al., 2015). The catalyst characteristics are summarised in Table 4.9. Although the ion exchange capacity of Aquivion PFSA (1.0 mequiv/g) used in this study is lower than that of Amberlyst 15 (4.7 mequiv/g), the Hammett acidity function of Amberlyst 15 ($H_0 = −2$) is considerably

lower than that of the superacid Aquivion ($H_0 = -12$) (Karam et al., 2016). Thus, the influences of the different acidity strengths of catalysts were observed in the present work.

The surface area, pore volume, particle size distribution and acidity strength of these three catalysts differed. The distribution phenomenon of each catalyst was also examined in a polar and nonpolar solvent (within a layer of immiscible toluene–water phase), and result is demonstrated in Figure 4.40. Aquivion were located on the interface between toluene and water. Nevertheless, Aquivion exhibited an amphiphilic property because it was only located on the interface between toluene and water, unlike the Me&Et-PhSO$_3$H-SiO$_2$-ZrO$_2$, which was distributed in the toluene phase. By contrast, Amberlyst 15 was immersed in the bottom-water phase.

Table 4.9: Comparison of the textural properties of ZrO$_2$-SiO$_2$-Me&EtPhSO$_3$H catalyst with those of commercial Amberlyst 15 and Aquivion catalyst

Catalysts	BET			Acidity	Particle size distribution (μm)
	Area (m^2/g)	Pore volume (cm^3/g)	Average pore diameter (nm)		
ZrO$_2$-SiO$_2$-Me&Et-PhSO$_3$H_70	79.75	0.0247	3.77	0.62 mmol/g	5.01
Amberlyst 15	42.5	0.290	28.8	4.7 mequiv./g	300
Aquivion PFSA-superacid*	<0.1	-	-	0.98-1.06 mmol/g	660

*The characterization data of Aquivion was obtained from (Fang et al., 2015)
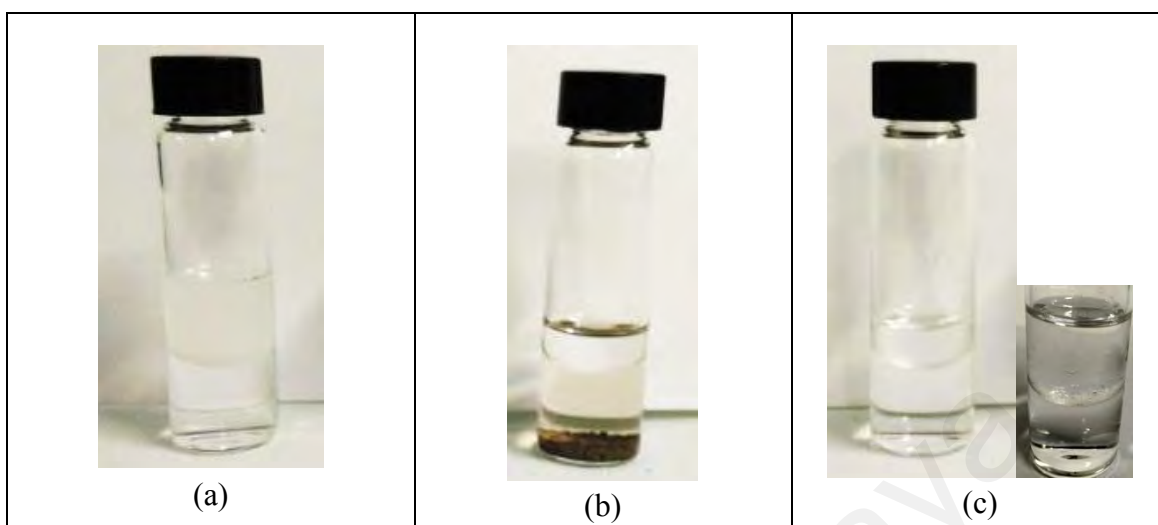
Figure 4.40: Sample photos of catalyst dispersed in toluene (top) and water (bottom): (a) Me&Et-PhSO$_3$H-SiO$_2$-ZrO$_2$, (b) Amberlyst 15 and (c) Aquivion

Three sets of experiments were performed under optimised conditions in glycerol esterification with OA in the presence of different catalysts, namely, ZrO$_2$-SiO$_2$-Me&EtPhSO$_3$H, Amberlyst 15 and Aquivion. Aquivion afforded the highest conversion, which was nearly 99% in 240 min reaction time (Figure 4.41 (a)). Approximately 98% conversion was obtained within 120 min reaction time. The formation rates of GDO and GTO were the fastest for Aquivion (S$_{GDO}$ = 69% and S$_{GTO}$ = 30%), although an equimolar ratio of reactants was used. This result was attributed to the strong acidity of Aquivion. A relatively low selectivity of GMO was obtained for Aquivion-catalysed reaction (< 3%). This finding suggested that the superstrong acidity of Aquivion is suitable in producing large GTO molecules at the OA-to-glycerol molar ratio of 3:1. Further lowering the loading amount of Aquivion (optimisation of catalyst concentration) is necessary to attain high yield and selectivity of GMO. Superstrong acid potentially produces undesirable side reaction products, such as acrolein, polyglycerol, alkene and polyglycerol esters. A long reaction time is unadvisable for

128

Aquivion-catalysed reaction because the yield and GTO selectivity were reduced (Figure 4.41(b)).

Results showed that Amberlyst 15 obtained a higher yield and selectivity for GDO and GTO (S_{GDO} = 65% and S_{GTO} = 12%) than those of the two other catalysts; this result can be attributed to the lower acidity strength of Amberlyst 15 (H_0 = −2) than that of Aquivion (H_0 = −12) and its larger pore size (28.8 nm) than that of ZrO_2-SiO_2-Me&EtPhSO$_3$H (3.77 nm). Prolonging the reaction time of Amberlyst 15 to 8 h increased the GDO and GTO selectivities (S_{GDO} = 74% and S_{GTO} = 16%).

ZrO_2-SiO_2-Me&EtPhSO$_3$H obtained the highest yield and GMO selectivity (60%), which proved that catalyst acidity is vital in controlling the conversion rate and yield. Firstly, a moderate acidity level of catalyst or suitable loading amount of catalyst is required to produce a high-yield product, and excess acidity may lead to side reaction. Secondly, textural properties, such as pore size/pore volume, influence the selectivity of a product significantly by controlling the pore size of catalyst to form the desired selectivity product.
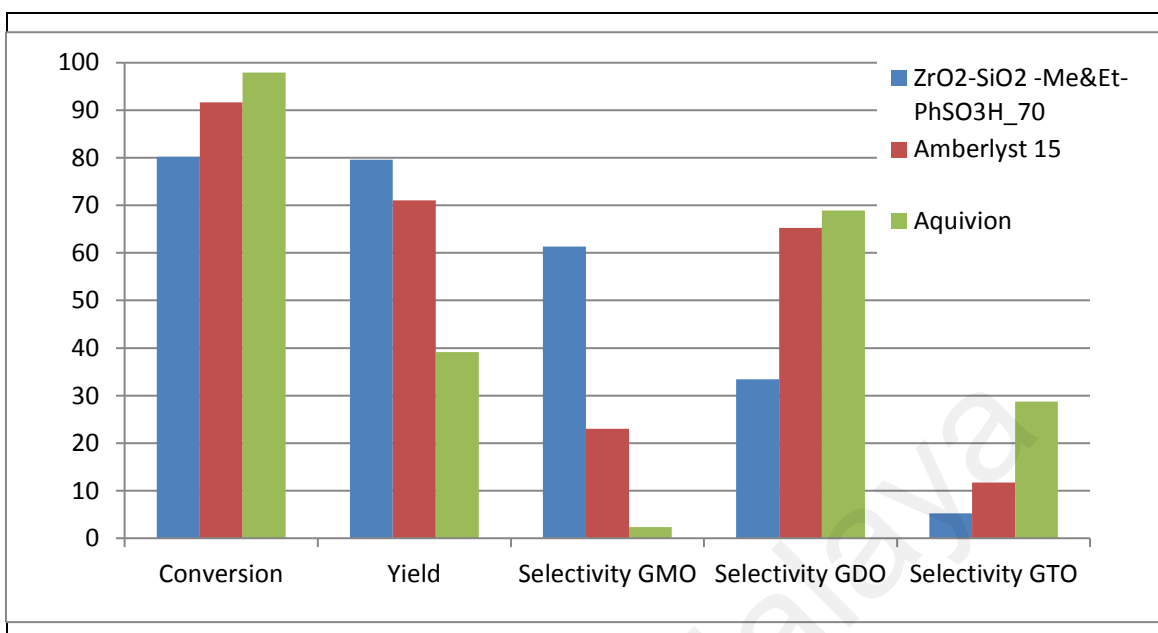
(a)
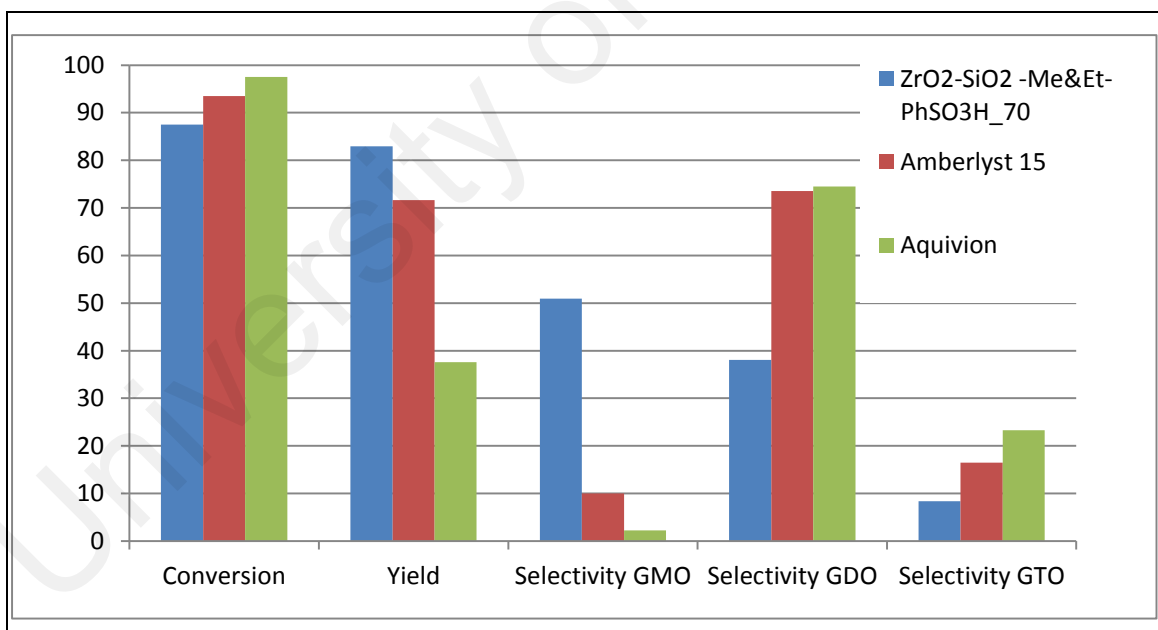
(b)

Figure 4.41: Comparison of the catalytic activities of ZrO$_2$-SiO$_2$-Me&EtPhSO$_3$H, Amberlyst 15 and Aquivion catalysts. All reactions were conducted at the constant acidity of 1.55 mmol H$^+$, equimolar ratio of OA and glycerol, reaction temperature of 160 °C and stirring speed of 650 rpm for 240 min (a) and 480 min (b)

The colour of the reaction medium catalysed by Me&Et-PhSO$_3$H-SiO$_2$-ZrO$_2$, Amberlyst 15 and Aquivion are displayed in Figure 4.42. The product colour increased according to the darkness level as follows: Me&Et-PhSO$_3$H-SiO$_2$-ZrO$_2$ > Amberlyst 15 > Aquivion. The darkest product mixture colour was that of Aquivion. This work revealed that the catalyst acid strength affected the colour product because the colour produced by Aquivion was similar to that of homogeneous catalyst, such as H$_2$SO$_4$ product.

To examine the influence of the strong acid strength of Aquivion, catalyst stability studies were carried out by using filtered and reused catalyst directly under optimised reaction conditions for 180 min. In Figure 4.43, the increased number of catalyst reusable times also increased the product yield. Notable increases in GMO selectivity in the third experimental run were also observed. The resultant trend confirmed the loss of strong catalyst active sites of Aquivion might attribute to the increasing of yield. Therefore, low catalyst acidity/moderate acidity amount is essential for glycerol esterification with OA.
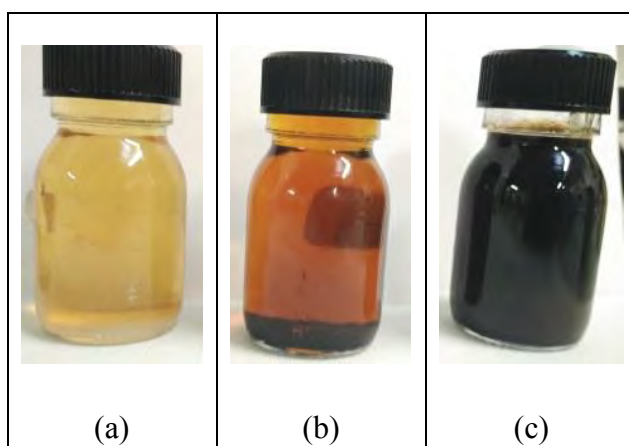
Figure 4.42: Colour of products catalysed by (a) Me&Et-PhSO$_3$H-SiO$_2$-ZrO$_2$, (b) Amberlyst 15 and (c) Aquivion
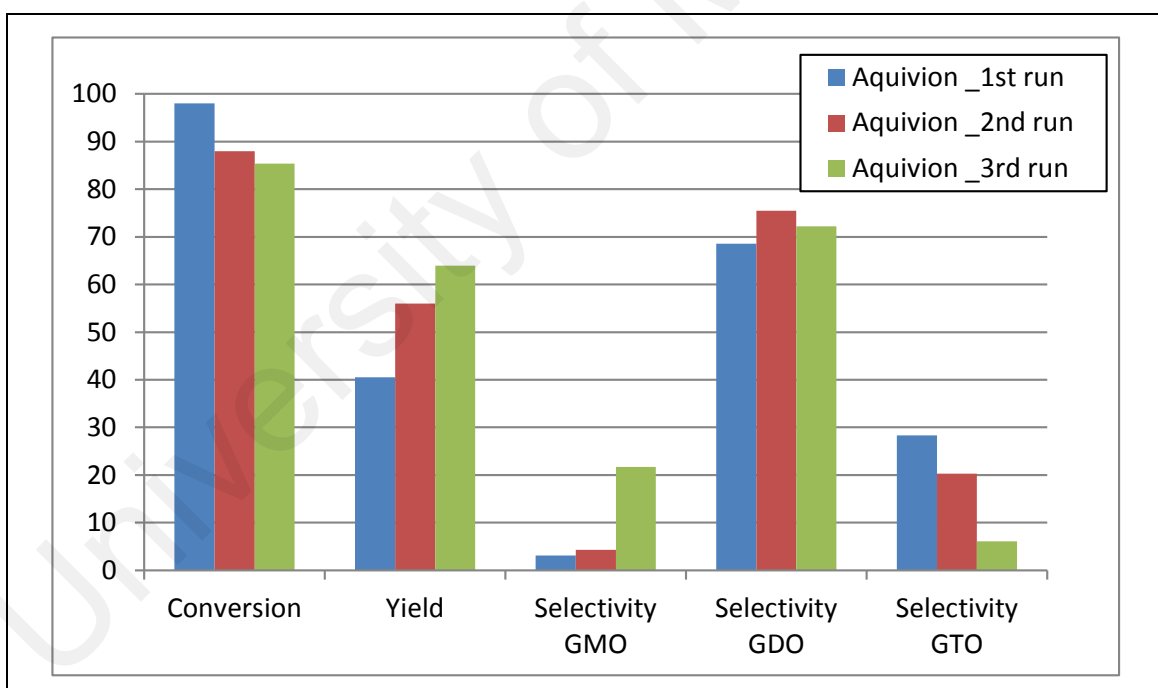
Figure 4.43: Catalyst stability studies on Aquivion at optimised reaction conditions: 1.55 mmol H$^+$, equimolar ratio of OA and glycerol, reaction temperature of 160 °C and stirring speed of 650 rpm for 180 min

CHAPTER 5: CONCLUSION AND RECOMMENDATION

5.1 Conclusion

This work developed a novel highly hydrophobic heterogeneous acid catalyst using ZrO_2-SiO_2 support. Silication enabled the adherence of SiO_2 on ZrO_2 support and resulted in the formation of ZrO_2-SiO_2. In addition, the loading amounts of TMMS and CSPETS were found vital in controlling the hydrophobicity and acidity of the catalyst. ZrO_2-SiO_2-Me&Et-PhSO$_3$H_70 catalyst with 70 mol% of TMMS and 0.62 mmol/g acidity was the optimal catalyst for glycerol esterification with OA. The catalyst hydrophobicity decreased with increased acidity. Furthermore, at constant catalyst acidity, a catalyst with increased hydrophobicity showed an improved yield. A comparative study on two catalysts with the same acidities (0.62 mmol/g) but different loadings of TMMS agent (ZrO_2-SiO_2-Me&EtPhSO$_3$H_50h and ZrO_2-SiO_2-Me&EtPhSO$_3$H_70) proved that ZrO_2-SiO_2-Me&EtPhSO$_3$H_70 with high TMMS agent amount can increase the product yield from 28.9% to 37.4% at 100 °C, 300 rpm and equimolar ratio of OA and glycerol.

ZrO_2-SiO_2-Me&Et-PhSO$_3$H_70 catalyst was applied during process optimisation study. Result showed an 80% conversion with a 59.4% GMO selectivity and 34.6% GDO selectivity (combined GMO and GDO selectivity = 94.8%) at the optimised conditions of equimolar OA-to-glycerol ratio, 160 °C reaction temperature and 5 wt% catalyst concentration with respect to the OA weight for 4 h. After prolonging the reaction time to 8 h under the same operating parameters, 88.2% conversion with 53.5% GMO selectivity and 40.0% GDO selectivity (combined GMO and GDO selectivity = 94%) were obtained. This work discovered that increasing the reaction temperature

accelerates the conversion rate but decreases the selectivity of GMO. The equimolar ratio of OA to glycerol was suggested to increase the selectivities of GMO and GDO. This work also confirmed that 5 wt% ZrO_2-SiO_2-Me&Et-$PhSO_3H$_70 catalyst concentration is the optimal level for the catalytic study of glycerol with OA. Moreover, the GMO selectivity decreased with the increased catalyst concentration. This effect was highly attributed to the increased number of available acidic sites of the catalyst. Therefore, a strongly acidic catalyst promoted the formation of a low-GMO-selectivity product mixture.

A comparative study on ZrO_2-SiO_2-Me&Et-$PhSO_3H$ with different SO_4^{2-}/ZrO_2 catalysts validated the following points: (i) the structural crystallinity of SO_4^{2-}/ZrO_2 was affected with the type of zirconia precursor and (ii) the importance of catalyst pore volume or high accessibility of the organic reactants to the active sites. The catalyst pore volume was correlated with the selectivity of the reaction; a large pore volume enabled the formation of large-molecular-size GDO and GTO. Furthermore, highly uniform pores measuring less than 5 nm attained high GMO selectivity. Comparison of the performance of ZrO_2-SiO_2-Me&Et-$PhSO_3H$ and commercially available Amberlyst 15 and Aquivion noted that catalyst acidity is a key parameter for catalytic activity and conversion rate. Nevertheless, high acidity/acid strength reduced the product yield in the glycerol esterification of OA. The mild acidity of ZrO_2-SiO_2-Me&Et-$PhSO_3H$ with a hydrophobic surface was recommended for the catalytic esterification of glycerol with OA at equimolar ratio of reactants to attain a high selectivity of GMO. Superacid Aquivion was recommended to produce GTO at a OA-to-glycerol moral ratio of 3:1.

This study proved that the textural properties (pore volume and pore size), acidity and hydrophobicity of heterogeneous acid catalysts play vital roles in controlling the

activity and selectivity of reactions. Therefore, the acid strength and the number of available acid sites influence the conversion rate of reaction, and the hydrophobicity and pore volume of solid catalysts significantly affect the selectivity of the product.

5.2 Recommendation

This work developed hydrophobicity-enhanced heterogeneous acid catalyst using ZrO_2-SiO_2 support. It was proven that catalyst hydrophobicity plays an important role to enhance formation rate of GMO. However, the stability of the catalyst is not suitable to robust usage and not ready for commercial use. Therefore, two suggestions are recommended to improve designing of high thermal stability of catalyst. First, oxidative cleavage of tetrasulfide bridges in sulfonic acid functionalized hybrid silicas catalyst is suggested to produce strong $-SO_3H$ bond between acid sites and catalyst support. Second, it is essential to study different method in preparation of porous, mesoporous or hollow silica-based catalyst, for instance, surfactant addition or combination with hard-soft template methods. An accessible and permeable pores, especially radially oriented channels is vital for small molecules, bio-macromolecules or even nanoparticles to easily move into or out of the porous matrices.

In addition, kinetic study should be done in future for batch and continuous processes. The designed hydrophobicity-advanced heterogeneous acid catalyst in this work can be applied in typical esterification of carboxylic acid with non-polar reactant, for instance, acetylation for the production of bio-additives, etherification production of glycerol tertiary butyl ether, biodegradable surfactant production derived from glycerol-fatty alcohol as well as water-sensitive biomass conversion synthesis.

Meanwhile, commercial strong acidity Aquivion catalyst is suggested for production of GTO biolubricant. The process optimization works is needed in order to maximize GTO yield.

REFERENCES

Åkerman, C. O., Gaber, Y., Ghani, N. A., Lämsä, M., & Hatti-Kaul, R. (2011). Clean synthesis of biolubricants for low temperature applications using heterogeneous catalysts. *Journal of Molecular Catalysis B: Enzymatic, 72*(3), 263-269.

Alcañiz-Monge, J., Bakkali, B. E., Trautwein, G., & Reinoso, S. (2018). Zirconia-supported tungstophosphoric heteropolyacid as heterogeneous acid catalyst for biodiesel production. *Applied Catalysis B: Environmental, 224*(Supplement C), 194-203.

Anneken, D. J., Both, S., Christoph, R., Fieg, G., Steinberner, U., & Westfechtel, A. (2000). Fatty Acids *Ullmann's Encyclopedia of Industrial Chemistry*: Wiley-VCH Verlag GmbH & Co. KGaA.

Aranda, D. A. G., Santos, R. T. P., Tapanes, N. C. O., Ramos, A. L. D., & Antunes, O. A. C. (2008). Acid-Catalyzed Homogeneous Esterification Reaction for Biodiesel Production from Palm Fatty Acids. *Catalysis Letters, 122*(1), 20-25.

Ayoub, M., & Abdullah, A. Z. (2012). Critical review on the current scenario and significance of crude glycerol resulting from biodiesel industry towards more sustainable renewable energy industry. *Renewable and Sustainable Energy Reviews, 16*(5), 2671-2686.

Babajide, O. (2013). Sustaining Biodiesel Production via Value-Added Applications of Glycerol. *Journal of Energy, 2013*, 1-7.

Bagheri, S., Julkapli, N. M., & Yehye, W. A. (2015). Catalytic conversion of biodiesel derived raw glycerol to value added products. *Renewable and Sustainable Energy Reviews, 41*, 113-127.

Balaraju, M., Nikhitha, P., Jagadeeswaraiah, K., Srilatha, K., Sai Prasad, P. S., & Lingaiah, N. (2010). Acetylation of glycerol to synthesize bioadditives over niobic acid supported tungstophosphoric acid catalysts. *Fuel Processing Technology, 91*(2), 249-253.

Barauskas, J., Misiunas, A., Gunnarsson, T., Tiberg, F., & Johnsson, M. (2006). "Sponge" Nanoparticle Dispersions in Aqueous Mixtures of Diglycerol Monooleate, Glycerol Dioleate, and Polysorbate 80. *Langmuir, 22*(14), 6328-6334.

Bazuła, P. A., Arnal, P. M., Galeano, C., Zibrowius, B., Schmidt, W., & Schüth, F. (2014). Highly microporous monodisperse silica spheres synthesized by the Stöber process. *Microporous and Mesoporous Materials, 200*(Supplement C), 317-325.

Bondioli, P. (2004). The Preparation of Fatty Acid Esters by Means of Catalytic Reactions. *Topics in Catalysis, 27*(1-4), 77-82.

BP. (June 2017). *BP Statistical Review of World Energy*. Retrieved from https://www.bp.com/content/dam/bp/en/corporate/pdf/energy-economics/statistical-review-2017/bp-statistical-review-of-world-energy-2017-full-report.pdf

Brockmann, R., Jeromin, L., Johannisbauer, W., Meyer, H., Michel, O., & Plachenka, J. (1987). Germany Patent No. US4655879 A. US Patent: K. A. A. Henkel.

Chen, J., Chen, J., Zhang, X., Gao, J., & Yang, Q. (2016). Efficient and stable PS-SO3H/SiO2 hollow nanospheres with tunable surface properties for acid catalyzed reactions. *Applied Catalysis A: General, 516*, 1-8.

Choi, S. J., Oh, J. M., & Choy, J. H. (2008). Human-related application and nanotoxicology of inorganic particles: complementary aspects. *Journal of Materials Chemistry, 18*(6), 615-620.

CIMBRIA SKET. (2008). Glycerine Distillation (Refining) Technology. Retrieved from http://www.cimbria-sket.de/downloads/Glycerine_english_2008-11.pdf

Corma, A., Hamid, S. B. A., Iborra, S., & Velty, A. (2005). Lewis and Brönsted basic active sites on solid catalysts and their role in the synthesis of monoglycerides. *Journal of Catalysis, 234*(2), 340-347.

Corma, A., Iborra, S., Miquel, S., & Primo, J. (1998). Production of Food Emulsifiers, Monoglycerides, by Glycerolysis of Fats with Solid Base Catalysts. *Journal of Catalysis, 173*, 315-321.

de Jong, M. C., Feijt, R., Zondervan, E., Nijhuis, T. A., & de Haan, A. B. (2009). Reaction kinetics of the esterification of myristic acid with isopropanol and n-propanol using p-toluene sulphonic acid as catalyst. *Applied Catalysis A: General, 365*(1), 141-147.

Diao, Y., He, H., Yang, P., Wang, L., & Zhang, S. (2015). Optimizing the structure of supported Pd catalyst for direct oxidative esterification of methacrolein with methanol. *Chemical Engineering Science, 135*, 128-136.

Díaz, I., Márquez-Alvarez, C., Mohino, F., Pérez-Pariente, J. n., & Sastre, E. (2000). Combined Alkyl and Sulfonic Acid Functionalization of MCM-41-Type Silica: Part 2. Esterification of Glycerol with Fatty Acids. *Journal of Catalysis, 193*(2), 295-302.

Díaz, I., Mohino, F., Blasco, T., Sastre, E., & Pérez-Pariente, J. n. (2005). Influence of the alkyl chain length of HSO3-R-MCM-41 on the esterification of glycerol with fatty acids. *Microporous and Mesoporous Materials, 80*(1–3), 33-42.

Díaz, I., Mohino, F., Pérez-Pariente, J. n., & Sastre, E. (2003). Synthesis of MCM-41 materials functionalised with dialkylsilane groups and their catalytic activity in the esterification of glycerol with fatty acids. *Applied Catalysis A: General, 242*(1), 161-169.

Dorin Bombos, Mihaela Bombos, Ion Bolocan, Gabriel Vasilievici, & Zaharia, E. (2010). Esterification of glycerol with technical olein in heterogeneous catalysis. *REV. CHIM. (Bucharest), 61*, 784.

Estevez, R., López, M. I., Jiménez-Sanchidrián, C., Luna, D., Romero-Salguero, F. J., & Bautista, F. M. (2016). Etherification of glycerol with tert-butyl alcohol over sulfonated hybrid silicas. *Applied Catalysis A: General, 526*, 155-163.

Fang, W., Fan, Z., Shi, H., Wang, S., Shen, W., Xu, H., . . . Pera-Titus, M. (2016). Aquivion[registered sign]-carbon composites via hydrothermal carbonization: amphiphilic catalysts for solvent-free biphasic acetalization. *Journal of Materials Chemistry A, 4*(12), 4380-4385.

Fang, W., Wang, S., Liebens, A., De Campo, F., Xu, H., Shen, W., . . . Clacens, J.-M. (2015). Silica-immobilized Aquivion PFSA superacid: application to heterogeneous direct etherification of glycerol with n-butanol. *Catalysis Science & Technology, 5*(8), 3980-3990.

Faria, E. A., Marques, J. S., Dias, I. M., Andrade, R. D. A., Suarez, P. A. Z., & Prado, A. G. S. (2009). Nanosized and reusable SiO2/ZrO2 catalyst for highly efficient biodiesel production by soybean transesterification. *Journal of the Brazilian Chemical Society, 20*, 1732-1737.

Ferretti, C. A., Fuente, S., Ferullo, R., Castellani, N., Apesteguía, C. R., & Di Cosimo, J. I. (2012). Monoglyceride synthesis by glycerolysis of methyl oleate on MgO:

Catalytic and DFT study of the active site. *Applied Catalysis A: General, 413–414*(0), 322-331.

Ferretti, C. A., Soldano, A., Apesteguía, C. R., & Di Cosimo, J. I. (2010). Monoglyceride synthesis by glycerolysis of methyl oleate on solid acid–base catalysts. *Chemical Engineering Journal, 161*(3), 346-354.

Food and Agriculture Organization of the United Nations (OECD). (2015). *OECD-FAO Agricultural Outlook 2015*. Retrieved from Paris: http://dx.org/10.1787/agr_outlook-2015-en

Frost & Sullivan Research Service. (2014). World fatty esters markets (technical insights). Retrieved from http://www.frost.com/prod/servlet/report-brochure.pag?id=D483-01-00-00-00

Frusteri, F., Arena, F., Bonura, G., Cannilla, C., Spadaro, L., & Di Blasi, O. (2009). Catalytic etherification of glycerol by tert-butyl alcohol to produce oxygenated additives for diesel fuel. *Applied Catalysis A: General, 367*(1–2), 77-83.

Galarneau, A., Cambon, H., Martin, T., Ménorval, L.-C. D., Brunel, D., Renzo, F. D., & Fajula, F. (2002). SBA-15 versus MCM-41: are they the same materials? In A. Sayari & M. Jaroniec (Eds.), *Studies in Surface Science and Catalysis* (Vol. 141, pp. 395-402): Elsevier.

Gaudin, P., Jacquot, R., Marion, P., Pouilloux, Y., & Jérôme, F. (2011). Acid-Catalyzed Etherification of Glycerol with Long-Alkyl-Chain Alcohols. *ChemSusChem, 4*(6), 719-722.

GlobeNewswire, N. (2017). Lubricants Market worth over $74bn by 2022: Global Market Insights Inc. Retrieved from https://globenewswire.com/news-release/2017/03/13/934926/0/en/Lubricants-Market-worth-over-74bn-by-2022-Global-Market-Insights-Inc.html

Grosch, G. H., Larbig, H., Lorenz, R., Junge, D., & Kammel, U. (2002). Supported double metal cyanide catalysts, method for producing them, and their use for producing polyether alcohols: U. S. Patents.

Gryglewicz, S., Piechocki, W., & Gryglewicz, G. (2003). Preparation of polyol esters based on vegetable and animal fats. *Bioresource Technology, 87*(1), 35-39.

Gu, Y., Azzouzi, A., Pouilloux, Y., Jérôme, F., & Barrault, J. (2008). Heterogeneously catalyzed etherification of glycerol: new pathways for transformation of glycerol to more valuable chemicals. *Green Chemistry, 10*(2), 164–167.

Gürbüz, E., Bond, J. Q., Dumesic, J. A., & Román-Leshkov, Y. (2013). Chapter 8 - Role of Acid Catalysis in the Conversion of Lignocellulosic Biomass to Fuels and Chemicals. In K. S. T. A. L. Stöcker (Ed.), *The Role of Catalysis for the Sustainable Production of Bio-fuels and Bio-chemicals* (pp. 261-288). Amsterdam: Elsevier.

Hamerski, F., & Corazza, M. L. (2014). LDH-catalyzed esterification of lauric acid with glycerol in solvent-free system. *Applied Catalysis A: General, 475*(0), 242-248.

Hamerski, F., Prado, M. A., da Silva, V. R., Voll, F. A. P., & Corazza, M. L. (2016). Kinetics of layered double hydroxide catalyzed esterification of fatty acids with glycerol. *Reaction Kinetics, Mechanisms and Catalysis, 117*(1), 253-268.

Hasan, Z., Yoon, J. W., & Jhung, S. H. (2014). Esterification and acetylation reactions over in situ synthesized mesoporous sulfonated silica. *Chemical Engineering Journal*.

Hermida, L., Abdullah, A. Z., & Mohamed, A. R. (2011). Synthesis of monoglyceride through glycerol esterification with lauric acid over propyl sulfonic acid post-synthesis functionalized SBA-15 mesoporous catalyst. *Chemical Engineering Journal, 174*(2–3), 668-676.

Hongxia Zhao, Jiangang Chen, & Sun, Y. (2003). Effect Of Calcination Temperature on the Performance of Co/ZrO2 Catalyts for Fischer-Tropsch Synthesis *Prepr. Pap. -Am. Chem. Soc., Div. Fuel Chem., 48(2)*(2), 733.

Hoo, P.-Y., & Abdullah, A. Z. (2014). Direct synthesis of mesoporous 12-tungstophosphoric acid SBA-15 catalyst for selective esterification of glycerol and lauric acid to monolaurate. *Chemical Engineering Journal, 250*, 274-287.

International Process Plants. (2009). Fatty Acid Plants. Retrieved from http://www.ippe.com/plants/600497/fattyacid.pdf

Isahak, W. N. R. W., Ismail, M., Nordin, N. M., Jahim, J. M., & Yarmo, M. A. (2011). Synthesis, Characterization and Catalytic Performance of H3SiW12O40/SiO2 Prepared by Sol-Gel Technique. *Journal of Nanotechnology*.

Isahak, W. N. R. W., Ramli, Z. A. C., Ismail, M., & Yarmo, M. A. (2014). Highly Selective Glycerol Esterification over Silicotungstic Acid Nanoparticles on Ionic Liquid Catalyst. *Industrial & Engineering Chemistry Research, 53*(25), 10285-10293.

Jérôme, F., Pouilloux, Y., & Barrault, J. (2008). Rational Design of Solid Catalysts for the Selective Use of Glycerol as a Natural Organic Building Block. *ChemSusChem, 1*(7), 586-613.

Johnson Matthey Catalysts VERTEC™. (2003). Direct esterification

technology   Retrieved   from http://www.jmcatalysts.com/vertec/pdfs/directesterification.pdf

Karam, A., Sayoud, N., De Oliveira Vigier, K., Lai, J., Liebens, A., Oldani, C., & Jérôme, F. (2016). Heterogeneously-acid catalyzed oligomerization of glycerol over recyclable superacid Aquivion® PFSA. *Journal of Molecular Catalysis A: Chemical, 422*, 84-88.

Kathy Wai Yu, L., Christopher J. H., P., & Ben J., B. (2013). A Simple Quantitative Approach for the Determination of Long and Medium Chain Lipids in Bio-relevant Matrices by High Performance Liquid Chromatography with Refractive Index Detection. *AAPS PharmSciTech*.

Khayoon, M. S., Triwahyono, S., Hameed, B. H., & Jalil, A. A. (2014). Improved production of fuel oxygenates via glycerol acetylation with acetic acid. *Chemical Engineering Journal, 243*(0), 473-484.

Kirk-Othmer. (2013). Glycerine *Chemical Technology of Cosmetics*. Canada: John Wiley & Sons, Inc. Hoboken, New Jersey.

Kiss, A. A., Dimian, A. C., & Rothenberg, G. (2007). Biodiesel by Catalytic Reactive Distillation Powered by Metal Oxides. *Energy & Fuels, 22*(1), 598-604.

Kiss, A. A., Dimian, A. C., & Rothenberg, G. (2008). Biodiesel by Catalytic Reactive Distillation Powered by Metal Oxides. *Energy & Fuels, 22*(1), 598-604.

Kong PS, Aroua MK, & Raman AA. (2011). Kinetics study of esterification reaction of 2-methyl-4-chlorophenoxyacetic acid (MCPA acid). *International Journal of Chemical Reactor Engineering, 9*, 112.

Kong, P. S., Aroua, M. K., & Daud, W. M. A. W. (2015). Catalytic esterification of bioglycerol to value-added products. *Reviews in Chemical Engineering, 31*(5), 437–451.

Kong, P. S., Aroua, M. K., & Daud, W. M. A. W. (2016). Conversion of crude and pure glycerol into derivatives: A feasibility evaluation. *Renewable and Sustainable Energy Reviews, 63*, 533-555.

Kong, P. S., Aroua, M. K., Daud, W. M. A. W., Cognet, P., & Pérès, Y. (2016). Enhanced microwave catalytic-esterification of industrial grade glycerol over Brønsted-based methane sulfonic acid in production of biolubricant. *Process Safety and Environmental Protection, 104, Part A*, 323-333.

Kong, P. S., Aroua, M. K., Daud, W. M. A. W., Lee, H. V., Cognet, P., & Peres, Y. (2016). Catalytic role of solid acid catalysts in glycerol acetylation for the production of bio-additives: a review. *RSC Advances, 6*(73), 68885-68905.

Konwar, L. J., Boro, J., & Deka, D. (2014). Review on latest developments in biodiesel production using carbon-based catalysts. *Renewable and Sustainable Energy Reviews, 29*, 546-564.

Konwar, L. J., Mäki-Arvela, P., Kumar, N., Mikkola, J.-P., Sarma, A. K., & Deka, D. (2016). Selective esterification of fatty acids with glycerol to monoglycerides over –SO3H functionalized carbon catalysts. *Reaction Kinetics, Mechanisms and Catalysis, 119*(1), 121-138.

Kotwal, M., Deshpande, S. S., & Srinivas, D. (2011). Esterification of fatty acids with glycerol over Fe–Zn double-metal cyanide catalyst. *Catalysis Communications, 12*(14), 1302-1306.

Kotwal, M., Kumar, A., & Darbha, S. (2013). Three-dimensional, mesoporous titanosilicates as catalysts for producing biodiesel and biolubricants. *Journal of Molecular Catalysis A: Chemical, 377*, 65-73.

Kozhevnikov, I. V. (1998). Catalysis by heteropoly acids and multicomponent polyoxometalates in liquid-phase reactions. *Chemical Reviews, 98*(1), 171-198.

Krüger, R. L., Valério, A., Balen, M., Ninow, J. L., Vladimir Oliveira, J., de Oliveira, D., & Corazza, M. L. (2010). Improvement of mono and diacylglycerol production via enzymatic glycerolysis in tert-butanol system. *European Journal of Lipid Science and Technology, 112*(8), 921-927.

Kulkarni, C. V., Wachter, W., Iglesias-Salto, G., Engelskirchen, S., & Ahualli, S. (2011). Monoolein: a magic lipid? *Physical Chemistry Chemical Physics, 13*(8), 3004-3021.

Kuśtrowski, P., Chmielarz, L., Bożek, E., Sawalha, M., & Roessner, F. (2004). Acidity and basicity of hydrotalcite derived mixed Mg–Al oxides studied by test reaction of MBOH conversion and temperature programmed desorption of NH3 and CO2. *Materials Research Bulletin, 39*(2), 263-281.

Kuwahara, Y., Kaburagi, W., Nemoto, K., & Fujitani, T. (2014). Esterification of levulinic acid with ethanol over sulfated Si-doped ZrO2 solid acid catalyst: Study of the structure–activity relationships. *Applied Catalysis A: General, 476*, 186-196.

Labauze, G., & Vasseur, D. (2007). Rubber composition for a tire tread: U.S. Patents.

Le-Khac, B. (1996). Highly active double metal cyanide catalysts: United States Patents.

Leoneti, A. B., Aragão-Leoneti, V., & de Oliveira, S. V. W. B. (2012). Glycerol as a by-product of biodiesel production in Brazil: Alternatives for the use of unrefined glycerol. *Renewable Energy, 45*(0), 138-145.

Li, L., Li, B., Dong, J., & Zhang, J. (2016). Roles of silanes and silicones in forming superhydrophobic and superoleophobic materials. *Journal of Materials Chemistry A, 4*(36), 13677-13725.

Ma, F., & Hanna, M. A. (1999). Biodiesel production: a review. *Bioresource Technology, 70*(1), 1-15.

Macierzanka, A., & Szeląg, H. (2004). Esterification Kinetics of Glycerol with Fatty Acids in the Presence of Zinc Carboxylates: Preparation of Modified Acylglycerol Emulsifiers. *Industrial & Engineering Chemistry Research, 43*(24), 7744-7753.

Markovska, I., Yovkova, F., Minov, G., Rusev, D., & Lyubchev, L. (2013). Investigation of Silane Modified Ceramic Surface of Porous Mullite Ceramics *International Journal of Environmental, Chemical, Ecological, Geological and Geophysical Engineering, 7*(7).

Márquez-Alvarez, C., Sastre, E., & Pérez-Pariente, J. (2004). Solid Catalysts for the Synthesis of Fatty Esters of Glycerol, Polyglycerols and Sorbitol from Renewable Resources. *Topics in Catalysis, 27*(1-4), 105-117.

Matthias, T., Katsumi, K., Alexander, V. N., James, P. O., Francisco, R.-R., Jean, R., & Kenneth, S. W. S. (2015). Physisorption of gases, with special reference to the evaluation of surface area and pore size distribution (IUPAC Technical Report). *Pure Appl. Chem*.

Mobaraki, A., Movassagh, B., & Karimi, B. (2014). Hydrophobicity-enhanced magnetic solid sulfonic acid: A simple approach to improve the mass transfer of reaction partners on the surface of the heterogeneous catalyst in water-generating reactions. *Applied Catalysis A: General, 472*, 123-133.

Montoya, C., Cochard, B., Flori, A., Cros, D. C., Lopes, R., Cuellar, T., . . . Billotte, N. (2014). Genetic Architecture of Palm Oil Fatty Acid Composition in Cultivated Oil Palm (Elaeis guineensis Jacq.) Compared to Its Wild Relative E. oleifera (H.B.K) Cortés. *PLOS ONE, 9(*(6), e101628.

Nagendramma, P., & Kaul, S. (2012). Development of ecofriendly/biodegradable lubricants: An overview. *Renewable and Sustainable Energy Reviews, 16*(1), 764-774.

Nanda, M. R., Yuan, Z., Qin, W., Ghaziaskar, H. S., Poirier, M.-A., & Xu, C. C. (2014). Thermodynamic and kinetic studies of a catalytic process to convert glycerol into solketal as an oxygenated fuel additive. *Fuel, 117*(Part A), 470-477.

Ogino, I., Suzuki, Y., & Mukai, S. R. (2017). Esterification of levulinic acid with ethanol catalyzed by sulfonated carbon catalysts: Promotional effects of additional functional groups. *Catalysis Today*.

Oh, J., Yang, S., Kim, C., Choi, I., Kim, J. H., & Lee, H. (2013a). Synthesis of biolubricants using sulfated zirconia catalysts. *Applied Catalysis A: General, 455*(Supplement C), 164-171.

Oh, J., Yang, S., Kim, C., Choi, I., Kim, J. H., & Lee, H. (2013b). Synthesis of biolubricants using sulfated zirconia catalysts. *Applied Catalysis A: General, 455*, 164-171.

Okamura, M., Takagaki, A., Toda, M., Kondo, J. N., Domen, K., Tatsumi, T., . . . Hayashi, S. (2006). Acid-catalyzed reactions on flexible polycyclic aromatic carbon in amorphous carbon. *Chemistry of Materials, 18*(13), 3039-3045.

Okuhara, T. (2002). Water-Tolerant Solid Acid Catalysts. *Chem. Rev., 102*, 3641-3666.

Oleoline. (2012). Glycerine Market Report. www.oleoline.com/wp-content/uploads/products.

Oleoline. (2017). Oleoline Glycerine Market Report Retrieved from http://www.hbint.com/datas/media/590204fd077a6e381ef1a252/sample-quarterly-glycerine.pdf

Organic Materials Review Institute. (2001). Glycerol Monooleate Retrieved from https://www.ams.usda.gov/sites/default/files/media/Glycerin%20Oleate%20TR.pdf

Pagliaro, M., & Rossi, M. (2010). Future of Glycerol. UK: The Royal Society of Chemistry.

Pérez-Pariente, J. n., Díaz, I., Mohino, F., & Sastre, E. (2003). Selective synthesis of fatty monoglycerides by using functionalised mesoporous catalysts. *Applied Catalysis A: General, 254*(2), 173-188.

Pouilloux, Y., Abro, S., Vanhove, C., & Barrault, J. (1999). Reaction of glycerol with fatty acids in the presence of ion-exchange resins: Preparation of monoglycerides. *Journal of Molecular Catalysis A: Chemical, 149*(1–2), 243-254.

Quispe, C. A. G., Coronado, C. J. R., & Carvalho Jr, J. A. (2013). Glycerol: Production, consumption, prices, characterization and new trends in combustion. *Renewable and Sustainable Energy Reviews, 27*(0), 475-493.

Rahman, I. A., & Padavettan, V. (2012). Synthesis of Silica Nanoparticles by Sol-Gel: Size-Dependent Properties, Surface Modification, and Applications in Silica-Polymer Nanocomposites-A Review. *Journal of Nanomaterials, 2012*, 15.

Rashad, M. M., & Baioumy, H. M. (2008). Effect of thermal treatment on the crystal structure and morphology of zirconia nanopowders produced by three different routes. *Journal of Materials Processing Technology, 195*(1–3), 178-185.

Refaat, A. A. (2009). Correlation between the chemical structure of biodiesel and its physical properties. *International Journal of Environment Science and Technology, 6*(4), 677–694.

Rodríguez-Castellón, E., Jiménez-López, A., Maireles-Torres, P., Jones, D. J., Rozière, J., Trombetta, M., . . . Storaro, L. (2003). Textural and structural properties and surface acidity characterization of mesoporous silica-zirconia molecular sieves. *Journal of Solid State Chemistry, 175*(2), 159-169.

Sánchez, J. A., Hernández, D. L., Moreno, J. A., Mondragón, F., & Fernández, J. J. (2011). Alternative carbon based acid catalyst for selective esterification of glycerol to acetylglycerols. *Applied Catalysis A: General, 405*(1–2), 55-60.

Saravanan, K., Tyagi, B., & Bajaj, H. C. (2016). Esterification of stearic acid with methanol over mesoporous ordered sulfated ZrO2–SiO2 mixed oxide aerogel catalyst. *Journal of Porous Materials*, 1-10.

Sebastian, J., & Srinivas, D. (2013). Influence of method of preparation of solid, double-metal cyanide complexes on their catalytic activity for synthesis of hyperbranched polymers. *Applied Catalysis A: General, 464–465*(0), 51-60.

Shaikhutdinov, S., & Freund, H.-J. (2013). Metal-Supported Aluminosilicate Ultrathin Films as a Versatile Tool for Studying the Surface Chemistry of Zeolites. *ChemPhysChem, 14*(1), 71-77.

Singh, D., Patidar, P., Ganesh, A., & Mahajani, S. (2013). Esterification of Oleic Acid with Glycerol in the Presence of Supported Zinc Oxide as Catalyst. *Industrial & Engineering Chemistry Research, 52*(42), 14776-14786.

Sivaiah, M. V., Robles-Manuel, S., Valange, S., & Barrault, J. (2012). Recent developments in acid and base-catalyzed etherification of glycerol to polyglycerols. *Catalysis Today, 198*(1), 305-313.

Soares, V. L. P., Lachter, E. R., Rodrigues Jr, J. d. A., Batista, L. N., & Nascimento, R. S. V. (2011). New Applications for Soybean Biodiesel Glycerol. *Applications and Technology, Prof. Tzi-Bun Ng (Ed.)*.

Stawicka, K., Trejda, M., & Ziolek, M. (2013). The production of biofuels additives on sulphonated MCF materials modified with Nb and Ta—Towards efficient solid catalysts of esterification. *Applied Catalysis A: General, 467*(0), 325-334.

Stephane Pariente, Tanchoux, N., & Fajula, F. (2009). Etherification of glycerol with ethanol over solid acid catalysts. *Green Chemistry, 11*, 1256-1261.

Su, C.-H. (2013). Kinetic study of free fatty acid esterification reaction catalyzed by recoverable and reusable hydrochloric acid. *Bioresource Technology, 130*, 522-528.

Suprun, W., Lutecki, M., Haber, T., & Papp, H. (2009). Acidic catalysts for the dehydration of glycerol: Activity and deactivation. *Journal of Molecular Catalysis A: Chemical, 309*(1–2), 71-78.

Tao, M.-L., Guan, H.-Y., Wang, X.-H., Liu, Y.-C., & Louh, R.-F. (2015). Fabrication of sulfonated carbon catalyst from biomass waste and its use for glycerol esterification. *Fuel Processing Technology, 138*, 355-360.

The Soap and Detergent Association. (1990). *Glycerine: an overview-terms technical data properties performance*. Retrieved from New York: http://www.aciscience.org/docs/glycerine_-_an_overview.pdf

Thengumpillil, N. B. K., Penumarthy, V., & Ayyagari, A. L. (2002). Process for the preparation of a monoglyceride: U.S. Patents.

Thompson, J., & He, B. (2006). Characterization of crude glycerol from biodiesel production from multiple feedstocks. *Applied Engineering in Agriculture, 22*(2), 261.

Trinh, H., Yusup, S., & Uemura, Y. (2018). Optimization and kinetic study of ultrasonic assisted esterification process from rubber seed oil. *Bioresource Technology, 247*(Supplement C), 51-57.

Troncea, S. B., Wuttke, S., Kemnitz, E., Coman, S. M., & Parvulescu, V. I. (2011). Hydroxylated magnesium fluorides as environmentally friendly catalysts for glycerol acetylation. *Applied Catalysis B: Environmental, 107*(3), 260-267.

USDA AMS Agricultural Analytics Division. (2013). *Glycerin Handling/Processing Technical Evaluation Report*. Retrieved from http://www.ams.usda.gov/sites/default/files/media/Glycerin%20Petition%20to%20remove%20TR%202013.pdf

Varhadi, P., Kotwal, M., & Srinivas, D. (2013). Zirconium phenyl phosphonate phosphite as a highly active, reusable, solid acid catalyst for producing fatty acid polyol esters. *Applied Catalysis A: General, 462–463*(0), 129-136.

Vol'eva, V. B., Belostotskaya, I. S., Malkova, A. V., Komissarova, N. L., Kurkovskaya, L. N., Usachev, S. V., & Makarov, G. G. (2012). New approach to the synthesis of 1,3-dioxolanes. *Russian Journal of Organic Chemistry, 48*(5), 638-641.

Voll, F., Krüger, R. L., de Castilhos, F., Filho, L. C., Cabral, V., Ninow, J., & Corazza, M. L. (2011). Kinetic modeling of lipase-catalyzed glycerolysis of olive oil. *Biochemical Engineering Journal, 56*(3), 107-115.

Wang, P., Liu, H., Niu, J., Li, R., & Ma, J. (2014). Entangled Pd complexes over Fe3O4@SiO2 as supported catalysts for hydrogenation and Suzuki reactions. *Catalysis Science & Technology, 4*(5), 1333-1339.

Wang, X.-D., Shen, Z.-X., Sang, T., Cheng, X.-B., Li, M.-F., Chen, L.-Y., & Wang, Z.-S. (2010). Preparation of spherical silica particles by Stöber process with high concentration of tetra-ethyl-orthosilicate. *Journal of Colloid and Interface Science, 341*(1), 23-29.

Wee, L., Lescouet, T., Fritsch, J., Bonino, F., Rose, M., Sui, Z., . . . Martens, J. (2013). Synthesis of Monoglycerides by Esterification of Oleic Acid with Glycerol in Heterogeneous Catalytic Process Using Tin–Organic Framework Catalyst. *Catalysis Letters, 143*(4), 356-363.

Wee, L. H., Lescouet, T., Fritsch, J., Bonino, F., Rose, M., Sui, Z., . . . Martens, J. A. (2013). Synthesis of Monoglycerides by Esterification of Oleic Acid with Glycerol in Heterogeneous Catalytic Process Using Tin–Organic Framework Catalyst. *Catalysis Letters, 143*(4), 356-363.

Yan, S., Salley, S. O., & Ng, K. S. (2009). Simultaneous transesterification and esterification of unrefined or waste oils over ZnO-La 2 O 3 catalysts. *Applied Catalysis A: General, 353*(2), 203-212.

Yang, F., Hanna, M., & Sun, R. (2012). Value-added uses for crude glycerol--a byproduct of biodiesel production. *Biotechnology for Biofuels, 5*(1), 1-10.

Yoneda, T. (2009). Method for stabilizing oil-based thickening gel composition: U. S. Patents.

Yusoff, M. H. M., & Abdullah, A. Z. (2016). Catalytic behavior of sulfated zirconia supported on SBA-15 as catalyst in selective glycerol esterification with palmitic acid to monopalmitin. *Journal of the Taiwan Institute of Chemical Engineers, 60*, 199-204.

Zabeti, M., Wan Daud, W. M. A., & Aroua, M. K. (2009). Activity of solid catalysts for biodiesel production: A review. *Fuel Processing Technology, 90*(6), 770-777.

Zauba. (2016). Retrieved from https://www.zauba.com/import-mono-oleate-hs-code.html

Zhang, Z., Huang, H., Ma, X., Li, G., Wang, Y., Sun, G., . . . Li, A. (2017). Production of diacylglycerols by esterification of oleic acid with glycerol catalyzed by diatomite loaded SO_4^{2-}/TiO_2. *Journal of Industrial and Engineering Chemistry, 53*, 307-316.

Zhou, C.-H. C., Beltramini, Jorge N. , Fan, Y.-X., & Lu, G. Q. M. (2008). Chemoselective catalytic conversion of glycerol as a biorenewable source to valuable commodity chemicals. *Chemical Society Reviews, 37*, 527–549.

Zhou, L., Al-Zaini, E., & Adesina, A. A. (2013). Catalytic characteristics and parameters optimization of the glycerol acetylation over solid acid catalysts. *Fuel, 103*, 617-625.

Zhu, S., Zhu, Y., Gao, X., Mo, T., Zhu, Y., & Li, Y. (2013). Production of bioadditives from glycerol esterification over zirconia supported heteropolyacids. *Bioresource Technology, 130*(0), 45-51.

Zięba, A., Drelinkiewicz, A., Chmielarz, P., Matachowski, L., & Stejskal, J. (2010). Transesterification of triacetin with methanol on various solid acid catalysts: A role of catalyst properties. *Applied Catalysis A: General, 387*(1–2), 13-25.

LIST OF PUBLICATIONS AND PAPERS PRESENTED

LIST OF PUBLICATIONS

Kong, P. S., Aroua, M. K., Daud, W. M. A. W., Cognet, P., & Pérès, Y. (2016). Enhanced microwave catalytic-esterification of industrial grade glycerol over Brønsted-based methane sulfonic acid in production of biolubricant. *Process Safety and Environmental Protection, 104*, Part A, 323-333.

Kong, P. S., Aroua, M. K., Daud, W. M. A. W., Lee, H. V., Cognet, P., & Peres, Y. (2016). Catalytic role of solid acid catalysts in glycerol acetylation for the production of bio-additives: a review. *RSC Advances, 6*(73), 68885-68905.

Kong, P. S., Aroua, M. K., & Daud, W. M. A. W. (2016). Conversion of crude and pure glycerol into derivatives: A feasibility evaluation. *Renewable and Sustainable Energy Reviews, 63*, 533-555.

Kong, P. S., Aroua, M. K., & Daud, W. M. A. W. (2015). Catalytic esterification of bioglycerol to value-added products. *Reviews in Chemical Engineering, 31*(5), 437–451.

Kong, P. S., Cognet, P., Pérès, Y., Daud, W. M. A. W., & Aroua, M. K. (2018). Development of a novel hydrophobic ZrO_2-SiO_2 based acid catalyst for catalytic esterification of glycerol with oleic acid. *Industrial & Engineering Chemistry Research,* Under revision.

LIST OF PAPERS PRESENTED

Kong, P. S., Aroua, M. K., Daud, W. M. A. W., Cognet, P., Pérès, Y., & Jerome, F. Development of hydrophobicity-enhanced SiO_2-ZrO_2 solid acid catalyst for glycerol esterification reaction. *4th International Symposium on Green Chemistry (ISGC)*, 16-19 May 2017, La Rochelle, France.

Kong, P. S., Aroua, M. K., Daud, W. M. A. W., Cognet, P., Pérès, Y., & Jerome, F. Development of hydrophobicity-enhanced SiO_2-ZrO_2 solid acid catalyst for glycerol esterification reaction. *Journée Scientifique INCREASE*, 14 March 2017, Paris, France.

Kong, P. S., Aroua, M. K., & Daud, W. M. A. W. Comparative study on production of biolubricant via conventional and microwave heating. *3rd International Symposium on Green Chemistry (ISGC)*, May 2015, La Rochelle, France.